Binding Motifs of Carboplatin and Oxaliplatin with Guanine: A Combined MS/MS, IRMPD, and Theoretical Study

Barbara Chiavarino, Lucretia Rotari, Maria Elisa Crestoni, Davide Corinti, Simonetta Fornarini, Debora Scuderi, Jean-Yves Salpin

Binding motifs of carboplatin and oxaliplatin with guanine: a combined MS/MS, IRMPD and theoretical study

Barbara Chiavarino[1], Lucretia Rotari[1], Maria Elisa Crestoni[1], Davide Corinti[1], Simonetta Fornarini[1], Debora Scuderi[2] and Jean-Yves Salpin[3*]*

1) Dipartimento di Chimica e Tecnologie del Farmaco, Università di Roma "La Sapienza", P.le A. Moro 5, I-00185 Roma, ITALY

2) Université Paris-Saclay, CNRS, Institut de Chimie Physique, 91405, Orsay, France.

3) Université Paris-Saclay, Univ Evry, CY Cergy Paris Université, CNRS, LAMBE, 91025, Evry-Courcouronnes, France

Corresponding authors:

Dr Barbara Chiavarino
e-mail: barbara.chiavarino@uniroma1.it

Dr Jean-Yves Salpin
e-mail: jeanyves.salpin@univ-evry.fr

ORCID Numbers

Barbara Chiavarino: https://orcid.org/0000-0002-1585-7061

Lucretia Rotari: https://orcid.org/0000-0001-5086-7487

Davide Corinti: https://orcid.org/0000-0001-8064-3492

Maria Elisa Crestoni: https://orcid.org/0000-0002-0991-5034

Simonetta Fornarini: https://orcid.org/0000-0002-6312-5738

Debora Scuderi: https://orcid.org/0000-0003-3931-8481

Jean-Yves Salpin: https://orcid.org/0000-0003-0979-1251

Abstract

Complexes generated in the gas phase involving the purine nucleobase guanine bound to second and third generation platinum drugs, namely carboplatin (CarboPt) and oxaliplatin (OxaliPt), were investigated by combining tandem mass spectrometry, collision induced dissociation (CID), infrared multiple photon dissociation spectroscopy (IRMPD) and density functional theory (DFT) calculations.

As first step, a spectroscopic characterization of the protonated platinum drugs was accomplished. Protonation of both CarboPt and OxaliPt in the gas phase occurs on one of the two carbonyl groups of the cyclobutanedicarboxylate and oxalate ligand, respectively. Such protonation has been postulated by several theoretical studies as a key preliminary step in the hydrolysis of Pt drugs under acidic conditions.

Subsequently, the protonated drugs react with guanine in solution to generate a complex of general formula [Pt drug + H + guanine]$^+$, which was then mass-selected. CID experiments provided evidence for the presence of strong binding between guanine and platinum-based drugs within the complexes. The structure of the two complexes has also been examined by comparing the experimental IRMPD spectra recorded in two spectral regions with DFT-computed IR spectra. For each system, the IRMPD spectra agree with the vibrational spectra calculated for the global minimum structures, which present a monodentate complexation of Pt onto the N7 position of canonical guanine. This binding scheme is therefore akin to that observed for cisplatin, while other coordination sites yield substantially less stable species. Interestingly, in the case of oxaliplatin, the IRMPD spectra are consistent with the presence of two isomeric forms very close in energy.

Introduction.

Discovered in the late 60's, cisplatin (*cis*-diamminedichloroplatinum(II); *cis*-[$Pt(NH_3)_2Cl_2$]), has since revolutionized the field of cancer therapy, and is widely used as an anticancer drug, especially to treat lung, ovarian, testicular, head, and neck cancers.[1] Its mechanism of action is now well described.[2] After passive diffusion through the cell wall, the mechanism starts with hydrolysis of cisplatin by removal of a first chloro ligand, leading to the biologically active complex *cis*-$[Pt(NH_3)_2(H_2O)Cl]^+$. The latter in turn interacts with the N7 position of guanine (G), thereby generating a monofunctional adduct by substitution of water. Then, displacement of the second chloro ligand and coordination to the N7 position of an adjacent purine results in the formation of intrastrand crosslinks,[3] mainly 1,2-d(GpG) and, to a lesser extent, 1,2-d(ApG), which induce strong distortion of DNA[4] and ultimately cell death.

In spite of its clinical success, this first generation of Pt-based anticancer drugs suffers from the appearance of severe side effects, such as nausea, nephro-, oto- and neurotoxicity,[5] as well as acquired resistance of tumor cells.[6] Consequently, many efforts were devoted to the development of new Pt-based drugs, by systematically varying the metal ligand sphere, notably to reduce the high rate of hydrolysis of cisPt, recognized as an important factor of its toxicity. Forty years of intensive research finally resulted in the worldwide approval of the second and third generation platinum drugs, namely carboplatin (CarboPt) and oxaliplatin (OxaliPt), respectively (Scheme 1).

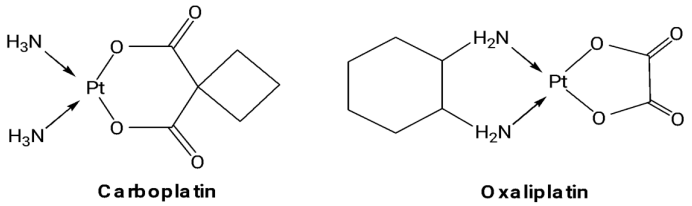

Scheme 1

As shown in Scheme 1, carboplatin and oxaliplatin present malonato and oxalato ligands, respectively, able to decrease the rate of hydrolysis by orders of magnitude when compared to that of cisplatin.[7] CarboPt is used primarily to treat ovarian cancer, whereas OxaliPt is particularly active against colorectal tumors.[8] However, in retrospect, neither carboplatin nor oxaliplatin have achieved the broad-spectrum application of cisplatin.[2b]

It is generally admitted that the mechanism of action of CarboPt and OxaliPt within the cells is retracing that of cisPt. However, given the presence of bulkier substituents, and notably of the very stable 1,2-diamino-cyclohexane (DACH) ligand in oxaliplatin, one may reasonably wonder how their mode of interaction at the molecular level compares to that described for cisPt. This question has motivated the present study, which reports the structural characterization of the bare complexes arising from the interaction between CarboPt and OxaliPt with guanine, and the comparison with our previous works on cisPt. We performed this scrutiny by combining tandem mass spectrometry experiments, density functional theory calculations (DFT), and IRMPD (Infrared Multiple Photon Dissociation) spectroscopy of mass-selected ions. This latter technique is particularly powerful for the structural characterization of free/isolated metal ions/biomolecules complexes,[9] and particularly for the interactions with DNA building blocks.[10] Two distinct IR frequency domains were presently examined. We used a Fourier Tranform Ion Cyclotron Resonance (FT-ICR) setup coupled to the CLIO (Centre Laser Infrarouge d'Orsay) free electron laser to record IRMPD spectra in the 800-1900 cm^{-1} energy region.[11] Furthermore, we also examined the NH and OH stretches region between 2900 and 3700 cm^{-1} by means of a tunable OPO/OPA system (optical parametric oscillator/optical parameter amplifier (OPO/OPA) combined with a Paul ion trap mass spectrometer.[12]

Experimental

2.1 Materials

Carboplatin (cis-diammine-[1,1-cyclobutanedicarboxylato]platinum(II)) and oxaliplatin [(1R,2R-diamminocyclohexane)oxalatoplatinum(II)], 2′-deoxyguanosine-5′-monophosphate (5'-dGMP), methanol and water used in this work were research grade products from commercial sources (Sigma-Aldrich s.r.l. Milan, Italy) and were used without any further purification. Stock aqueous solutions of 5'-dGMP and the two drugs were prepared at 10^{-3}M concentration. To circumvent the poor solubility of guanine in any solvent, we used 5'-dGMP to generate the complexes of interest in the gas phase by loss of the deoxyribosyl-phosphate moiety. To this end, a 10^{-5}M water:methanol solution of Pt drug and 5'-dGMP were mixed together in the molar ratio of (1:1) and then let to react at room temperature for 24 h.

2.2 CID experiments

The CID experiments were performed using two different mass spectrometers both equipped with an electrospray ionization (ESI) source. The solutions prepared as described were delivered to the ESI source using a syringe pump at a flow rate of 10 μL min^{-1}. To draw the fragmentation scheme of the investigated complex ions, MS^n spectra were recorded in a linear ion trap mass spectrometer (LTQ XL from Thermo Scientific™). Typical operating parameters were set as follows: temperature: 250°C, spray voltage: 5000 V and sheath gas flow rate: 10 (arbitrary units). Conversely, CID spectra at variable energy of the adducts of interest were obtained using a commercial hybrid triple-quadrupole linear ion trap mass spectrometer (2000 Q-Trap instrument from Applied Biosystems) with a $Q1q2Q_{LIT}$ configuration. In this case, the source parameters used were ion spray voltage: 5500 V, declustering potential: 80 V, and entrance potential: 4 V. In the CID measurements, the complex ions of interest were mass-selected in Q1 and let to collide with N_2 in the quadrupole collision cell q2 at variable collision

energies (E_{lab} = 5-50 eV). The nominal pressure measured at the vicinity of q2 was 3.3×10^{-5} mbar. Note however that the actual pressure in the collision cell is in fact in the order of 10^{-2} mbar.[13]At this pressure and given the dimension of q2 (~20 cms long), the mean free path for a N_2 molecule is about 5 mm. So, the complexes under examination (which have higher collision cross-sections) certainly undergo multiple collisions along their path through q2, as also already reported for QTRAP instruments.[14] The dissociation products were monitored by scanning Q_{LIT} using the enhanced mode of operation, where the ions were trapped in Q_{LIT} for 10 accumulation cycles to increase both resolution and signal intensity. Breakdown curves were generated by plotting the relative abundance of the ions in the resulting CID mass spectra as a function of collision energy. Quantitative threshold information is not directly available.[15] However, to compare the breakdown curves of different ions, the laboratory-frame collision energy (E_{lab}) was first converted to the center-of-mass frame (E_{CM}) according to the equation $E_{CM} = [m/(m + M)]E_{lab}$, where m and M are the masses of the collision gas and of the ion, respectively. Phenomenological threshold energies (TE) of selected fragmentation pathways were then derived from linear extrapolation of the sigmoidal increase of the fragment abundances for comparative purposes.[15b, 16]

2.3 IRMPD experiments

IRMPD experiments have been carried out in two spectral ranges. The fingerprint range (800-2000 cm^{-1}) was explored using the beamline of the free electron laser (FEL) of the Centre Laser Infrarouge d'Orsay (CLIO).[17] The FEL radiation is delivered in trains of 8 μs-long macropulses at a repetition rate of 25 Hz, each containing few hundred micropulses (0.5-3 ps long). Typical macropulse energies are 40 mJ. For the present study, the electron energy of the FEL was adjusted at 44.4 MeV to optimize and ensure a fairly stable laser power (900-1100 mW) in the explored frequency range of interest. The FEL beamline was coupled to a hybrid FT-ICR

tandem mass spectrometer (APEX-Qe Bruker) equipped with a 7.0 T actively shielded magnet and a quadrupole-hexapole interface for mass-filtering and ion accumulation. This experimental setup has already been described in details elsewhere.[11] Ions of interest were mass-selected in the quadrupole, accumulated and collisionally cooled during 300 ms in a hexapole containing argon buffer gas and then transferred into the ICR cell where they were irradiated with the IR FEL light for 200 to 500 ms. The resulting photofragment ions are then mass-analyzed. To avoid saturation effects of the most intense absorptions, IRMPD spectra were also recorded using one or two attenuators to decrease the irradiation power.

To examine the vibrational modes associated with the XH (X = C, N, O) stretches, IRMPD spectra were also recorded in the 2900-3700 cm^{-1} energy range by means of an optical parametric oscillator/amplifier (OPO/OPA, LaserVision) system coupled to a Paul ion trap mass spectrometer (Esquire 6000+, Bruker Daltonics), as already reported.[12] This parametric converter is pumped by the 1064 nm fundamental of a non seeded Nd:YAG laser (Continuum Surelite II) operating at 9 Hz repetition rates and generates a typical output energy of ca. 19 mJ/pulse in the spectral range of investigation with 3-4 cm^{-1} bandwidth. In the trap, ions were accumulated for 5-50 msec prior to IR irradiation. The typical irradiation time used in the experiment is 0.5 to 4 sec. In several cases, we improved the IRMPD signal intensity by irradiating the sampled ions with an auxiliary CO_2 laser (Universal Laser Systems, Inc., Scottsdale, AZ, USA). To this end, a 15 ms long CO_2 pulse of 13 W, corresponding to an energy of 260 mJ, followed each OPO/OPA pulse, delayed by 10 μs.[18]

IRMPD spectra presented in this work depict the photofragmentation yield R ($R = -\ln[I_{precursor}/(I_{precursor} + \Sigma I_{product})]$, where $I_{precursor}$ and $I_{product}$ are the integrated intensities of the mass peaks of the precursor and of the product ions, respectively) as a function of the frequency of the IR radiation.[17b, 19]

2.4 Theoretical study

Quantum chemical calculations were carried out in the framework of the Density Functional Theory (DFT), by using the hybrid B3LYP functional,[20] as implemented in the Gaussian-16 set of programs.[21] Provided the use of an appropriate scaling factor, Hybrid DFT methods such as B3LYP have been shown to be very efficient to describe both position and relative intensities of IR band.[22] Furthermore, a recent computational study has shown that the B3LYP functional performs also well for the structural and IR characterization of Pt complexes.[23] Geometry optimization was performed without any symmetry constraint with the 6-311G** basis set. The platinum atom was described by using the Los Alamos effective core potential (ECP) in combination with the LACV3P** basis set.[24] Harmonic vibrational frequencies were also computed at this level to estimate the zero-point vibrational energy (ZPE) corrections, and to characterize the stationary points as local minima or saddle points. The successful combination of the Los Alamos ECP+basis sets with the B3LYP functional for the investigation of both the electronic properties and reaction pathways of platinum-containing compounds is rather well documented,[25] including several computational studies on cisplatin, carboplatin and oxaliplatin.[26,27] In addition, so far we obtained an overall good agreement by using this approach, between the experimental IRMPD spectra and the harmonic vibrational spectra for different complexes involving cisplatin. [10e, j, m, q]

The infrared absorption spectra of the various structures were calculated within the harmonic approximation. Calculated frequencies were scaled by a factor of 0.974 in the fingerprint region and by 0.957 in the X-H stretch region for a better agreement with the experimental spectrum, as detailed in a previous study.[10e] Finally, to be consistent with the experimental spectral resolution, the calculated absorption spectra have been convoluted with a Lorentzian profile of 15 cm^{-1} FWHM (full width at half maximum) in the 800–2000 cm^{-1} region, while a FWHM of 5 cm^{-1} was used for the 2900–3700 cm^{-1} frequency range. Throughout this paper total energies

are expressed in Hartrees and relative energies in kJ mol^{-1}. For the sake of simplicity, the basis set used for Pt will be referred to as 6-311G**.

3.Results and Discussion

3.1 Collision-induced dissociation experiments

The mass spectrum of the methanolic/aqueous solution containing CarboPt and 5'-dGMP recorded in ESI-MS displays a cluster at *m/z* 522-524 whose isotopic pattern is in perfect agreement with the calculated isotopic pattern for the $[CarboPt+H+G]^+$ complex, as reported in Figure S1. Similarly, the ESI mass spectrum of the OxaliPt - 5'-dGMP solution shows a cluster at *m/z* 548-550, corresponding to $[OxaliPt+H+G]^+$ complex, as depicted in Figure S2. The complex observed is therefore different from the ions observed in a previous ESI study of OxaliPt/nucleobase mixtures, which were characterized by the loss of the oxalate ligand.[28]

To attain the fragmentation pattern of the $[CarboPt+H+G]^+$ and $[OxaliPt+H+G]^+$ adducts ions, MS^n experiments have been performed in a linear ion trap mass spectrometer. Figure S3 shows the CID spectrum of $[CarboPt+H+G]^+$ recorded at 15 eV, where the precursor ion exhibits three dissociation channels. The most abundant product ion at *m/z* 505 is obtained by the elimination of a single ammonia molecule, the product ion at *m/z* 461 from the combined loss of NH_3 and CO_2, and the *m/z* 371 species, formally ascribed to protonated carboplatin, $[CarboPt+H]^+$, by elimination of neutral guanine. MS^3 experiments performed on each primary fragments has allowed to draw the fragmentation scheme for $[CarboPt+G+H]^+$ adduct (Figure S4).

The CID spectrum of $[OxaliPt+H+G]^+$ is characterized by four principal dissociation routes (Figure S5). The first dissociation product at *m/z* 504 is due to elimination of CO_2, while the second one, at *m/z* 458, consists in the loss of $[C_2H_2O_4]$. Elimination of guanine yields protonated oxaliplatin at *m/z* 397, $[OxaliPt+H]^+$, whereas the product ion at *m/z* 353 is due to

the combined elimination of guanine and CO_2. The overall fragmentation scheme of $[OxaliPt+H+G]^+$ is reported in Figure S6.

Since both complexes lose neutral guanine yielding the respective protonated Pt-drug as primary fragment ion, this dissociation pathway was further investigated. A qualitative evaluation of the energy involved in Pt drug and guanine binding in $[CarboPt+H+G]^+$ and $[OxaliPt+H+G]^+$ adducts have been gathered by exploiting CID at variable energy. The ion abundance of precursor and product ions as a function of the collision energy expressed in the center of mass framework (E_{CM}) is given in Figure S7. Linear extrapolation of the rise of the breakdown curves provides a phenomenological threshold energy (TE) of 0.56 ± 0.20 eV for the appearance of protonated carboplatin (Figure S7a), while the values of TE for the appearance of the ion at *m/z* 397, corresponding to protonated oxaliplatin, and the ion at *m/z* 353, corresponding to $[OxaliPt+H-(CO_2)]^+$, are 0.93 ± 0.20 eV and 1.02 ± 0.20 eV, respectively (Figure S7b). Since the sizes of $[OxaliPt+H+G]^+$ and $[CarboPt+H+G]^+$ are comparable and the CID experiments are conducted under the same collision gas pressure, both complexes undergo a comparable number of collisions during the experiments. For the same reason, relevant differences in kinetic shift effects are not expected due to the similar degrees of vibrational freedom of the complexes, and have not been considered in the phenomenological comparison. These TE values do not provide a direct, absolute measurement of the threshold energy for dissociation, but suggest that oxaliplatin is more strongly bound to guanine in comparison with carboplatin. This trend could be correlated to the minor drug resistance observed in the clinical application of oxaliplatin. Among the various factors that contribute to platinum-resistance cells, including decreased cellular drug accumulation, enhanced detoxification system and reduced apoptosis, the DNA repair process plays the most important role.[29] The stronger binding observed in the isolated $[OxaliPt+H+G]^+$ complex may reflect the lower aptitude of the

OxalipPt-DNA crosslinks adducts to undergo DNA repair processes compared to CarboPt-DNA adducts.

3.2 IRMPD spectroscopy of the reactive species $[CarboPt+H]^+$ and $[OxaliPt+H]^+$

ESI mass spectra (Figure S1 and S2) show that protonation of the platinum drug is systematically observed, leading to $[CarboPt+H]^+$ and $[OxaliPt+H]^+$, which in turn form an adduct with guanine in solution to generate a complex of general formula [Pt drug + H + G]$^+$. The interaction mechanism therefore differs from that occurring with cisplatin, which is promoted by dechlorination, leading to cis-$[Pt(NH_3)_2(G)Cl]^+$ ions.[10e] Protonation on CarboPt and OxaliPt is also observed in the ESI mass spectra of methanolic/aqueous solution of the individual drugs in the absence of the nucleobase (Figure S8). Before examining in details the structure of the two Pt/G complexes, we recorded the IRMPD spectra of the drugs in protonated form, because several computational studies suggested a key role of protonation in the ring opening process allowing the metallic center to interact with the nucleobase during a subsequent step.[30]

The IRMPD spectra recorded in the fingerprint region for the $[CarboPt+H]^+$ and $[OxaliPt+H]^+$ ions are displayed in Figure 1, whereas data obtained in the XH (X = C, N, O) stretching region are summarized in the supporting information.

The photofragmentation spectrum of protonated oxaliplatin in the fingerprint region (recorded at 1250 cm^{-1}) is characterized by loss of carbon dioxide, followed by elimination of water and carbon monoxide (Figure S9, upper panel). Elimination of the intact DACH ligand is not observed. Scanning the laser wavelength results in the IRMPD spectrum displayed in Figure 1a that shows three sharp features at 1248, 1669 and 1759 cm^{-1}, and other weaker bands at 1063, 1150 and 1444 cm^{-1}.

To obtain structural information from this spectrum, a comparison with the calculated IR spectra of potential structures is mandatory. The geometry of the optimized structures for the $[OxaliPt+H]^+$ ions are given in Figure S10. The harmonic vibrational spectra obtained for the two most stable forms are displayed in Figure 1. Elimination of water as a photofragment suggested protonation of the oxalate ligand, consistently such protonation results in the most stable computed forms. The global minimum obtained, **Oxal_H1**, is in agreement with a previous theoretical study.[26c] It is characterized by a proton located on an oxygen atom not interacting with the metallic center, the proton being in an 'inside' position. The various features in the experimental spectrum are nicely reproduced by the computed spectrum of the isomer **Oxal_H1**. Given this good agreement, the vibrational modes of $[OxaliPt+H]^+$ can be assigned as described in Table S2. Notably, the band observed experimentally at 1444 cm^{-1} probably corresponds to the stretch of the protonated carbonyl group, whereas the C=O stretch of the second carbonyl, computed at 1765 cm^{-1} and red-shifted due to the formation of an internal hydrogen bond, accounts for the very intense band at 1759 cm^{-1}.

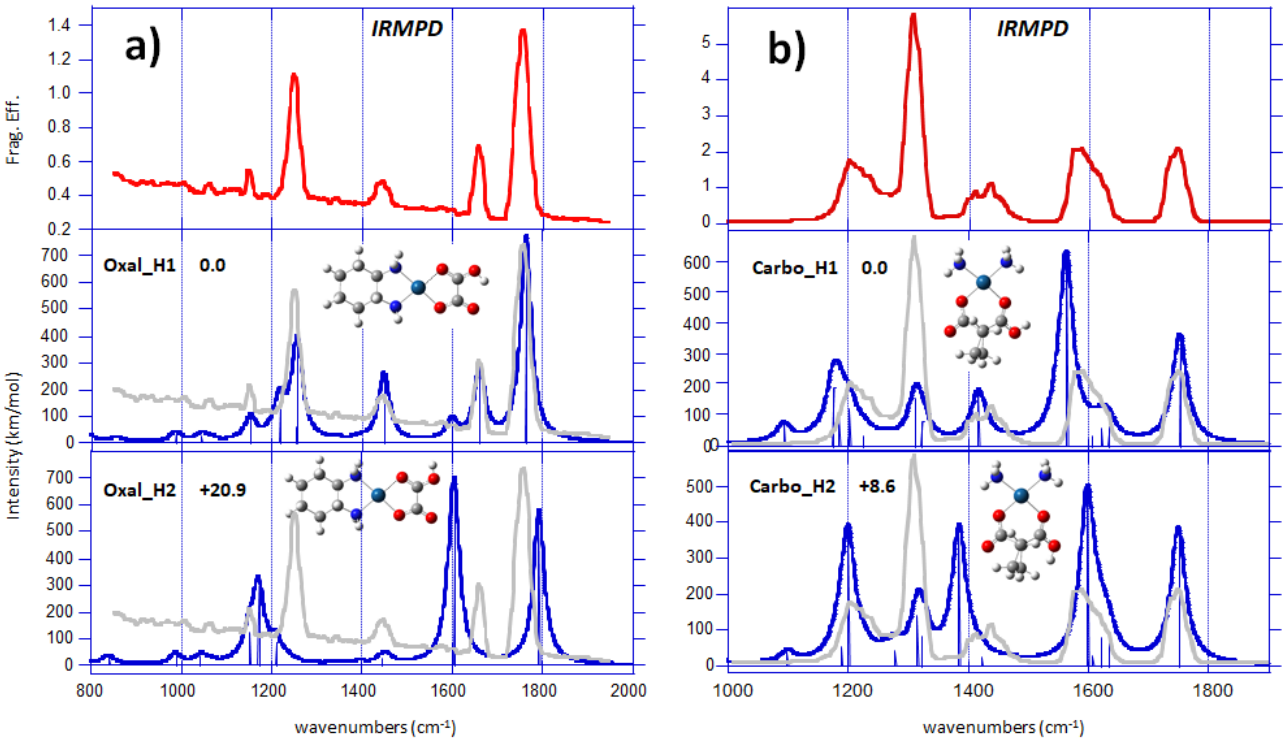

Figure 1. Experimental IRMPD spectrum of **a)** $[OxaliPt+H]^+$ and **b)** $[CarboPt+H]^+$ ions in the fingerprint region, compared with the IR spectra of their two most stable computed forms at the B3LYP/6-311G** level. For $[OxaliPt+H]^+$: irradiation time 2s combined with CO_2 activation of 15 ms; for $[CarboPt+H]^+$: irradiation time 500 ms and 1 attenuator.

Examination of Figure 1 also shows that the agreement of the **Oxal_H2** structure with the experimental features at 1248, 1669 and 1759 cm^{-1} is less satisfactory. In addition, OPO experiments are consistent with data obtained in the fingerprint region. As shown in Figure S11, the agreement in the X-H stretch region is again much better with **Oxal_H1**. Furthermore, the **Oxal_H2** structure is 20.9 kJ mol^{-1} less stable than the global minimum, supporting the evidence that its presence in the gas phase can be reasonably excluded. Finally, the **Oxal_H3** form, characterized by protonation onto an oxygen that interacts with Pt, turned out to be notably less stable (+78.7 kJ mol^{-1}) and its formation is therefore deemed unlikely (Figure S12). The IRMPD spectrum of $[CarboPt+H]^+$ in the fingerprint range is presented in Figure 1b. This spectrum is characterized by three broad features at 1180-1255, 1390-1460, 1560-1630 cm^{-1}

and two sharper bands centered at 1305 and 1745 cm^{-1}. Unsurprisingly, the photofragmentation differs from that of protonated OxaliPt and is associated with subsequent elimination of ammonia, carbon dioxide and the second ammonia (Figure S9 lower panel).

Given the results obtained with OxaliPt, we focused our theoretical survey on the protonation of the carboxylate group of the 1,1-cyclobutanedicarboxylato moiety. The two most stable forms are displayed in Figure 1b and are again associated with the protonation of an oxygen atom not interacting with Pt. **Carbo_H1** and **Carbo_H2** only differ by rotation of the hydroxyl group and, not unexpectedly, examination of Figure 1b indicates that the spectra of the two forms reproduce the experimental trace reasonably well. Vibrational assignment for **Carbo_H1** is provided in the supporting information (Table S3). The broad feature between 1180-1255 cm^{-1} is accounted for by several OH and CH bending modes, whereas the sharp band at 1305 cm^{-1} is attributed to ammonia bending vibrations. Interestingly, the broad signal observed at 1390-1460 cm^{-1} may result from the combination of at least two bands at ca. 1405 and 1435 cm^{-1}, which likely correspond to the ν(C⎓O-H) stretching vibration computed at 1385 and 1415 cm^{-1}, for **Carbo_H2** and **Carbo_H1**, respectively. Moreover, the ν(C=O(OH)) stretching mode computed at 1563 and 1598 cm^{-1} for **Carbo_H1** and **Carbo_H2**, respectively, may account for the asymmetrical shape of the experimental band located between 1560 and 1630 cm^{-1}. Finally, the sharp band at 1745 cm^{-1} can be attributed to the ν(C=O(OPt)) vibration. In the XH-stretching range, the two structures exhibit very similar spectra (Figure S11), which are again in very good agreement with the experimental contour. These different findings, combined with the fact that **Carbo_H1** and **Carbo_H2** are close in energy (8.6 kJ mol^{-1}), suggest that a mixture of these two forms is likely to be sampled in the gas phase.

In summary, our study demonstrates that under our experimental condition, protonation of both CarboPt and OxaliPt occurs on one of the two carbonyl groups. Such protonation has been postulated by several theoretical studies as a key preliminary step in the hydrolysis of the Pt

drugs under acidic conditions, because protonation lowers the activation barrier associated with the ring-opening process and allows the subsequent interaction with the nucleobase.[30] When comparing the geometry of the neutral and protonated forms of carboplatin and oxaliplatin (Figure S10), one may notice that the oxygen protonation results in a significant lengthening of the associated Pt-O bond (+ 0.060 Å and + 0.088 Å, respectively).

3.3 IRMPD spectroscopy of $[CarboPt+H+G]^+$ complex

The main purpose of the present paper is to determine the structure of the adducts $[CarboPt+H+G]^+$ and $[OxaliPt+H+G]^+$ observed with guanine (G), ions which formally correspond to the interaction of the protonated Pt drugs with intact G. To this end, we focused our theoretical survey by considering almost exclusively the canonical form of the nucleobase. We made several attempts by considering tautomeric forms of guanine, but as the resulting structures were systematically less stable, we did not push forward this exploration. Similarly, preliminary calculations have shown that protonation preferentially occurs onto the Pt drug, and not on the nucleobase. Given the fact that the results obtained for protonated carboplatin and oxaliplatin suggest the significant lengthening of one of the Pt-O bonds, we considered that one coordination site of Pt could become accessible, and that guanine could interact directly with the metal at either the N3, N7, O6 or NH_2 positions. Consequently, the names used to label the different structures are composed of three distinct parts: i) the name of the Pt drug (Carbo/Oxal), ii) the guanine site of interaction with Pt, and iii) an additional number if different forms for a particular interaction site are mentioned. Figure 2 shows representative optimized geometries for the different binding sites of guanine with protonated carboplatin.

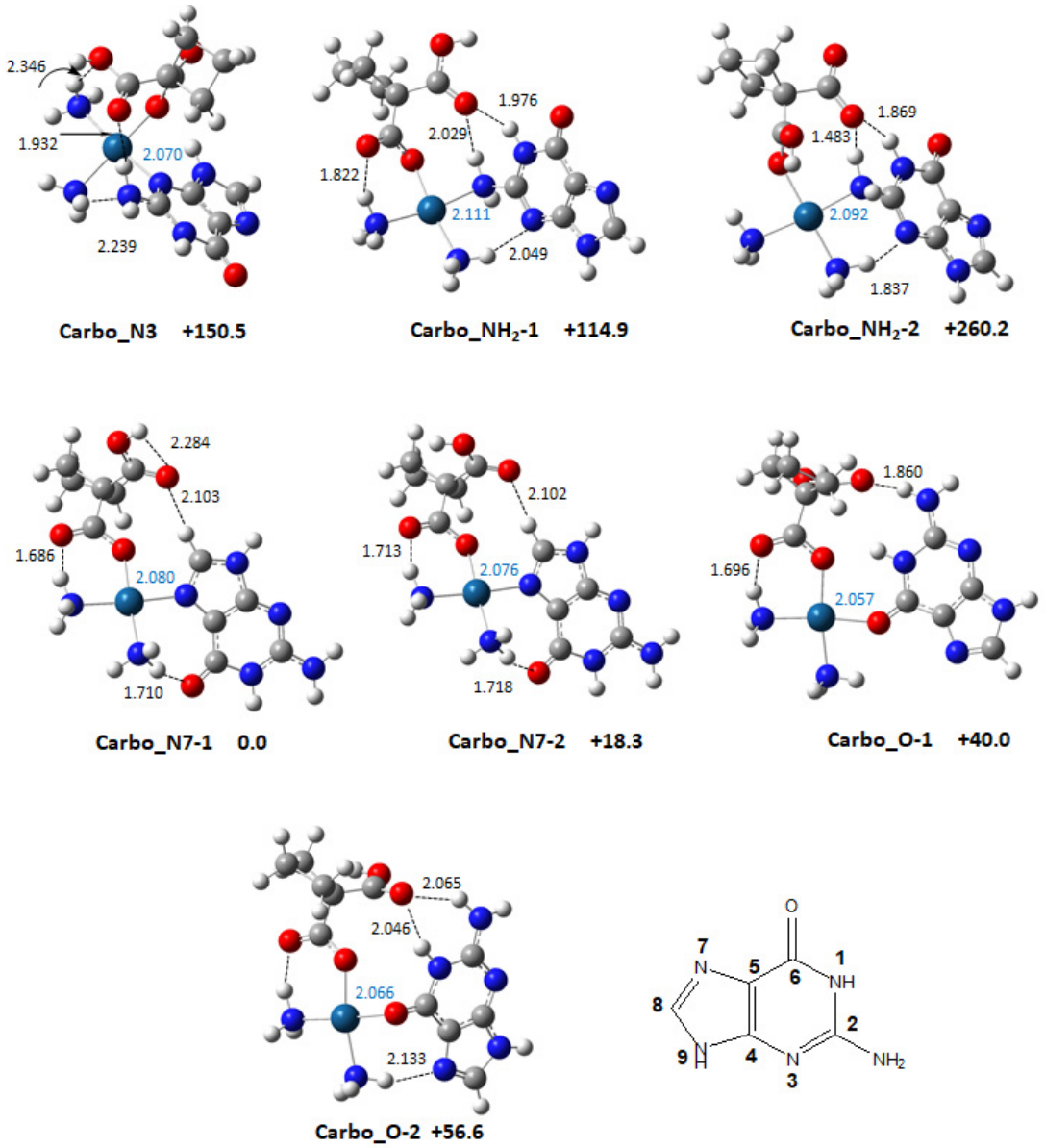

Figure 2. Representative structures computed for the $[CarboPt+H+G]^+$ complex. Bond lengths are in Angströms, relative free energies in kJ mol^{-1}.

First, a square planar coordination scheme is systematically observed around platinum. One can also note that the guanine amino group is the less favorable binding site. One of the key results of this computational survey is that interaction of Pt with COO is systematically preferred over interaction with COOH, regardless of guanine binding site. This is illustrated for example by the comparison between the two forms **Carbo_NH_2-1** and **Carbo_NH_2-2**.

Examination of Figure 2 also indicates that the N7 position of guanine is the preferred platination target. This finding is not surprising given the previous results reported in the literature[8, 31], and it is similar to what we determined in the gas phase with cisplatin.[10e] The most stable form, **Carbo_N7-1,** is characterized by an interaction with N7 together with several stabilizing weak contacts, as already observed for the [CarboPt+H_2O+G] complex[31]. One may notice: i) an interaction between the hydrogen atom on C8 and the protonated carboxylic group, ii) hydrogen bonds between the ammonia ligands and the carbonyl of G on one hand, and the malonate carboxylate on the other hand, and iii) an interaction between the OH and C=O of COOH in syn configuration. The removal of the latter interaction results in a structure (**Carbo_N7-2**) 18.3 kJ mol^{-1} less stable than the global minimum. When G interacts with either N3 or O, several hydrogen bonds are also established within the complexes, but the resulting structures, although minima on the potential energy surface, are considerably less stable than those involving N7.

In the FT-ICR mass spectrometer, the whole isotopic cluster corresponding to the [CarboPt+H+G]$^+$ complex at *m/z* 522-526 was mass selected for subsequent IRMPD experiments. The fragmentation of this species upon irradiation by IR photons in resonance with an active vibrational mode in the fingerprint region (Figure S13) yields two product ions that were previously observed in the CID experiments, namely by loss of one (*m/z* 505-509) and two ammonia (*m/z* 498-492) molecules. This latter fragment was observed in MS^3 experiments on the ion at *m/z* 505. One can also observe two minor product ions associated with loss of NH_3 and CO_2 (cluster at *m/z* 461-465) and with the loss of G (cluster at 371-375), respectively. Formation of GH^+ is never observed upon IRMPD activation. These same photofragments are observed by IRMPD in the OPO region.

The experimental IRMPD spectrum of $[CarboPt+H+G]^+$ in the 1000–1800 cm^{-1} range is plotted in Figure 3a together with the IR spectra calculated for the species representative of different binding schemes (Figure 3b-e).

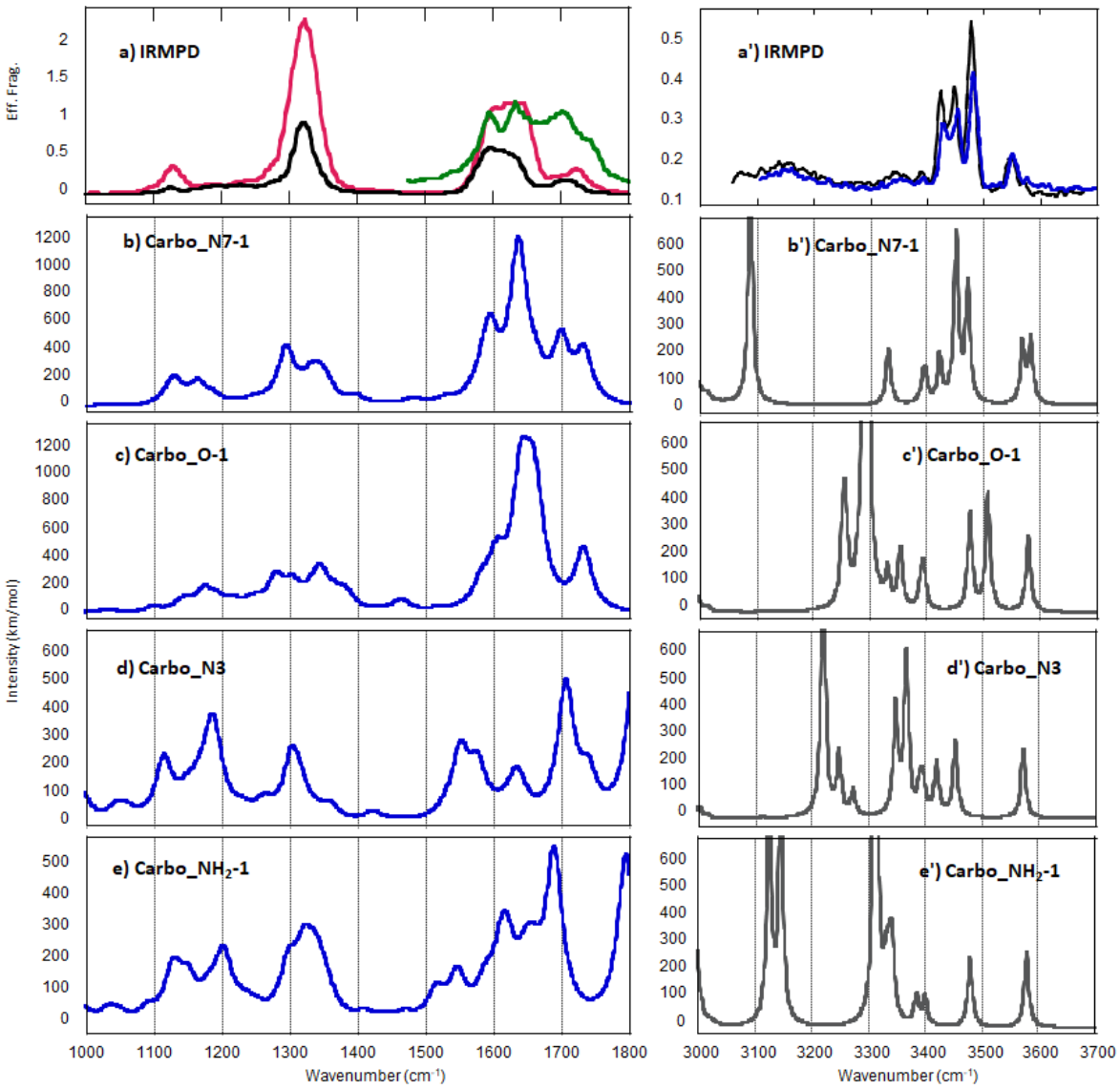

Figure 3. Experimental IRMPD spectrum of the $[CarboPt+H+G]^+$ complex (top) in both **a)** fingerprint (red trace: irradiation time 500 ms ; black trace : irradiation time 250 ms; green trace: irradiation time 500 ms, laser optimized in the 1600-1800 cm^{-1} range) and **a')** X–H region (black trace : irradiation time 1500 ms ; blue trace : irradiation time 1000 ms), compared with the computed IR spectra (**b)-e)** and **b')-e')**) of structures representative of different binding schemes and reported in Figure 2. See text for details.

The experimental trace shows two distinct features centered around 1130 and 1320 cm^{-1}, and a very broad signal spanning from 1565 to 1750 cm^{-1}, resulting from the combination of several absorptions. Comparison between panels a and b in Figure 3 shows that the experimental IRMPD spectrum is nicely reproduced by the computed spectrum of the global minimum **Carbo_N7-1**. Given this good agreement, the vibrational modes of $[CarboPt+H+G]^+$ can be interpreted as described in Table S4, which gathers both the experimental IRMPD features and the IR bands calculated for **Carbo_N7-1**. The band detected at 1130 cm^{-1} may comprise the combination of several bending modes and notably rocking of the methylene groups of the cyclobutane moiety. The very intense signal ranging between 1285 and 1355 cm^{-1} and centered at 1320 cm^{-1}, may be associated to several intense vibrational modes, and particularly the ν(C ⎓ O-Pt) and ν(C⎓ O-H) stretches (1295 cm^{-1} and 1334 cm^{-1}, respectively), the N1-H bending mode (1328 cm^{-1}), as well as the umbrella mode of both ammonia ligands (1341 cm^{-1} and 1353 cm^{-1}). Specific examination of the 1500-1800 cm^{-1} region indicates that these broad features can encompass at least four (if not more) absorptions. In this region, six particularly active vibrational modes are computed for the global minimum (Table S4): five stretches involving N3-C4, C2-N2, C=O(OPt), C=O (of G), C=O(OH) bonds, and the bending mode associated to the N-H bond engaged in the hydrogen bond with the guanine carbonyl group.

The $[CarboPt+H+G]^+$ complex has also been examined in the region from 3050 to 3700 cm^{-1}. The resulting spectrum (Figure 3a') is particularly informative with a combination of broad (~3150 and 3345 cm^{-1}) and sharp features (between 3390 and 3575 wavenumbers). Again, a reasonable agreement is observed with the spectrum computed for the global minimum **Carbo_N7-1**, especially in the region above 3300 cm^{-1} The broad band centered around 3345 cm^{-1} may be ascribed to a symmetric NH_2 stretching mode of the two ammonia ligands (computed at 3332 and 3334 cm^{-1}), whereas the computed asymmetric counterpart is consistent with the experimental band at 3390 cm^{-1}. The bands detected at 3425 and 3445 cm^{-1} may

correspond to the N1-H elongation and the symmetric NH_2 stretch of G, respectively. The most intense band at 3480 cm^{-1} is attributed to the stretch of the N9-H bond. Finally, the two bands detected at 3550 and 3575 cm^{-1} (weak) may correspond to the asymmetric NH_2 stretch of G on one hand (computed at 3570 cm^{-1}), and to the OH stretch of the COOH group (computed at 3584 cm^{-1}) on the other hand. The experimental IRMPD spectrum of $[CarboPt+H+G]^+$ shows also a broad and weak absorption around 3150 cm^{-1}. The nearest absorption computed for **Carbo_N7-1** that might account for this particular signal, is the very intense feature associated to the C8-H stretch, the proton being interacting with the carbonyl of the COOH group. Such broadening effects and low IRMPD efficiencies associated to the stretching vibrations of X-H groups involved in a hydrogen bond, have been already observed for example in the case of protonated nucleobases[32], and may find their origin in the anharmonicity of these modes.

Examination of Figures 3c-e and 3c'-e' shows that the alternate binding schemes (O, N3, NH_2) are globally less consistent with the experimental spectra. Concerning the **Carbo_O-1** form, a reasonable match is observed in the fingerprint region, but this is not the case in the OPO domain (Figure 3c'). As for the structures corresponding to the remaining binding sites, the agreement is not satisfactory. Given these discrepancies and the fact that these structures are significantly less stable than **Carbo_N7-1**, their formation during our experiments seems precluded. Finally, the comparison with the vibrational spectra computed for the **Carbo_N7-2** structure is given in the supporting information (Figure S14). At first glance, one can see that in the fingerprint region, the computed spectrum reproduces the experimental trace quite well. However, one noticeable difference is the ν(C=O(OH)) stretch computed at 1766 cm^{-1}, and therefore 33 cm^{-1} blue-shifted with respect to **Carbo_N7-1**, because of the lack of the internal hydrogen bond between C=O and OH. Therefore, in Figure S14b, this vibration does not correspond to any experimental signature, and the computed spectrum does not reproduce the absorption observed experimentally around 1740 cm^{-1}. Similarly, another consequence is the

OH stretch computed at 3625 cm^{-1} (blue-shift of 41 cm^{-1} compared to **Carbo_N7-1**), and therefore less consistent with the experimental spectrum. These findings and the relative free energy estimated for **Carbo_N7-2** (+18.3 kJ mol^{-1}) suggest that the **Carbo_N7-2** form might not be generated in the gas phase.

3.4 IRMPD spectroscopy of $[OxaliPt+H+G]^+$ complex

Concerning the computational survey of the $[OxaliPt+H+G]^+$ complex, we followed the same strategy as for the previously reported $[CarboPt+H+G]^+$ complex, by focusing on canonical guanine. Again, examination of Figure 4 shows a clear preference of the platinated agent towards the N7 position of guanine, as compared to either other interaction sites. Likewise the carboplatin case, N3 and NH_2 are the least favorable interaction sites of guanine.

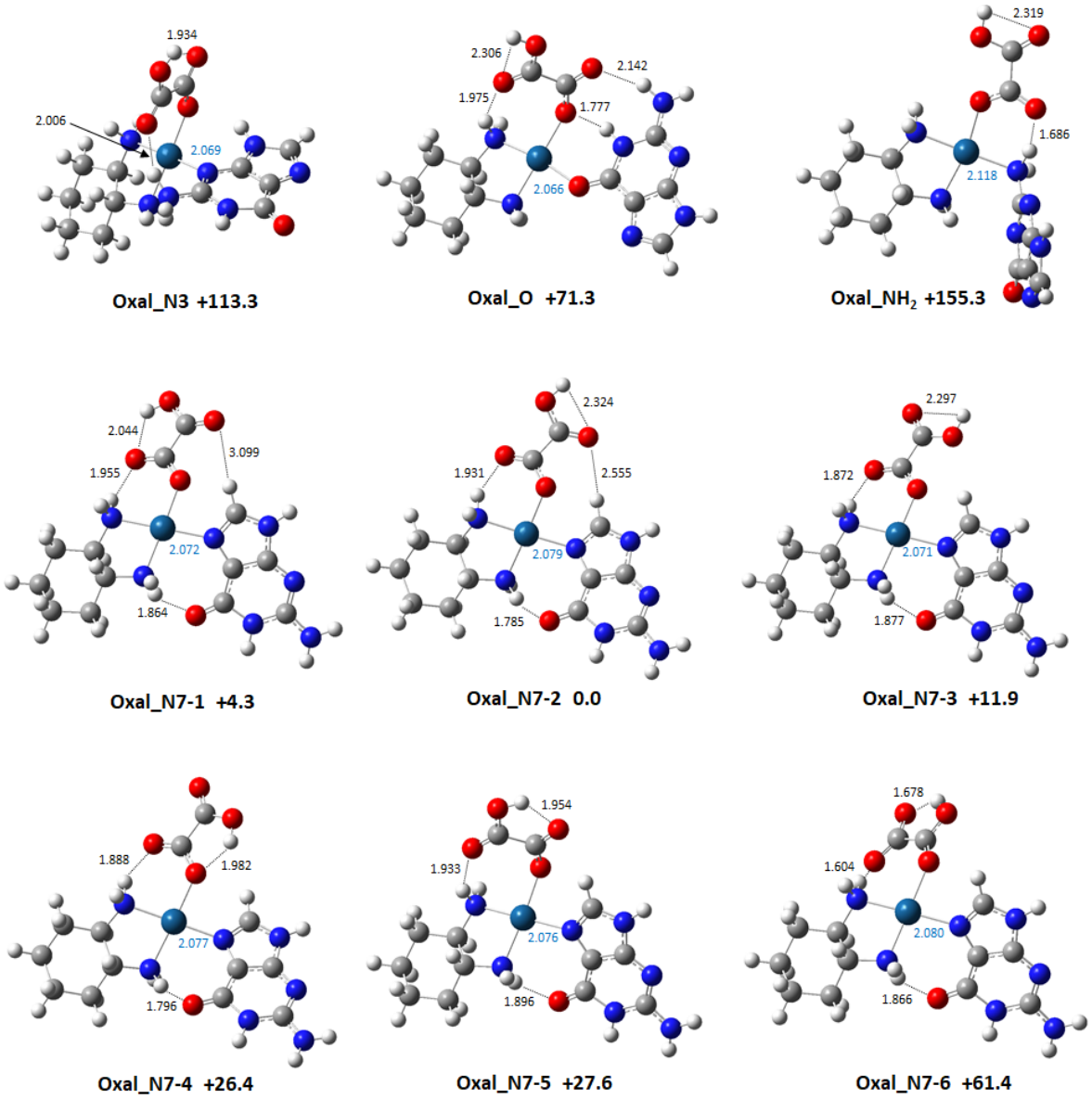

Figure 4. Representative structures computed for the [OxaliPt+H+G]$^{+}$ complex. Bond lengths are in Angströms, relative free energies in kJ mol^{-1}.

Notably, an important difference in comparison with carboplatin is the greater flexibility of the oxalate moiety once the nucleobase has interacted with the metal, which leads to a set of structures rather close in energy. This is presently illustrated in Figure 4 by six different forms involving the N7 platination, five of which lying within 28 kJ mol^{-1}. The sixth one, **Oxal_N7-6**, is much higher in free energy as it implies the coordination of Pt with COOH. Then, we can

focus on the two most stable structures, namely **Oxal_N7-1** and **Oxal_N7-2**, which are separated by only 4.3 kJ mol^{-1}. They share the same square planar organization around Pt, involving the two amino groups of the DACH moiety, interaction with the COO group of the oxalate ligand, and a monodentate interaction (N7) with G. Again, these structures also exhibit several weak stabilizing interactions, and **Oxal_N7-1** and **Oxal_N7-2** differ by the nature of the hydrogen bond established within the oxalate ligand. In the former conformer, the hydrogen bond is found between the two carboxylic groups and the oxalate ligand is planar, whereas in the latter the hydrogen bond involves only one carbonyl group, and the oxalate ligand is no longer planar (OCCO dihedral angle 31.5°) because of the establishment of an O···H-C8 interaction. Removal of this particular interaction (**Oxal_N7-3**) results in a geometry 11.9 kJ mol^{-1} less stable. In summary, given the small energy differences observed, the presence of a mixture of structures is possible.

As in the case of $[CarboPt+H+G]^+$, we recorded the photofragmentation spectrum of the $[OxaliPt+H+G]^+$ complex by selecting the whole isotopic cluster (*m/z* 548-552) and then irradiating with the CLIO FEL the selected ions by IR photons in resonance with an active vibrational mode (Figure S13). Four product ions, already observed under CID conditions, were detected. The most abundant species corresponds to loss of carbon dioxide, and the three other minor product ions are due to elimination of G, $G+CO_2$, and $C_2H_2O_4$. These four product ions were all considered to obtain the experimental IRMPD trace presented in Figure 5, presently recorded by irradiating the complex during 210 ms. Two broad features are observed, the first one between 1125 and 1210 cm^{-1} and the second one between 1250 and 1340 cm^{-1}.

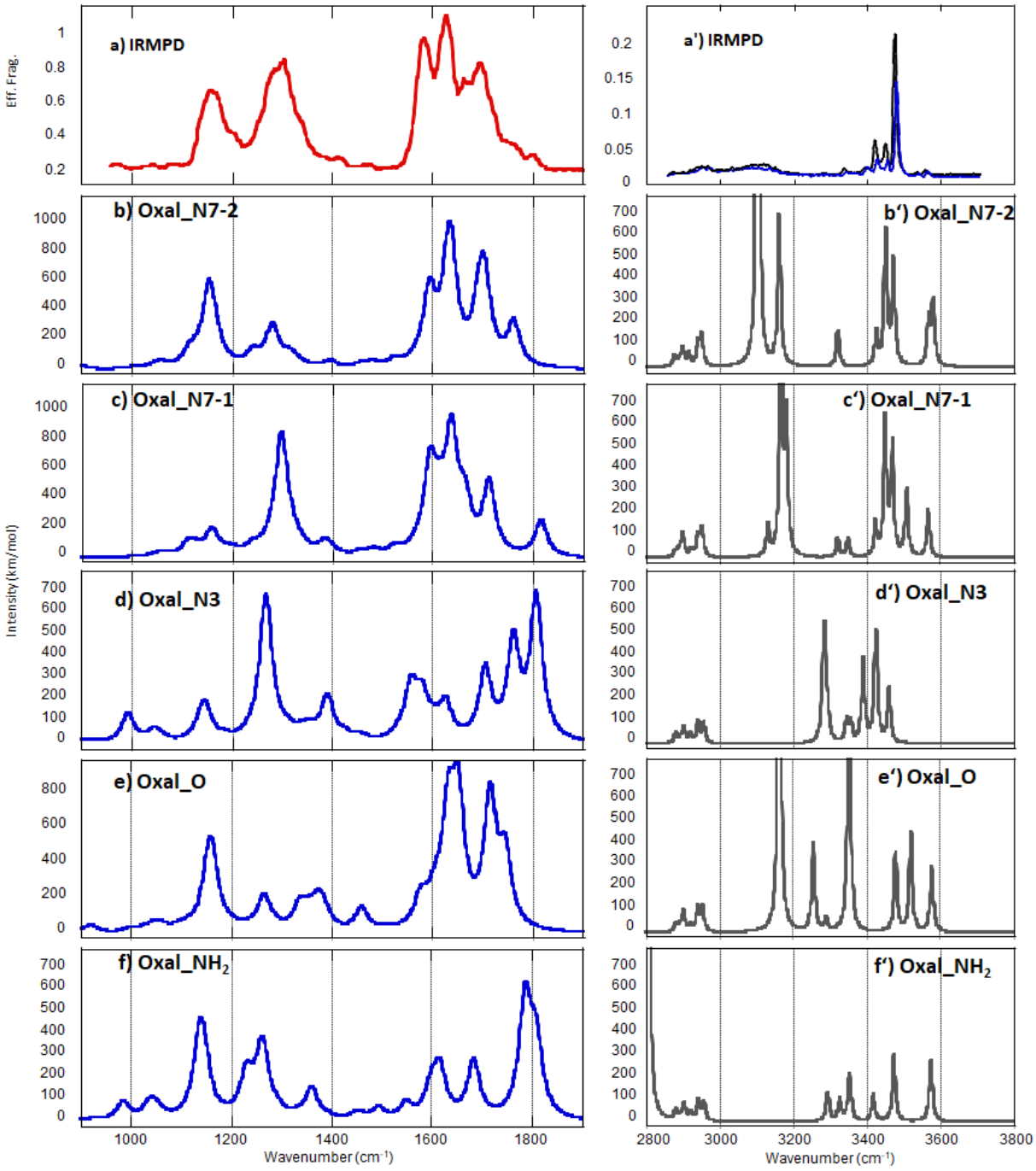

Figure 5. Experimental IRMPD spectrum of the $[OxaliPt+H+G]^+$ complex (top) in both **a)** fingerprint (irradiation time 210 ms) and **a')** X−H region (black trace : irradiation time 1500 ms ; blue trace : irradiation time 1000 ms), compared with the computed IR spectra (**b)-f)** and **b')-f')**) of structures representative of different binding schemes and reported in Figure 4. See text for details.

The region above 1550 cm^{-1} is characterized by at least three significant absorptions at about 1585, 1625, 1680, and a shoulder around 1755 cm^{-1}. Finally, two other weak signals are also observed at 1410 cm^{-1} and 1800 cm^{-1}. Comparison between panels a and b in Figure 5 shows that most of the experimental bands are nicely reproduced by the computed spectrum of the global minimum **Oxal_N7-2**. Assuming the formation of this particular structure, the experimental absorptions of the $[OxaliPt+H+G]^+$ complex can be interpreted by the computed IR modes listed in Table S5. The broad band detected around 1160 cm^{-1} may result from the contribution of several C-H of N-H bending modes of G and DACH, together with the intense OH bending mode of the protonated oxalate group. The large feature detected between 1250 and 1340 cm^{-1}, and centered around 1295 cm^{-1}, is consistent with five significant absorptions of **Oxal_N7-2**, and notably the ν(C⎓O-Pt) stretch. The weak feature at 1410 cm^{-1} may correspond to the δ(N9-H) bending mode. The intense band detected at c.a. 1585 cm^{-1} is attributed to the stretching of the N3-C4 bond, whereas the band at c.a 1625 cm^{-1} can correspond to the NH_2 scissoring of the DACH ligand, and to ν(C2N2). The C=O stretch of the carboxylate interacting with Pt, and of the guanine carbonyl, can account for the intense band observed at 1680 cm^{-1}. These two vibrations are significantly red shifted as compared to unperturbed carbonyl groups because of the establishment of hydrogen bonds with DACH amino groups. Finally, the shoulder observed around 1755 cm^{-1} can be ascribed to the remaining carbonyl group (of COOH) computed at 1762 cm^{-1}.

One can notice that the IR spectrum computed for the global minimum does not account for the small feature detected at 1800 cm^{-1}. This finding suggests that a mixture of forms could be generated for the $[OxaliPt+H+G]^+$ complex. The computed spectra of **Oxal_N7-1** and **Oxal_N7-2** are very similar, but one noticeable difference is the ν(C=O(OH)) stretching mode of **Oxal_N7-1** (1816 cm^{-1}), which is not engaged in any weak interaction, is blue-shifted by 54

cm^{-1} with respect to **Oxal_N7-2** and therefore may account for the small absorption observed at 1800 cm^{-1}. Also to be noted is that the IR spectrum computed for **Oxal_N7-1** does not reproduce the shoulder around 1755 cm^{-1}, thus reinforcing the likely presence of a mixture of two forms. The formation of **Oxal_N7-1** may also account for the very strong and broad signal centered around 1295 cm^{-1}, because a highly active mode is computed at 1302 cm^{-1} (supporting information, Table S6). Finally, examination of panels 5c-f shows that the agreement with the spectra computed for the remaining binding schemes is less satisfactory.

In summary, the data obtained in the fingerprint region suggest the formation of a mixture of at least two forms involving a monodentate interaction of the metal with the N7 position of guanine. This finding is also supported by the experimental data recorded in the 2900–3700 cm^{-1} spectral range (Figure 5a'). As in the Carboplatin case, the experimental spectrum presents a series of sharp (although sometimes weak) signals above 3300 cm^{-1}, which are presently well reproduced by assuming a mixture of **Oxal_N7-1** and **Oxal_N7-2** forms, and particularly those detected at 3418, 3445 and 3475 cm^{-1}, that can be attributed for both structures to the N1-H elongation, the symmetric NH_2 stretch of G, and the elongation of the N9-H bond, respectively (Supporting information). The weak broad band below 3000 cm^{-1} probably corresponds to the C-H stretches of the DACH ligand, whereas the broad feature around 3110 cm^{-1} may correspond to either C8-H or DACH N-H stretches, all engaged in hydrogen bonding. The signals detected at 3335 cm^{-1} and above 3500 cm^{-1} can also be ascribed to a computed vibration of either **Oxal_N7-1** or **Oxal_N7-2**. Again, the overall agreement with the computed spectra for structures arising from other interaction schemes is less satisfactory (Figures 5c'-f'). Given these discrepancies and the fact that these forms are sensibly less stable than **Oxal_N7-1/Oxal_N7-2** (> 40 kJ mol^{-1}), their formation during our experiments seems unlikely. Overall, the data obtained by scanning the two energy ranges strongly suggest a preferred interaction of protonated oxaliplatin with the N7 position of guanine. Furthermore, IRMPD data point to the

establishment of a stabilizing hydrogen bond between the pseudoequatorial amino group of the (R,R)-DACH ligand and the O6 atom of G, similar to the one observed in the crystal structure of an oxaliplatin 1,2-d(GpG) intrastrand cross-link in a DNA dodecamer duplex. [33]

Conclusions

The protonated forms of carboplatin and oxaliplatin, the second- and third-generation platinum-based anticancer drugs, generated by ESI-MS, were structurally characterized by combining IRMPD action spectroscopy and quantum-chemical calculations. Both platinum drugs result protonated on one of the two carbonyl groups of the malonato and oxalato ligand of carboplatin and oxaliplatin, respectively. This protonation causes a significant elongation of one of the Pt-O bonds with respect to the neutral form of the platinum drugs. Such evidence agrees with previous theoretical studies indicating protonation as a key step in the hydrolysis of platinum-based drugs by lowering the activation barrier associated with the ring opening process.

Subsequently, IRMPD spectroscopy was applied to structurally characterize the $[CarboPt+H+G]^+$ and $[OxaliPt+H+G]^+$ complexes, generated in solution and isolated in the mass spectrometer. Comparisons between experimental and calculated IR spectra showed that in both complexes the platinum atom binds directly and exclusively to the N7 position of guanine, as previously observed for cisplatin. In these complexes protonation is directed on carboplatin or oxaliplatin moiety and the platinum maintains the square planar geometry of the neutral drug as guanine replaces the protonated carbonyl group of the malonato or oxalato ligand. These geometries confirm the key role played by protonation in the hydrolysis reaction mechanism of carboplatin and oxaliplatin. Any relevant contribution of isomers, characterized by different coordination schemes between guanine and platinum, can be excluded. The

interaction mechanism therefore differs from that occurring with cisplatin, which is promoted by dechlorination.

Furthermore, the MS^2 spectra of both $[CarboPt+H+G]^+$ and $[OxaliPt+H+G]^+$ complexes display a product ion due to the loss of neutral guanine yielding the respective protonated Pt-drug. Further CID experiments at variable energies performed on both $[CarboPt+H+G]^+$ and $[OxaliPt+H+G]^+$ complexes found a significantly higher value of the phenomenological threshold energy for the appearance of protonated oxaliplatin compared to protonated carboplatin ion. This trend is indicative of a stronger Pt-G bonding in the $[OxaliPt+H+G]^+$ than in $[CarboPt+H+G]^+$. These findings are in agreement with the lower drug resistance observed in the oxaliplatin therapy respect to carboplatin treatment. The second part of this study, dedicated to the interaction with adenine, is under preparation and will report a very different behavior of the two purine bases in presence of these two Pt drugs.

The present results confirm IRMPD spectroscopy combined with DFT calculation and CID experiment as a powerful tool to elucidate the intrinsic interaction occurring between platinum agent and DNA nucleotide. As these studies have shown themselves on several occasions to be in agreement with the observations made in the condensed phase, they could be used to predict the coordination chemistry of potential new drugs with their final target.

Acknowledgements

The authors wish to thank the CLIO team (P Maître, J. M. Ortega, E. Loire, N. Jestin) for their support during the experiments. Financial support from the IR INFRANALYTICS FR2054 for conducting the research is gratefully acknowledged. Financial support has been provided by Sapienza Università di Roma (Progetti medi Ateneo 2022, grant number RM12218167307356 and Progetti Medi attrezzature scientifiche 2019, grant number MA31916B7482CC6E) and by the European Union (Project IC15-014 entitled ‘Interaction of carboplatin and oxaliplatin with

nucleic acids: an approach by IRMPD spectroscopy'). J-Y.S. is grateful to the computational centre of the Universidad Autónoma de Madrid for computing facilities.

Supporting Information Available

Detailed experimental mass spectra, CID, photofragmentation and IRMPD spectra of ions under examination; tables with experimental and computed vibrational bands for relevant structures of $[OxaliPt+H]^+$, $[CarboPt+H]^+$, $[OxaliPt+H+G]^+$, $[CarboPt+H+G]^+$ ions, as well as the cartesian coordinates of all the computed structures and complete ref. 21, are gathered into a supporting information.

Bibliography

(1) Platinum and Other Metal Coordination Compounds in Cancer Chemotherapy. In *Platinum and Other Metal Coordination Compounds in Cancer Chemotherapy*, Howell, S. B. Ed.; Plenum Press, 1996.

(2) (a) Jamieson, E. R.; Lippard, S. J. Structure, Recognition, and Processing of Cisplatin-DNA Adducts. *Chem. Rev.* **1999**, *99*, 2467-2498. (b) Boulikas, T.; Pantos, A.; Bellis, E.; Christofis, P. Designing platinum compounds in cancer structures and mechanisms. *Cancer Ther.* **2007**, *5*, 537-583.

(3) (a) Sherman, S. E.; Lippard, S. J. Structural aspects of platinum anticancer drug interactions with DNA. *Chem. Rev.* **1987**, *87*, 1153-1181. (b) Bancroft, D. P.; Lepre, C. A.; Lippard, S. J. Platinum-195 NMR kinetic and mechanistic studies of cis- and trans-diamminedichloroplatinum(II) binding to DNA. *J. Am. Chem. Soc.* **1990**, *112*, 6860-6871.

(4) (a) Sherman, S. E.; Gibson, D.; Wang, A. H.; Lippard, S. J. X-ray structure of the major adduct of the anticancer drug cisplatin with DNA: cis-[$Pt(NH_3)_2$(d(pGpG))]. *Science* **1985**, *230*, 412-417. (b) Sherman, S. E.; Gibson, D.; Wang, A. H. J.; Lippard, S. J. Crystal And Molecular-Structure Of Cis-[$Pt(NH_3)_2$(d(pGpG))] The Principal Adduct Formed By Cis-Diamminedichloroplatinum(II) With Dna. *J. Am. Chem. Soc.* **1988**, *110*, 7368-7381.

(5) (a) Loehrer, P. J.; Einhorn, L. H. Drugs 5 years later - Cisplatin. *Ann. Intern. Med.* **1984**, *100*, 704-713. (b) Bokemeyer, C.; Schmoll, H. J.; Harstrick, A. SIde-effects of GM-CSF treatment in advanced testicular cancer. *Eur.J. Cancer* **1993**, *29A*, 924-924. (c) Cornelison, T. L.; Reed, E. Nephrotoxicity and hydration management for Cisplatin, Carboplatin, and Ormalaplatin. *Gynecol. Oncol.* **1993**, *50*, 147-158.

(6) Kartalou, M.; Essigmann, J. M. Mechanisms of resistance to cisplatin. *Mutat. Res.* **2001**, *478*, 23-43.

(7) (a) Frey, U.; Ranford, J. D.; Sadler, P. J. Ring-opening reactions of the anticancer drug Carboplatin - NMR characterization of Cis-[$Pt(NH_3)_2$(CBDCA-O)(5'-GMP-N_7)] in solution. *Inorg. Chem.* **1993**, *32*, 1333-1340. (b) Hay, R. W.; Miller, S. Reactions of platinum(II) anticancer drugs. Kinetics of acid hydrolysis of cis-diammine(cyclobutane-1,1-dicarboxylato)platinum(II) "Carboplatin". *Polyhedron* **1998**, *17*, 2337-2343. (c) Zhu, C. B.; Raber, J.; Eriksson, L. A. Hydrolysis process of the second generation platinum-based anticancer drug cis-amminedichlorocyclohexylamineplatinum(II). *J. Phys. Chem. B* **2005**, *109*, 12195-12205. (d) Jerremalm, E.; Wallin, I.; Ehrsson, H. New Insights Into the Biotransformation and Pharmacokinetics of Oxaliplatin. *J. Pharm. Sci.* **2009**, *98*, 3879-3885.

(8) Johnstone, T. C.; Suntharalingam, K.; Lippard, S. J. The Next Generation of Platinum Drugs: Targeted Pt(II) Agents, Nanoparticle Delivery, and Pt(IV) Prodrugs. *Chem. Rev.* **2016**, *116*, 3436-3486.

(9) (a) MacAleese, L.; Maitre, P. Infrared spectroscopy of organometallic ions in the gas phase: From model to real world complexes. *Mass Spectrom. Rev.* **2007**, *26*, 583-605. (b) Fridgen, T. D. Infrared consequence spectroscopy of gaseous protonated and metal ion cationized complexes. *Mass Spectrom. Rev.* **2009**, *28*, 586-607. (c) Polfer, N. C.; Oomens, J. Vibrational Spectroscopy Of Bare And Solvated Ionic Complexes Of Biological Relevance. *Mass Spectrom. Rev.* **2009**, *28*, 468-494. (d) Brodbelt, J. S. Photodissociation mass spectrometry: new tools for characterization of biological molecules. *Chem. Soc. Rev.* **2014**, *43*, 2757-2783. (e) Polfer, N. C.; Rodgers, M. T. Toward analytical applications of ion spectroscopy: Experiment and Theory. *Int. J. Mass Spectrom.* **2019**, *445*.

(10) (a) Gillis, E. A. L.; Fridgen, T. D. The hydrated Li^+-adenine-thymine complex by IRMPD spectroscopy in the N-H/O-H stretching region. *Int. J. Mass Spectrom.* **2010**, *297*, 2-8. (b) Rajabi, K.; Gillis, E. A. L.; Fridgen, T. D. Structures of Alkali Metal Ion-Adenine Complexes and Hydrated Complexes by IRMPD Spectroscopy and Electronic Structure Calculations. *J. Phys. Chem. A* **2010**, *114*, 3449-3456. (c) Salpin, J.-Y.; Gamiette, L.; Tortajada, J.; Besson, T.; Maitre, P. Structure of Pb(2+)/dCMP and Pb(2+)/CMP complexes as characterized by tandem mass spectrometry and IRMPD spectroscopy. *Int. J. Mass Spectrom.* **2011**, *304*, 154-164. (d) Salpin, J.-Y.; Guillaumont, S.; Ortiz, D.; Tortajada, J.; Maitre, P. Direct Evidence for Tautomerization of the Uracil Moiety within the $Pb(^{2+})$/Uridine-5 '-monophosphate Complex: A Combined Tandem Mass Spectrometry and IRMPD study. *Inorg. Chem.* **2011**, *50*, 7769-7778. (e) Chiavarino, B.; Crestoni, M. E.; Fornarini, S.; Scuderi, D.; Salpin, J.-Y. Interaction of Cisplatin with Adenine and Guanine: A Combined IRMPD, MS/MS, and Theoretical Study. *J. Am. Chem. Soc.* **2013**, *135*, 1445-1455. (f) Yang, B.; Wu, R. R.; Polfer, N. C.; Berden, G.; Oomens, J.; Rodgers, M. T. IRMPD Action Spectroscopy of Alkali Metal Cation-Cytosine Complexes: Effects of Alkali Metal Cation Size on Gas Phase Conformation. *J. Am. Soc. Mass. Spectrom.* **2013**, *24*, 1523-1533. (g) Rodgers, M. T.; Nei, Y.-W.; Wu, R.; Yang, B.; Berden, G.; Oomens, J. Probing the effects of sodium cationization of the local structure of DNA and RNA via IRMPD studies of the DNA and RNA mononucleotides. *Abstr. Pap. Am. Chem. Soc.* **2014**, *248*. (h) Salpin, J.-Y.; Haldys, V.; Guillaumont, S.; Tortajada, J.; Hurtado, M.; Lamsabhi, A. M. Gas-Phase Interactions between Lead(II) Ions and Cytosine: Tandem Mass Spectrometry and Infrared Multiple-Photon Dissociation Spectroscopy Study. *ChemPhysChem* **2014**, *15*, 2959-2971. (i) Salpin, J.-Y.; MacAleese, L.; Chirot, F.; Dugourd, P. Structure of the Pb^{2+}-deprotonated dGMP complex in the gas phase: a combined MS-MS/IRMPD spectroscopy/ion mobility study. *Phys. Chem. Chem. Phys.* **2014**, *16*, 14127-14138. (j) Chiavarino, B.; Crestoni, M. E.; Fornarini, S.; Scuderi, D.; Salpin, J.-Y. Interaction of Cisplatin with 5 '-dGMP: A Combined IRMPD and Theoretical Study. *Inorg. Chem.* **2015**, *54*, 3513-3522. (k) Kaczan, C. M.; Rathur, A. I.; Wu, R. R.; Chen, Y.; Austin, C. A.; Berden, G.; Oomens, J.; Rodgers, M. T. Infrared multiple photon dissociation action spectroscopy of sodium cationized halouracils: Effects of sodium cationization and halogenation on gas-phase conformation. *Int. J. Mass Spectrom.* **2015**, *378*, 76-85. (l) Gao, J.; Berden, G.; Rodgers, M. T.; Oomens, J. Interaction of Cu^+ with cytosine and formation of i-motif-like C-M^+-C complexes: alkali versus coinage metals. *Phys. Chem. Chem. Phys.* **2016**, *18*, 7269-7277. (m) Chiavarino, B.; Crestoni, M. E.; Fornarini, S.; Scuderi, D.; Salpin, J.-Y. Undervalued N3 Coordination Revealed in the Cisplatin Complex with 2 '-Deoxyadenosine-5 '-monophosphate by a Combined IRMPD and Theoretical Study. *Inorg. Chem.* **2017**, *56*, 8793-8801, Article. (n) Power, B.; Rowe, S.; Fridgen, T. D. Ammoniated Complexes of Uracil and Transition Metal Ions: Structures of $M(Ura-H)(Ura)(NH_3)^{(+)}$ by IRMPD Spectroscopy and Computational Methods (M = Fe, Co, Ni, Cu, Zn, Cd). *J. Phys. Chem. B* **2017**, *121*, 58-65. (o) Power, B.; Haldys, V.; Salpin, J.-Y.; Fridgen, T. D. Structures of $[M(Ura-H)(Ura)]^+$ and $[M(Ura-H)(H_2O)n]^+$ (M = Cu, Zn, Pb; n=1-3) complexes in the gas phase by IRMPD spectroscopy in the fingerprint region and theoretical studies. *Int. J. Mass Spectrom.* **2018**, *429*, 56-65. (p) Salpin, J.-Y.; Haldys, V.; Latrous, L.; Guillemin, J.-C.; Tortajada, J.; Leon, E.; Mo, O.; Yanez, M.; Merced Montero-Campillo, M. Alkylation of uracil and thymine in the gas phase through interaction with alkylmercury compounds. *Int. J. Mass Spectrom.* **2019**, *436*, 153-165. (q) Corinti, D.; Crestoni, M. E.; Chiavarino, B.; Fornarini, S.; Scuderi, D.; Salpin, J.-Y. Insights into Cisplatin Binding to Uracil and Thiouracils from IRMPD Spectroscopy and Tandem Mass Spectrometry. *J. Am. Soc. Mass. Spectrom.* **2020**, *31*, 946-960. (r) Cruz-Ortiz, A. F.; Taccone, M. I.; Maitre, P.; Rossa, M.; Pino, G. A. On the Interaction between Deprotonated Cytosine $[C(-H)]^{(-)}$ and Ba^{2+}: Infrared Multiphoton Spectroscopy and Dynamics. *ChemPhysChem* **2020**, *21*, 2571-2582. (s) Cruz-Ortiz, A. F.; Molina, F. L.; Maitre, P.; Pino, G. A. Guanine Tautomerism in Ionic Complexes with Ag^+ Investigated by IRMPD Spectroscopy and Mass Spectrometry. *J. Phys. Chem. B* **2021**, *125*, 7137-7146.

(11) Bakker, J. M.; Besson, T.; Lemaire, J.; Scuderi, D.; Maitre, P. Gas-Phase Structure of a π-Allyl-Palladium Complex: Efficient Infrared Spectroscopy in a 7 T Fourier Transform Mass Spectrometer. *J. Phys. Chem. A* **2007**, *111*, 13415-13424.

(12) (a) Sinha, R. K.; Maitre, P.; Piccirillo, S.; Chiavarino, B.; Crestoni, M. E.; Fornarini, S. Cysteine radical cation: A distonic structure probed by gas phase IR spectroscopy. *Phys. Chem. Chem. Phys.* **2010**, *12*, 9794-9800, Article. (b) Chiavarino, B.; Crestoni, M. E.; Fornarini, S.; Taioli, S.; Mancini, I.; Tosi, P. Infrared spectroscopy of copper-resveratrol complexes: A joint experimental and theoretical study. *J. Chem. Phys.* **2012**, *137*, 024307.

(13) Chernushevich, I. V.; Loboda, A. V.; Thomson, B. A. An introduction to quadrupole-time-of-flight mass spectrometry. *J. Mass Spectrom.* **2001**, *36*, 849-865.

(14) Hopfgartner, G.; Varesio, E.; Tschäppät, V.; Grivet, C.; Bourgogne, E.; Leuthold, L. A. Triple quadrupole linear ion trap mass spectrometer for the analysis of small molecules and macromolecules. *J. Mass Spectrom.* **2004**, *39*, 845-855.

(15) (a) Zocher, E.; Sigrist, R.; Chen, P. Threshold CID investigation of isomeric Cu(I) azabox complexes. *Inorg. Chem.* **2007**, *46*, 11366-11370. (b) Schröder, D.; Schwarz, H.; Aliaga-Alcalde, N.; Neese, F. Fragmentation of the (cyclam-acetato)iron azide cation in the gas phase. *Eur. J. Inorg. Chem.* **2007**, 816-821. (c) Armentrout, P. B. Guided ion beam studies of transition metal-ligand thermochemistry. *Int. J. Mass Spectrom.* **2003**, *227*, 289-302. (d) Armentrout, P. B.; Kickel, B. L. Organometallic Ion Chemistry. In *Organometallic Ion Chemistry*, Freiser, B. S. Ed.; Kluwer Academic Publishers, 1996.

(16) (a) Milko, P.; Roithova, J.; Schroder, D.; Lemaire, J.; Schwarz, H.; Holthausen, M. C. The phenoxy/phenol/copper cation: A minimalistic model of bonding relations in active centers of mononuclear copper enzymes. *Chem. Eur. J.* **2008**, *14*, 4318-4327. (b) Bouchoux, G.; Salpin, J.-Y.; Leblanc, D. A relationship between the kinetics and thermochemistry of proton transfer reactions in the gas phase. *Int. J. Mass Spectrom. Ion Processes* **1996**, *153*, 37-48.

(17) (a) Glotin, F.; Ortega, J. M.; Prazeres, R.; Rippon, C. Activities of the CLIO infrared facility. *Nucl. Instrum. Methods Phys. Res. B* **1998**, *144*, 8-17. (b) Lemaire, J.; Boissel, P.; Heninger, M.; Mauclaire, G.; Bellec, G.; Mestdagh, H.; Simon, A.; Le Caer, S.; Ortega, J. M.; Glotin, F.; et al. Gas Phase Infrared Spectroscopy of Selectively Prepared Ions. *Phys. Rev. Lett.* **2002**, *89*, 273002-273001.

(18) Corinti, D.; Crestoni, M. E.; Fornarini, S.; Pieper, M.; Niehaus, K.; Giampà, M. An integrated approach to study novel properties of a MALDI matrix (4-maleicanhydridoproton sponge) for MS imaging analyses. *Anal. Bioanal. Chem.* **2019**, *411*, 953-964.

(19) Prell, J. S.; O'Brien, J. T.; Williams, E. R. IRPD Spectroscopy and Ensemble Measurements: Effects of Different Data Acquisition and Analysis Methods. *J. Am. Soc. Mass. Spectrom.* **2010**, *21*, 800-809.

(20) (a) Becke, A. D. Density-functional Thermochemistry .3. the Role of Exact Exchange. *J. Chem. Phys.* **1993**, *98*, 5648-5652. (b) Lee, C.; Yang, W.; Parr, R. G. Development of the Colle-Salvetti correlation-energy formula into a functional of the electron density. *Phys. Rev. B* **1988**, *37*, 785-789.

(21) *Gaussian 16 Rev. C.01*; Wallingford, CT, 2016.

(22) (a) Halls, M. D.; Schlegel, H. B. Comparison of the performance of local, gradient-corrected, and hybrid density functional models in predicting infrared intensities. *J. Chem. Phys.* **1998**, *109*, 10587-10593. (b) Halls, M. D.; Velkovski, J.; Schlegel, H. B. Harmonic frequency scaling factors for Hartree-Fock, S-VWN, B-LYP, B3-LYP, B3-PW91 and MP2 with the Sadlej pVTZ electric property basis set. *Theor. Chem. Acc.* **2001**, *105*, 413-421.

(23) He, C. C.; Kimutai, B.; Bao, X.; Hamlow, L.; Zhu, Y.; Strobehn, S. F.; Gao, J.; Berden, G.; Oomens, J.; Chow, C. S.; et al. Evaluation of Hybrid Theoretical Approaches for Structural Determination of a

Glycine-Linked Cisplatin Derivative via Infrared Multiple Photon Dissociation (IRMPD) Action Spectroscopy. *J. Phys. Chem. A* **2015**, *119*, 10980-10987.

(24) (a) Hay, P. J.; Wadt, W. R. Abinitio Effective Core Potentials For Molecular Calculations - Potentials For The Transition-Metal Atoms Sc To Hg. *J. Chem. Phys.* **1985**, *82*, 270-283. (b) Hay, P. J.; Wadt, W. R. Abinitio Effective Core Potentials For Molecular Calculations - Potentials For K To Au Including The Outermost Core Orbitals. *J. Chem. Phys.* **1985**, *82*, 299-310. (c) Wadt, W. R.; Hay, P. J. Abinitio Effective Core Potentials For Molecular Calculations - Potentials For Main Group Elements Na To Bi. *J. Chem. Phys.* **1985**, *82*, 284-298.

(25) (a) Navarro, J. A. R.; Romero, M. A.; Salas, J. M.; Quirós, M.; El Bahraoui, J.; Molina, J. Binuclear Platinum(II) Triazolopyrimidine Bridged Complexes. Preparation, Crystal Structure, NMR Spectroscopy, and ab Initio MO Investigation on the Bonding Nature of the Pt(II)···Pt(II) Interaction in the Model Compound $\{Pt_2[NHCHN(C(CH_2)(CH_3))]_4\}$. *Inorg. Chem.* **1996**, *35*, 7829-7835. (b) Holmes, R. J.; O'Hair, R. A. J.; McFadyen, W. D. Electrospray ionization tandem mass spectrometric studies of competitive pyridine loss from platinum(II) ethylenediamine complexes by the kinetic method. *Rapid Commun. Mass Spectrom.* **2000**, *14*, 2385-2392. (c) Pazderski, L.; Toušek, J.; Sitkowski, J.; Maliňáková, K.; Kozerski, L.; Szłyk, E. Experimental and quantum-chemical studies of 1H, 13C and ^{15}N NMR coordination shifts in Au(III), Pd(II) and Pt(II) chloride complexes with picolines. *Magn. Reson. Chem.* **2009**, *47*, 228-238. (d) Yongye, A. B.; Giulianotti, M. A.; Nefzi, A.; Houghten, R. A.; Martínez-Mayorga, K. Conformational landscape of platinum(II)-tetraamine complexes: DFT and NBO studies. *J. Comput. Aided Mol. Des.* **2010**, *24*, 225-235. (e) Rajeev, R.; Sunoj, R. B. Mechanistic insights on platinum- and palladium-pincer catalyzed coupling and cyclopropanation reactions between olefins. *Dalton Trans.* **2012**, *41*, 8430-8440. (f) Vacher, A.; Barrière, F.; Camerel, F.; Bergamini, J.-F.; Roisnel, T.; Lorcy, D. Cis and trans-bis(tetrathiafulvalene-acetylide) platinum(ii) complexes: syntheses, crystal structures, and influence of the ancillary ligands on their electronic properties. *Dalton Trans.* **2013**, *42*, 383-394.

(26) (a) Wysokiński, R.; Michalska, D. The performance of different density functional methods in the calculation of molecular structures and vibrational spectra of platinum(II) antitumor drugs: cisplatin and carboplatin. *J. Comput. Chem.* **2001**, *22*, 901-912. (b) Giese, B.; Deacon, G. B.; Kuduk-Jaworska, J.; McNaughton, D. Density functional theory and surface enhanced Raman Spectroscopy characterization of novel platinum drugs. *Biopolymers* **2002**, *67*, 294-297. (c) Shoeib, T.; Sharp, B. L. Interactions of oxaliplatin with the cytoplasmic thiol containing ligand glutathione. *Metallomics* **2012**, *4*, 1308-1320. (d) Moustafa, E. M.; Camp, C. L.; Youssef, A. S.; Amleh, A.; Reid, H. J.; Sharp, B. L.; Shoeib, T. Oxaliplatin complexes with carnosine and its derivatives: in vitro cytotoxicity, mass spectrometric and computational studies with a focus on complex fragmentation. *Metallomics* **2013**, *5*, 1537-1546. (e) Moustafa, E. M.; Korany, M.; Mohamed, N. A.; Shoeib, T. Carnosine complexes and binding energies to some biologically relevant metals and platinum containing anticancer drugs. *Inorg. Chim. Acta* **2014**, *421*, 123-135.

(27) (a) Moustafa, E. M.; Ritacco, I.; Sicilia, E.; Russo, N.; Shoeib, T. Collision-induced dissociation products of the protonated dipeptide carnosine: structural elucidation, fragmentation pathways and potential energy surface analysis. *Phys. Chem. Chem. Phys.* **2015**, *17*, 12673-12682. (b) Ritacco, I.; Moustafa, E. M.; Sicilia, E.; Russo, N.; Shoeib, T. Fragmentation pathways analysis for the gas phase dissociation of protonated carnosine-oxaliplatin complexes. *Dalton Trans.* **2015**, *44*, 4455-4467. (c) Ritacco, I.; Sicilia, E.; Shoeib, T.; Korany, M.; Russo, N. Mass Spectrometric and Computational Investigation of the Protonated Carnosine-Carboplatin Complex Fragmentation. *Inorg. Chem.* **2015**, *54*, 7885-7897.

(28) Kerr, S. L.; Shoeib, T.; Sharp, B. L. A study of oxaliplatin-nucleobase interactions using ion trap electrospray mass spectrometry. *Anal. Bioanal. Chem.* **2008**, *391*, 2339-2348.

(29) Zhou, J.; Kang, Y.; Chen, L.; Wang, H.; Liu, J.; Zeng, S.; Yu, L. The Drug-Resistance Mechanisms of Five Platinum-Based Antitumor Agents. *Front. Pharmacol.* **2020**, *11*, art. 343.

(30) (a) Pavelka, M.; Lucas, M. F. A.; Russo, N. On the hydrolysis mechanism of the second-generation anticancer drug carboplatin. *Chem. Eur. J.* **2007**, *13*, 10108-10116. (b) Lucas, M. F. A.; Pavelka, M.; Alberto, M. E.; Russo, N. Neutral and Acidic Hydrolysis Reactions of the Third Generation Anticancer Drug Oxaliplatin. *J. Phys. Chem. B* **2009**, *113*, 831-838.

(31) Alberto, M. E.; Butera, V.; Russo, N. Which One among the Pt-Containing Anticancer Drugs More Easily Forms Monoadducts with G and A DNA Bases? A Comparative Study among Oxaliplatin, Nedaplatin, and Carboplatin. *Inorg. Chem.* **2011**, *50*, 6965-6971.

(32) (a) Bakker, J. M.; Sinha, R. K.; Besson, T.; Brugnara, M.; Tosi, P.; Salpin, J.-Y.; Maitre, P. Tautomerism of Uracil Probed via Infrared Spectroscopy of Singly Hydrated Protonated Uracil. *J. Phys. Chem. A* **2008**, *112*, 12393-12400. (b) Bakker, J. M.; Salpin, J.-Y.; Maitre, P. Tautomerism of cytosine probed by gas phase IR spectroscopy. *Int. J. Mass Spectrom.* **2009**, *283*, 214-221.

(33) Spingler, B.; Whittington, D. A.; Lippard, S. J. 2.4 angstrom crystal structure of an oxaliplatin 1,2-d(GpG) intrastrand cross-link in a DNA dodecamer duplex. *Inorg. Chem.* **2001**, *40*, 5596-5602.

Table of content

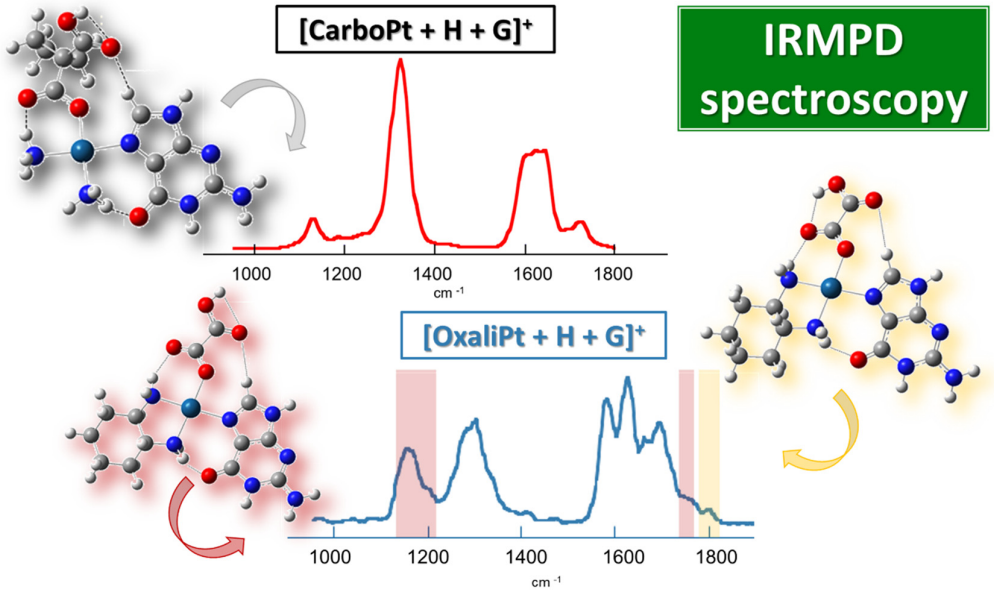

Synopsis: The structure of $[Pt\ drug + H]^+$ and $[Pt\ drug + H + guanine]^+$ complexes generated in the gas phase for the platinum drugs carboplatin and oxaliplatin, were investigated by combining collision induced dissociation (CID) experiments, infrared multiple photon dissociation spectroscopy (IRMPD) and density functional theory (DFT) calculations. Protonation of one COO group of the drugs promotes the ring opening process allowing the metallic center to interact with guanine; exclusively at its N7 position.

Binding motifs of carboplatin and oxaliplatin with guanine: a combined MS/MS, IRMPD and theoretical study

Barbara Chiavarino[1], Lucretia Rotari[1], Maria Elisa Crestoni[1], Davide Corinti[1], Simonetta Fornarini[1], Debora Scuderi[2] and Jean-Yves Salpin[3*]*

1) Dipartimento di Chimica e Tecnologie del Farmaco, Università di Roma "La Sapienza", P.le A. Moro 5, I-00185 Roma, ITALY

2) Université Paris-Saclay, CNRS, Institut de Chimie Physique, 91405, Orsay, France.

3) Université Paris-Saclay, Univ Evry, CY Cergy Paris Université, CNRS, LAMBE, 91025, Evry-Courcouronnes, France

Corresponding authors:

Dr Barbara Chiavarino
e-mail: barbara.chiavarino@uniroma1.it

Dr Jean-Yves Salpin
e-mail: jeanyves.salpin@univ-evry.fr

SUPPORTING INFORMATION: a total of 45 pages

Figure S1. Full scan positive-ion ESI mass spectrum of a 10^{-5}M water/methanol solution (1:1) of carboplatin and 5'-dGMP. The enclosed panel report the experimental (red) and theoretical (purple) isotope distribution for [CarboPt + H + G]$^+$ complex recorded in the FT-ICR MS.

.

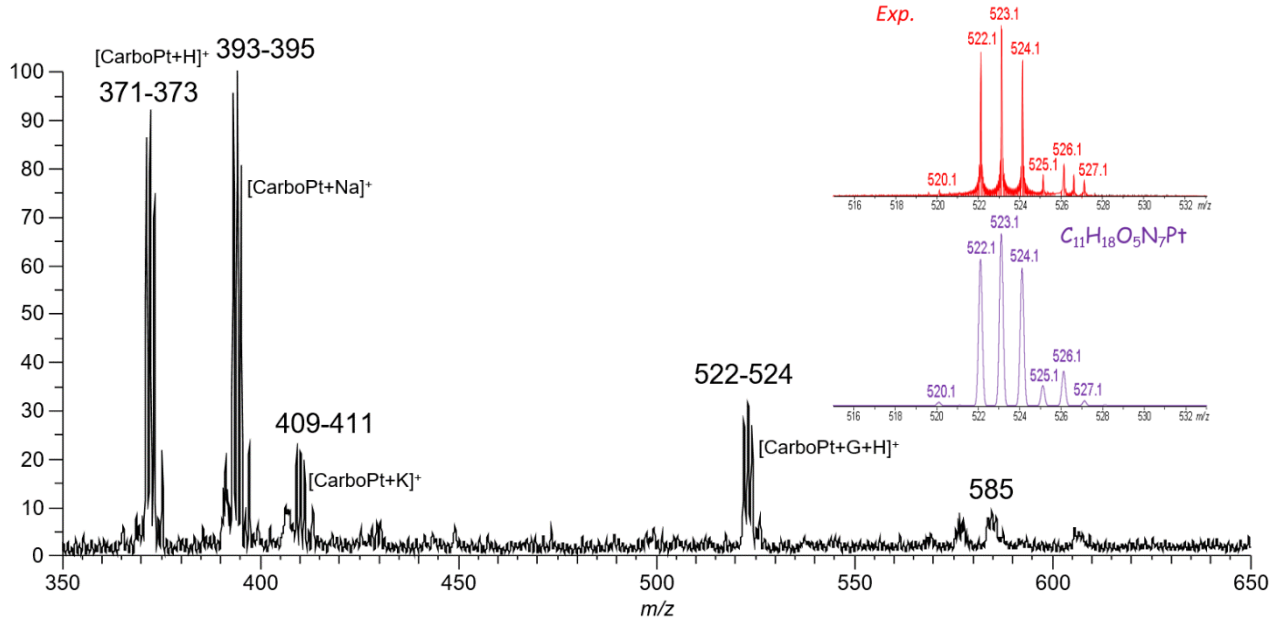

Figure S2. Full scan positive-ion ESI mass spectrum of a 10^{-5}M water/methanol (1:1) solution of oxaliplatin and 5'-dGMP.

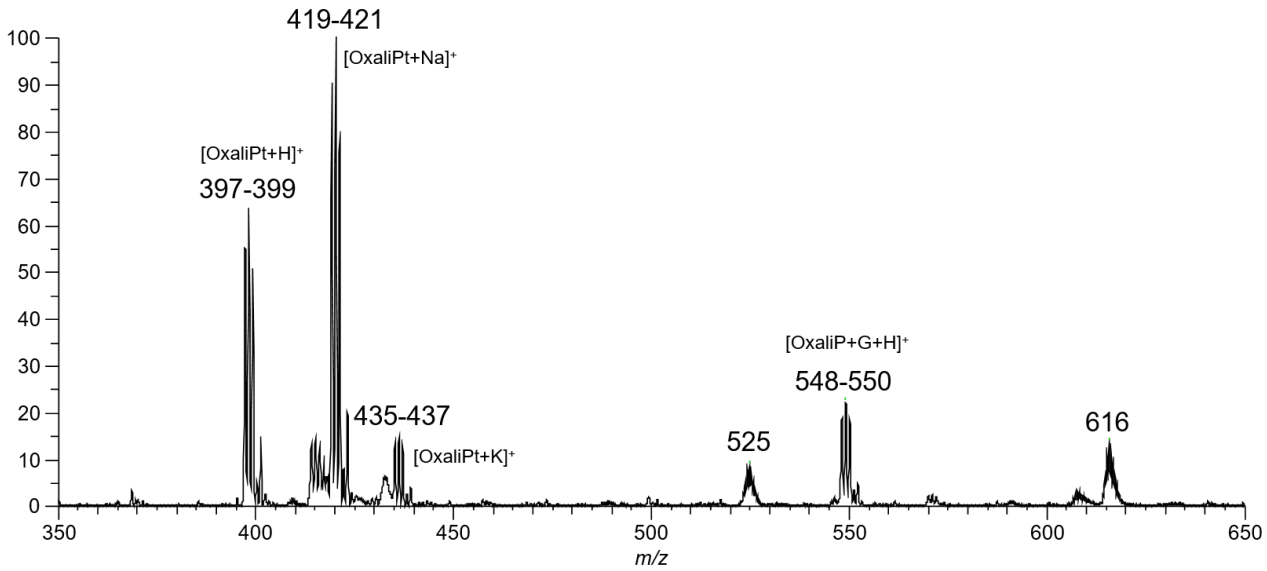

Figure S3. a) CID mass spectrum of [CarboPt + H + G]$^+$ complex ion recorded at CE 15 eV;**b)** MS^3 mass spectra of the ion at *m/z* 505 recorded at CE 13 eV; **c**) MS^3 mass spectra of the ion at *m/z* 371 recorded at CE 15 eV. N_2 is used as collision gas.

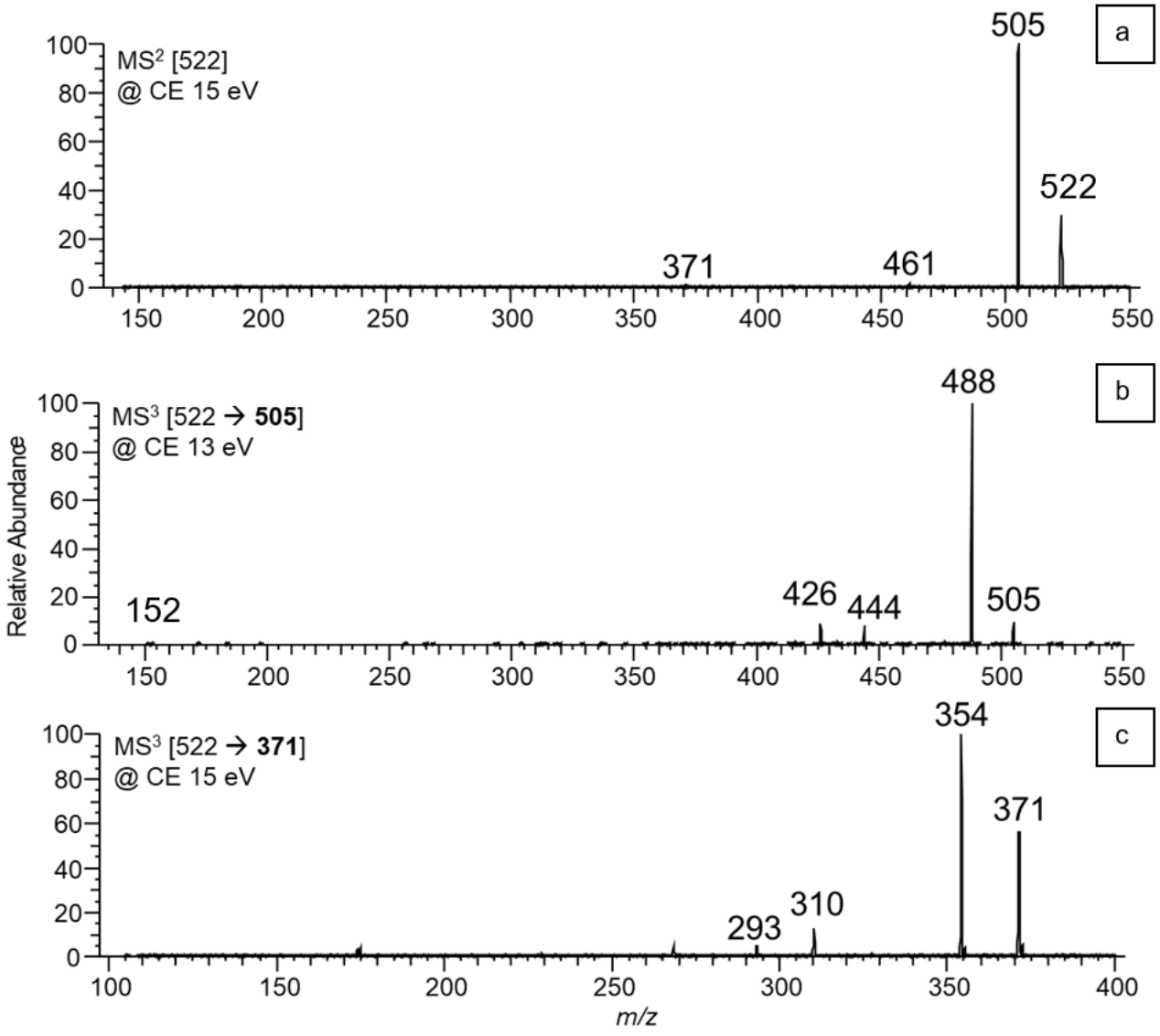

Figure S4. Fragmentation scheme for the [CarboPt + G + H]$^+$ adduct (*m/z* 522).

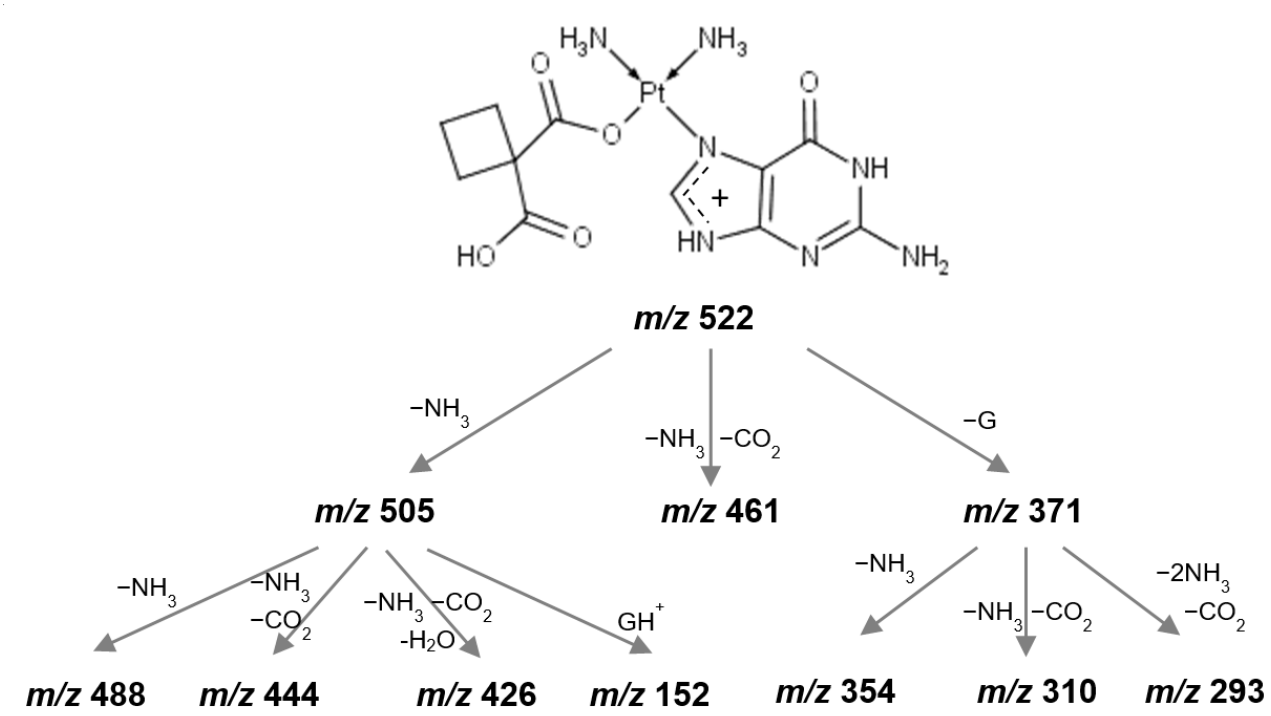

Figure S5. a) CID mass spectrum of $[OxaliPt + H + G]^+$ complex ion recorded at CE 15 eV; **b**) MS^3 mass spectra of the ion at *m/z* 504 recorded at CE 15 eV; **c**) MS^3 mass spectra of the ion at *m/z* 353 recorded at CE 20 eV; **d**) MS^3 mass spectra of the ion at *m/z* 397 recorded at CE 20 eV. N_2 is used as collision gas.

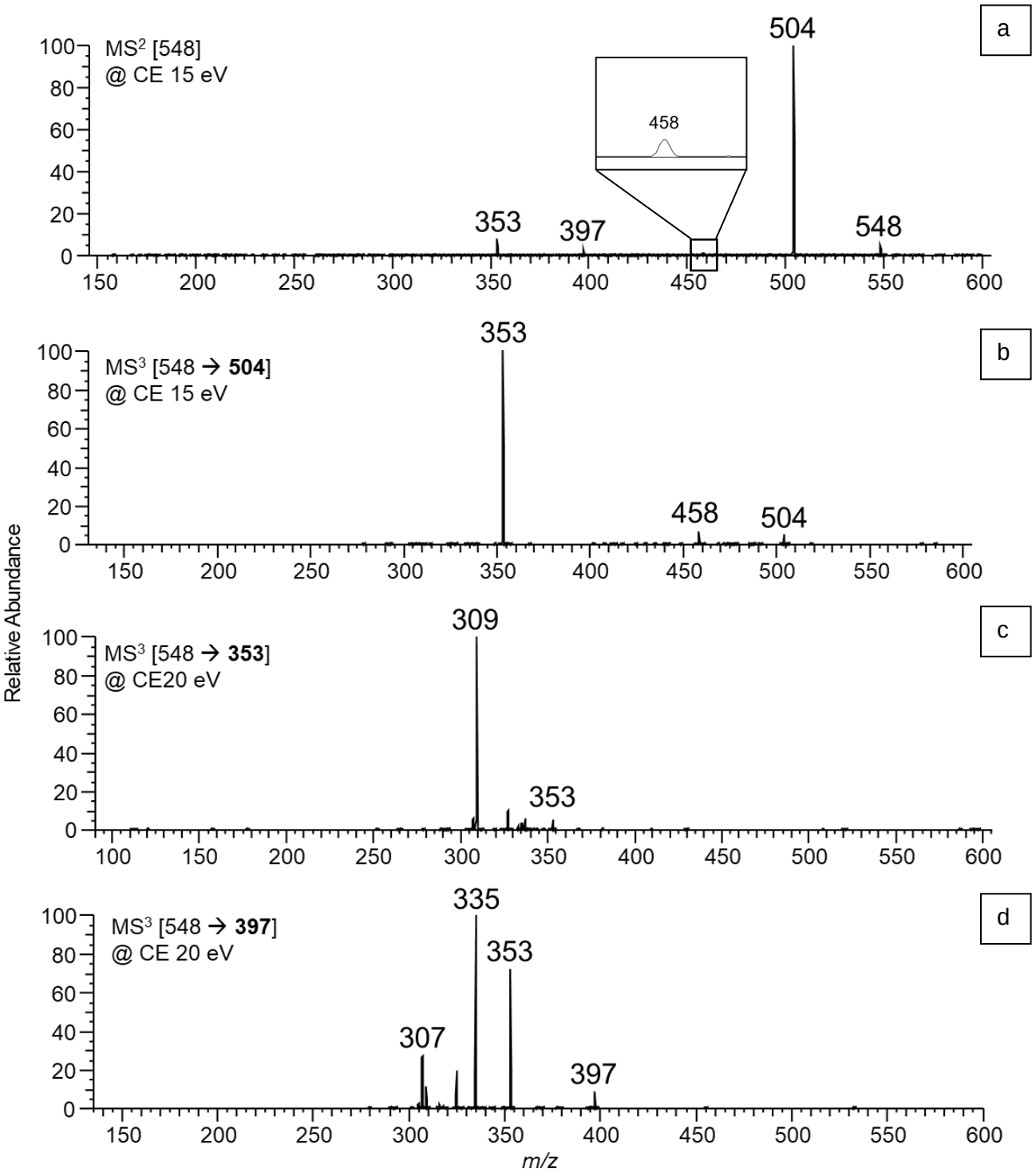

Figure S6. Fragmentation scheme for the [OxaliPt + G + H]$^+$ adduct (*m/z* 548).

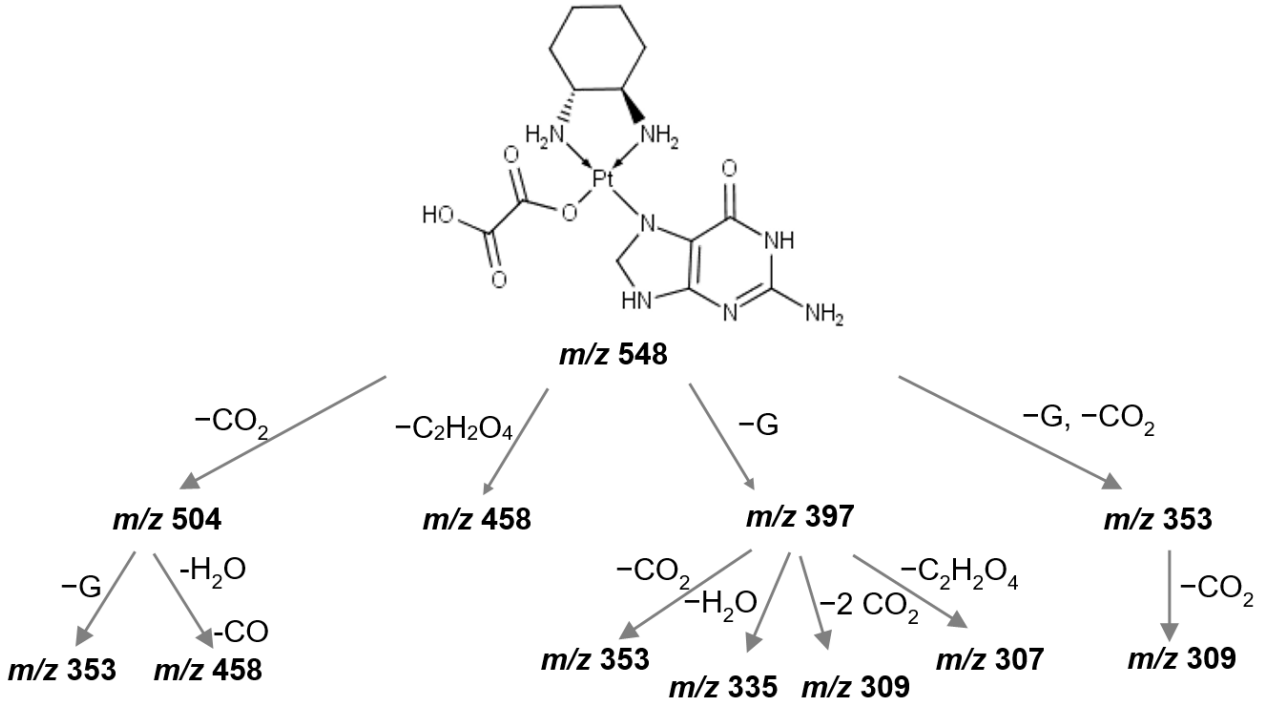

Figure S7. Relative abundance of the precursor and product ions as a function of collision energy (center of mass, E_{CM}) during CID of mass-selected [CarboPt + G + H]$^+$ (*m/z* 522) (**a**) and [OxaliPt + G + H]$^+$ (*m/z* 548) (**b**). Only ionic fragments generated by the loss of guanine are reported.

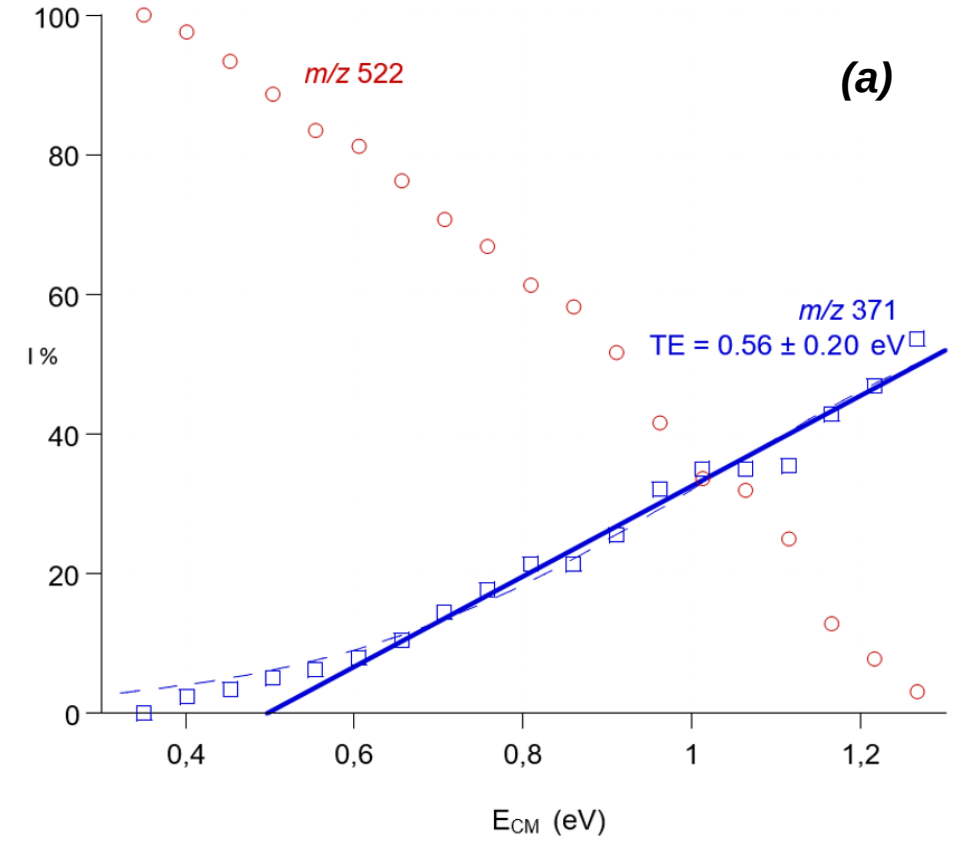

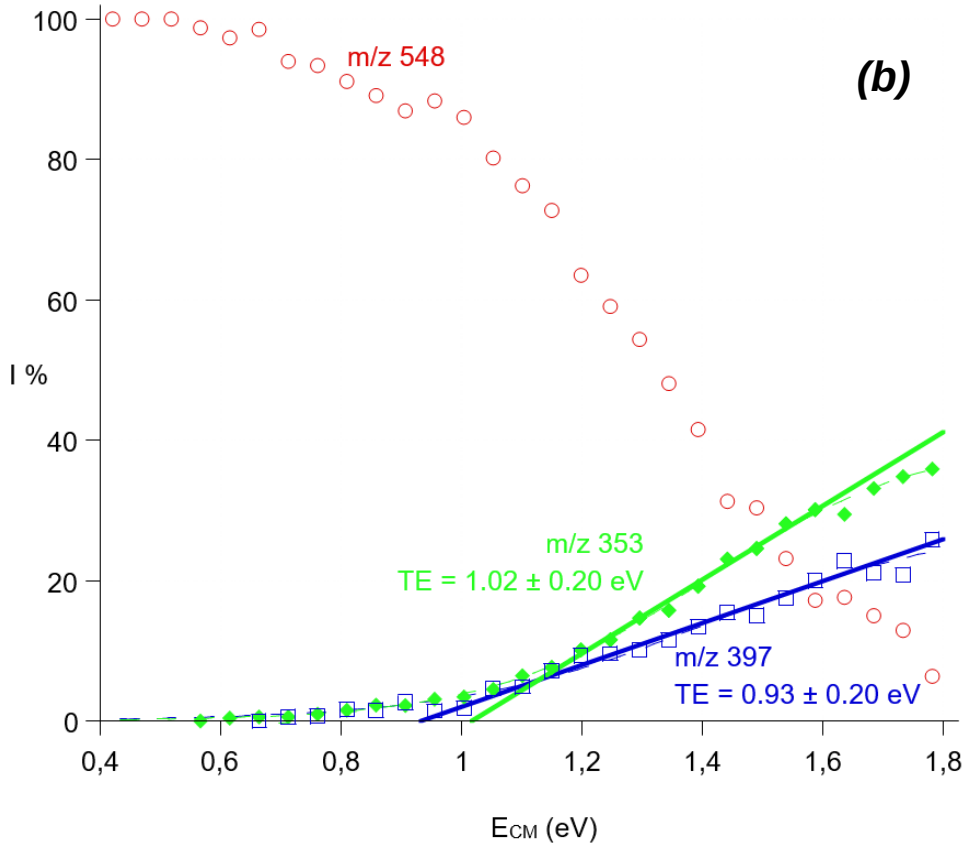

Figure S8. Full scan positive-ion ESI mass spectrum of a 10^{-5}M water/methanol (1:1) solution of Oxaliplatin and Carboplatin in the absence of the nucleobase.

Water/methanol solution of Oxaliplatin

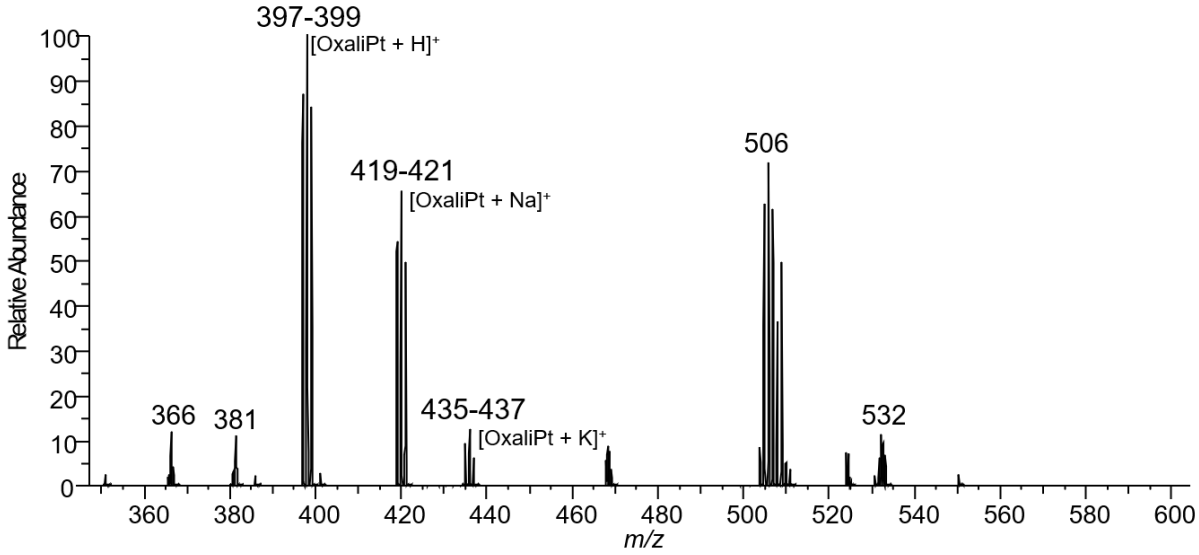

Water/methanol solution of Carboplatin

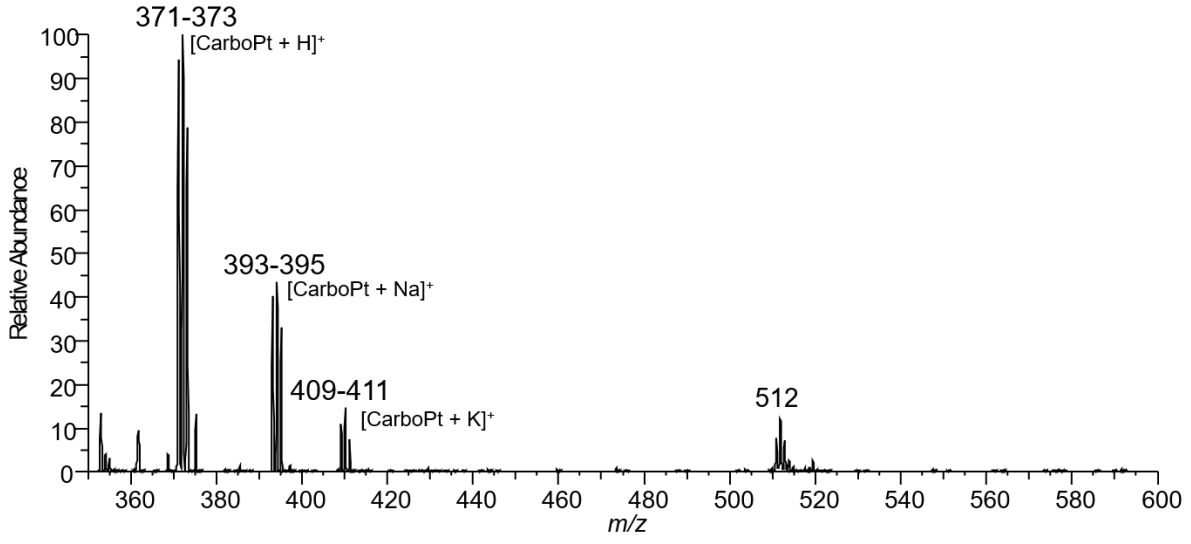

Figure S9. Photofragmentation mass spectra of $[OxaliPt + H]^+$ and $[CarboPt + H]^+$ recorded with the CLIO FEL tuned at 1250 and 1410 cm^{-1}, respectively.

$[OxaliPt + H]^+$ (isolation : *m/z* 397-399)

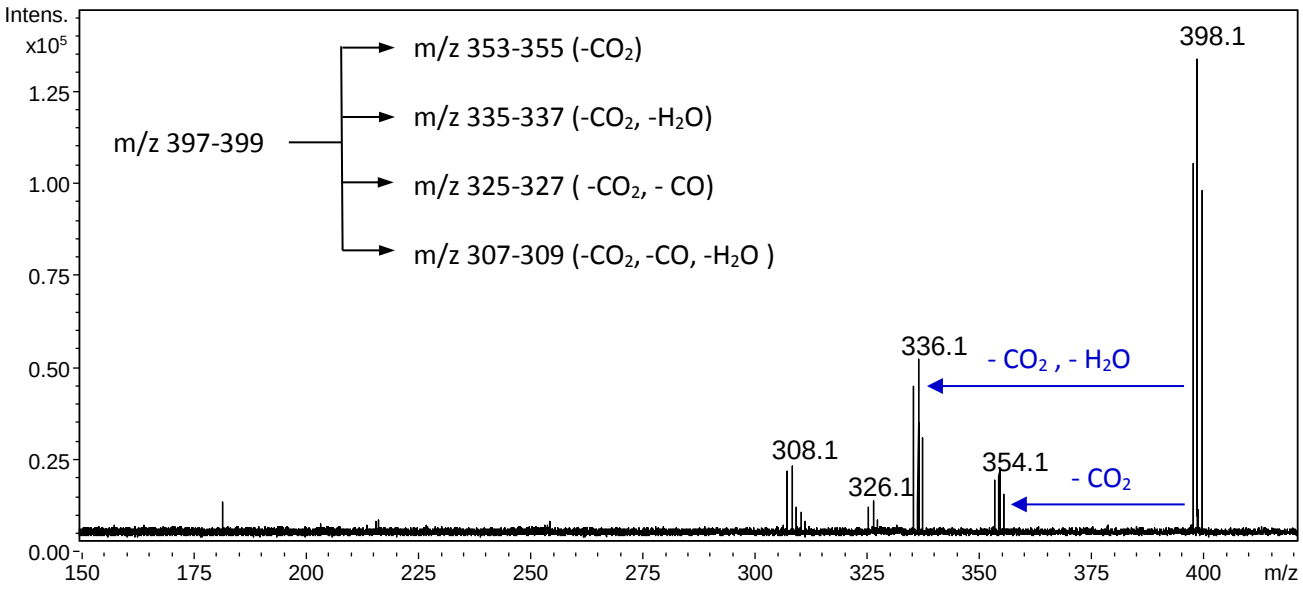

$[CarboPt + H]^+$ (isolation : *m/z* 371-375)

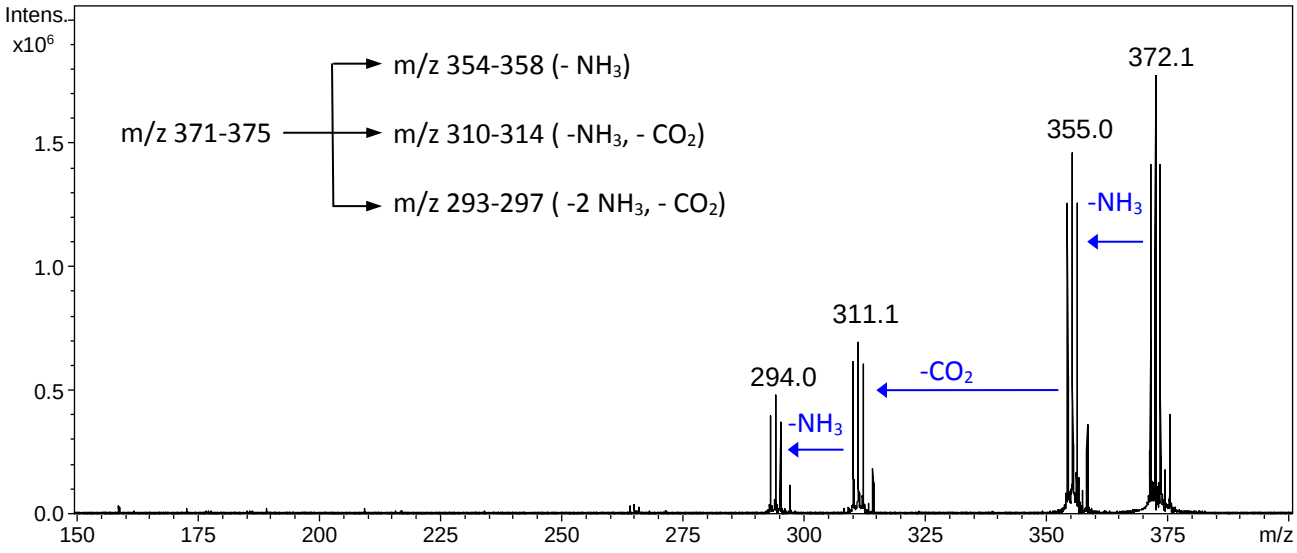

Figure S10. Structures computed for $[OxaliPt + H]^+$ and $[CarboPt + H]^+$. Bond lengths are in Angströms, relative free energies in kJ mol^{-1}.

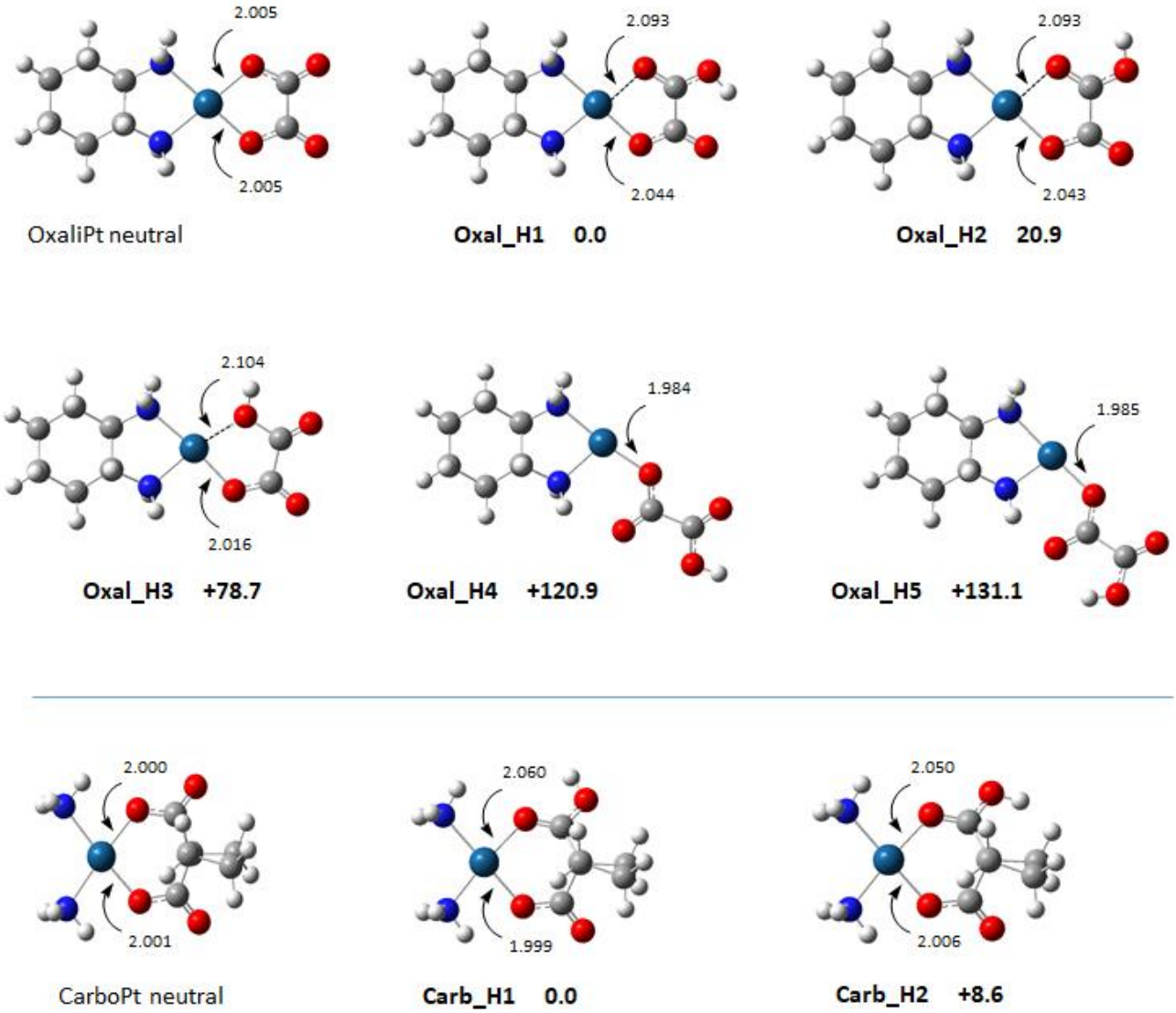

Figure S11. Experimental IRMPD spectrum of **a)** [OxaliPt + H]$^+$ and **b)** [CarboPt + H]$^+$ ions in the X-H (X = C,N,O) region, compared with the IR spectra of their two most stable computed forms at the B3LYP/6-311G** level. For [OxaliPt + H]$^+$: irradiation time 2s combined with CO_2 activation of 15ms; for [CarboPt + H]$^+$: irradiation time 4s.

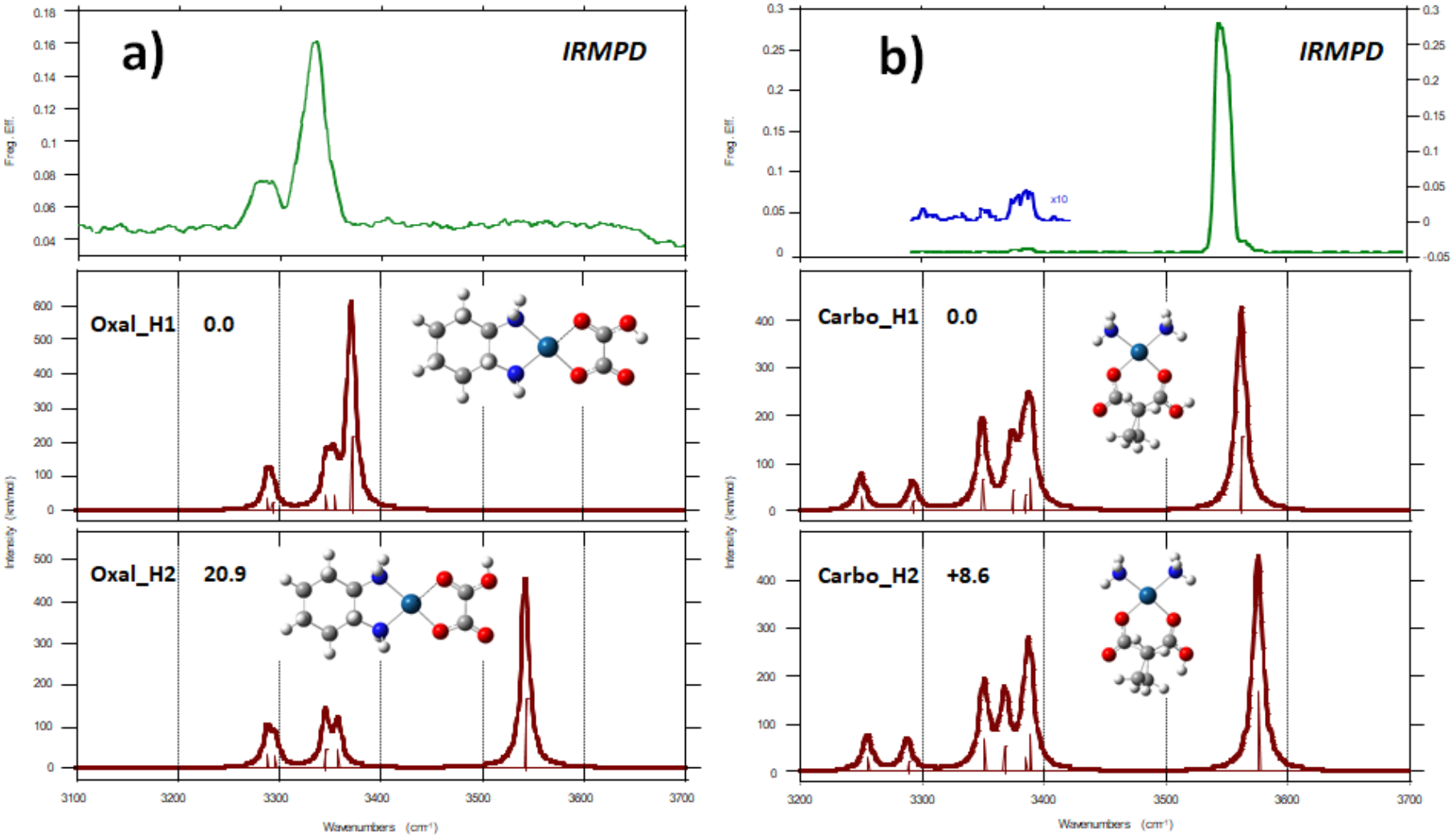

Figure S12. Experimental IRMPD spectrum of the [OxaliPt + H] $^{+}$ ion in the fingerprint region compared with the harmonic IR spectrum of **Oxal_H3** structure

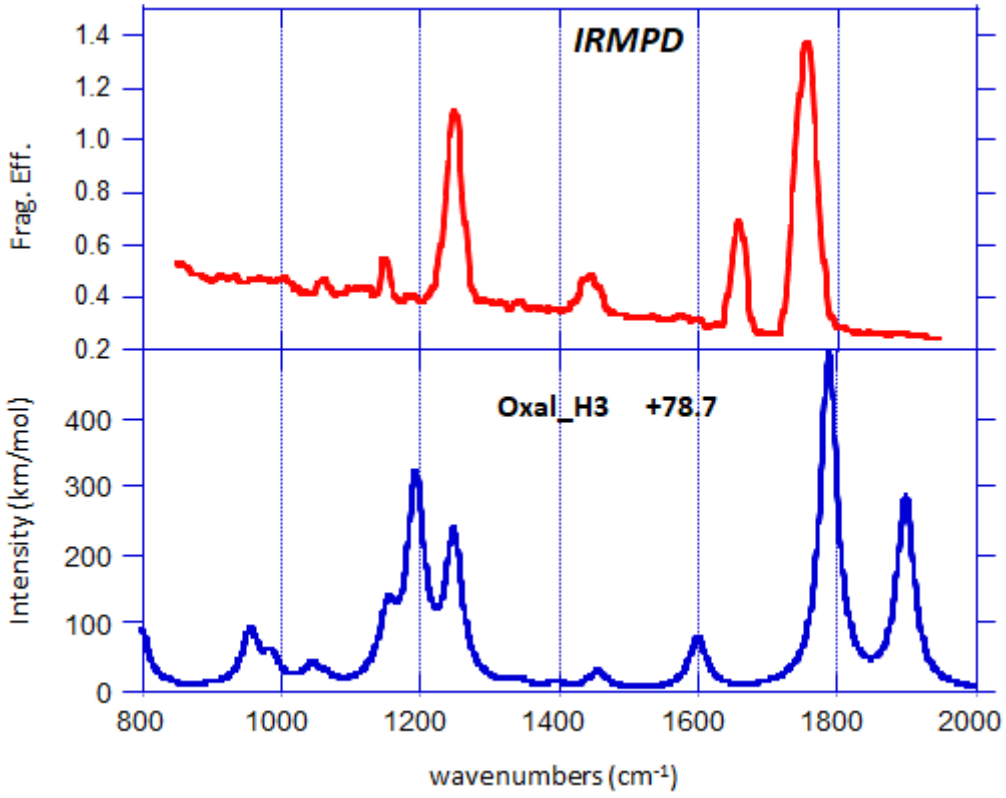

Figure S13. Photofragmentation mass spectra of $[OxaliPt + H + G]^+$ and $[CarboPt + H + G]^+$ recorded with the CLIO FEL tuned at 1248 and 1600 cm^{-1}, respectively.

$[OxaliPt + H + G]^+$ (isolation : *m/z* 548-552)

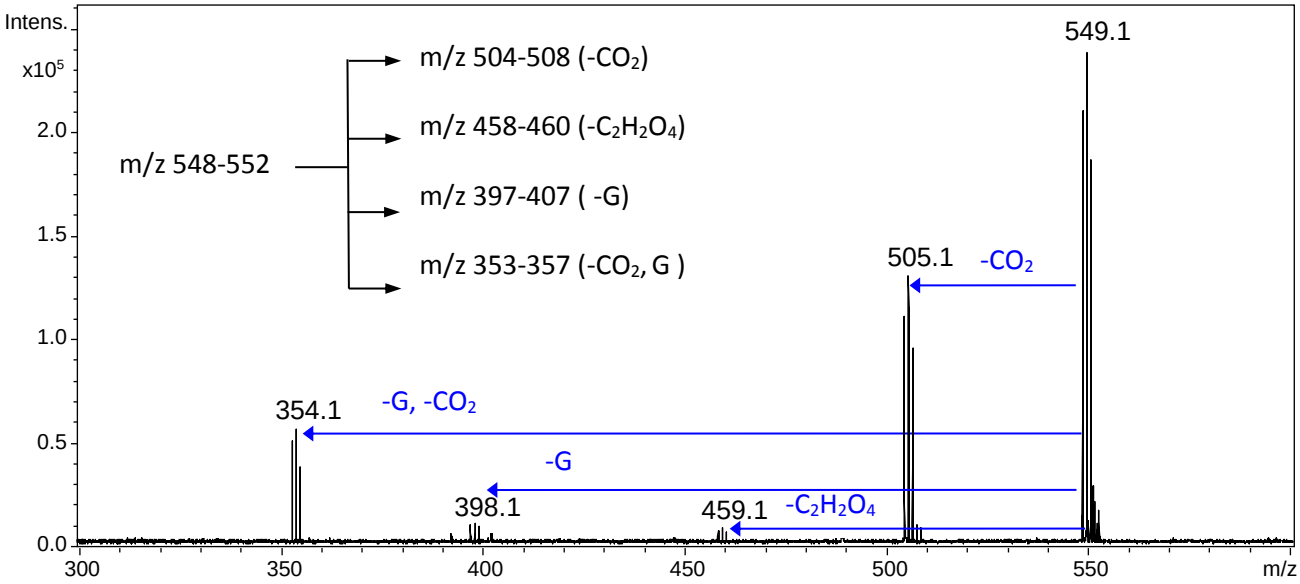

$[CarboPt + H + G]^+$ (isolation : *m/z* 522-526)

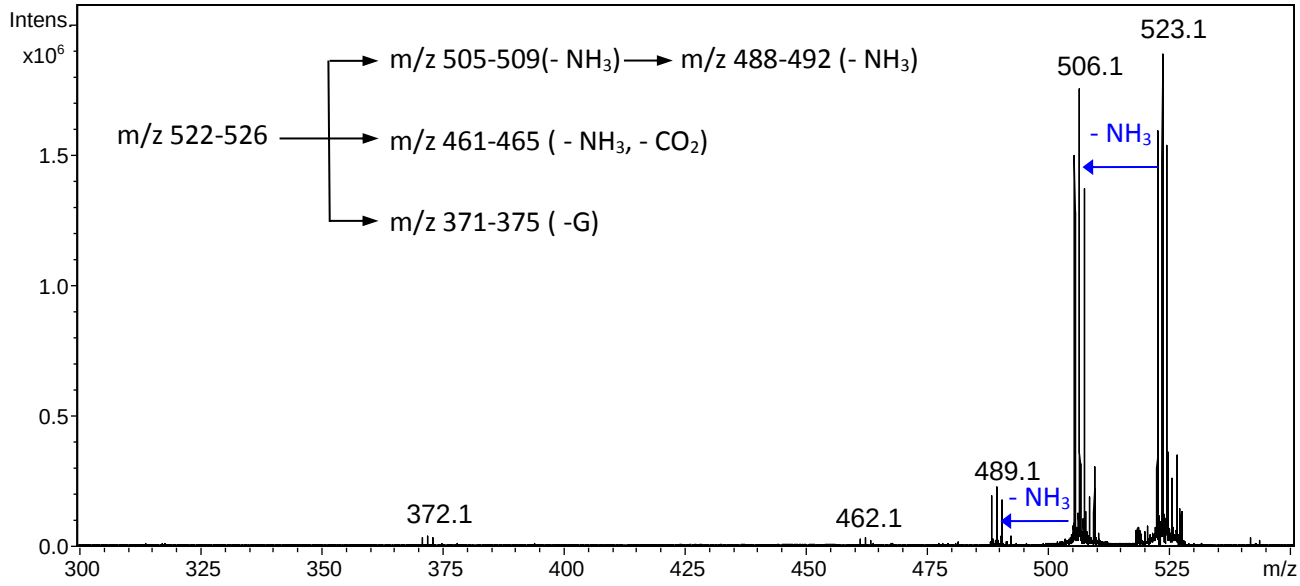

Figure S14. Experimental IRMPD spectrum of the [CarboPt + H + G]$^{+}$ complex (top) in both **a)** fingerprint (red trace: irradiation time 500 ms ; black trace : irradiation time 250 ms; green trace: irradiation time 500 ms, laser optimized in the 1600-1800 cm^{-1} range) and **a')** X−H region (black trace : irradiation time 1500 ms ; blue trace : irradiation time 1000 ms), compared with the computed IR spectra of the **Carbo_N7-2** structure.

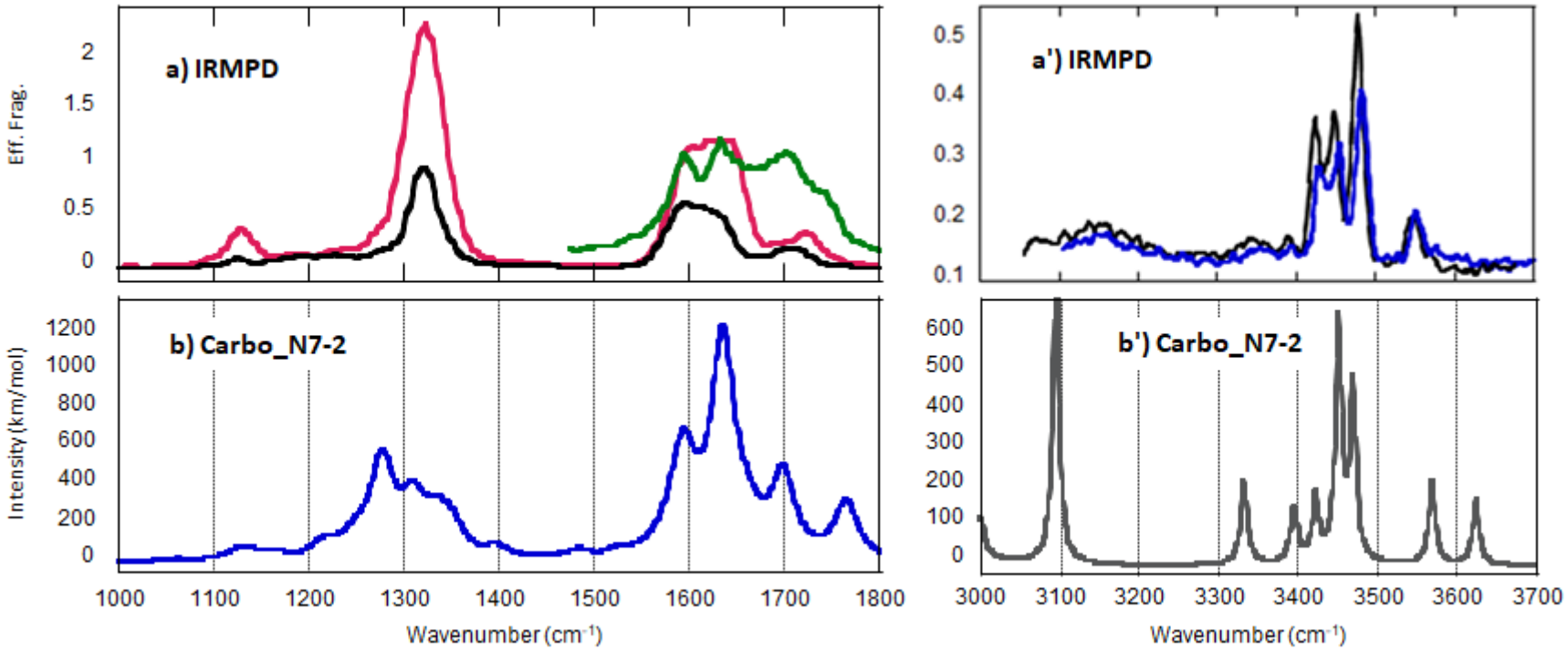

Table S1: Computational data associated with the complexes studied, obtained at the B3LYP/6-311G** level.

Structure	E+ZPE (Hartree)	ΔE (kJ mol^{-1})	H°$_{298}$ (Hartree)	ΔH°$_{298}$ (kJ mol^{-1})	G°$_{298}$ (Hartree)	ΔG°$_{298}$ (kJ mol^{-1})
[OxaliPt + H]$^+$						
Oxal_H1	-843.290645	**0.0**	-843.275249	**0.0**	-843.333149	**0.0**
Oxal_H2	-843.282395	21.7	-843.266843	22.1	-843.325187	20.9
Oxal_H3	-843.259461	81.9	-843.243457	83.5	-843.303176	78.7
Oxal_H4	-843.241844	128.1	-843.225775	129.9	-843.287087	120.9
Oxal_H5	-843.239007	135.6	-843.223048	137.1	-843.283217	131.1
[CarboPt + H]$^+$						
Carb_H1	-765.868291	**0.0**	-765.852228	**0.0**	-765.9116810	**0.0**
Carb_H2	-765.865453	7.5	-765.849481	7.2	-765.908397	8.6
[CarboPt + H + G]$^+$						
Carbo_N3	-1308.478380	143.5	-1308.452827	143.1	-1308.530475	150.5
Carbo_NH$_2$-1	-1308.491001	105.4	-1308.466155	108.1	-1308.546532	114.9
Carbo_NH$_2$-2	-1308.435448	260.3	-1308.410257	254.9	-1308.491189	260.2
Carbo_O-1	-1308.518983	34.9	-1308.493650	35.9	-1308.575074	40.0
Carbo_O-2	-1308.513624	49.0	-1308.488465	49.5	-1308.568765	56.5
Carbo_N7-1	-1308.532916	**0.0**	-1308.507335	**0.0**	-1308.590291	**0.0**
Carbo_N7-2	-1308.527073	15.7	-1308.50143	15.5	-1308.583336	18.3
[OxaliPt + H + G]$^+$						
Oxal_N3	-1385.906021	112.2	-1385.880658	111.6	-1385.961670	113.0
Oxal_NH$_2$	-1385.935512	164.5	-1385.909843	164.3	-1385.992052	155.3
Oxal_O	-1385.921502	71.6	-1385.896238	70.7	-1385.977553	71.3
Oxal_N7-1	-1385.947067	4.4	-1385.921489	4.4	-1386.003058	4.3
Oxal_N7-2	-1385.948756	**0.0**	-1385.923172	**0.0**	-1386.004708	**0.0**
Oxal_N7-3	-1385.942952	15.2	-1385.917188	15.7	-1386.000176	11.9
Oxal_N7-4	-1385.938734	26.3	-1385.913124	26.4	-1385.994786	26.1
Oxal_N7-5	-1385.937840	28.7	-1385.912155	28.9	-1385.994186	27.6
Oxal_N7-6	-1385.925821	60.2	-1385.900474	59.6	-1385.981325	61.4

Cartesian coordinates of the various computed structures in the xyz format

```
29
OxaliPt Neutral
 C                  0.00000000    0.00000000    0.00000000
 C                  0.00000000    0.00000000    1.53159418
 C                  1.43482447    0.00000000    2.08346622
 C                  2.25738308    1.16585463    1.51768793
 C                  2.24333087    1.17446501   -0.01951994
 C                  0.80873187    1.18339574   -0.55604071
 H                  1.40897827    0.04963928    3.17497211
 H                 -0.53169281    0.89128484    1.88995883
 H                 -0.55309546   -0.86909820    1.90057778
 H                  0.45932118   -0.92582923   -0.36346638
 H                  1.85063502    2.11433215    1.88845156
 H                  3.28854270    1.11027715    1.87567025
 H                  2.76154072    0.28315177   -0.39704392
 H                  0.31125091    2.10947190   -0.24758829
 H                  1.92097354   -0.94891957    1.82710097
 N                  0.72032126    1.15503428   -2.04761609
 H                  0.95724563    2.06272355   -2.44395576
 H                  1.38617115    0.48665454   -2.43497194
 Pt                -1.22831875    0.60223159   -2.63059892
 O                 -3.08205439    0.05654468   -3.16585349
 O                 -1.07951387    1.15856551   -4.55130639
 C                 -3.35562404    0.28753583   -4.44678436
 C                 -2.18470371    0.93571294   -5.25681642
 O                 -4.41307146    0.02524400   -4.95702543
 O                 -2.29189713    1.20479459   -6.42449940
 N                 -1.36618205    0.03766288   -0.60466806
 H                 -1.82399120   -0.86873569   -0.52719421
 H                 -1.95927970    0.70509903   -0.11177004
 H                  2.78622720    2.04354786   -0.40339509
```

```
30
Oxal_H1
 C                  0.00000000    0.00000000    0.00000000
 C                  0.00000000    0.00000000    1.52906112
 C                  1.44622434    0.00000000    2.05767789
 C                  2.26668070    1.16078190    1.47833710
 C                  2.23763900    1.17168545   -0.06114741
 C                  0.79242777    1.18252820   -0.56094929
 H                  1.43075597    0.05731516    3.14790786
 H                 -0.52691473    0.89171672    1.89206957
 H                 -0.54491042   -0.87117145    1.90361891
 H                  0.44694384   -0.92934298   -0.36839489
 H                  1.87643363    2.11336029    1.85442851
 H                  3.30214675    1.09608650    1.81861870
 H                  2.74833358    0.28025523   -0.44744797
 H                  0.30303178    2.11120785   -0.24860919
 H                  1.92404822   -0.95331004    1.80470621
 N                  0.66345949    1.14368795   -2.06221701
 H                  0.91606078    2.04837398   -2.46008497
 H                  1.32472302    0.46859856   -2.45087751
 Pt                -1.27496167    0.59258406   -2.58345006
 O                 -3.18018562    0.02396814   -3.05434733
 O                 -1.25646501    1.12294377   -4.60765789
 C                 -3.49887881    0.22895642   -4.29341205
 C                 -2.35670999    0.85872565   -5.12295121
 O                 -4.53537869    0.00167649   -4.87100651
 O                 -2.60409442    1.09254678   -6.36611664
 N                 -1.37866493    0.05279367   -0.60664688
 H                 -1.85095438   -0.84720970   -0.51070214
 H                 -1.95818332    0.73171118   -0.10825615
 H                  2.77373483    2.04296087   -0.44810389
 H                 -3.52996393    0.79754312   -6.52317403
```

30
Oxal_H2

C	0.00000000	0.00000000	0.00000000
C	0.00000000	0.00000000	1.52930198
C	1.44480486	0.00000000	2.06159265
C	2.26645775	1.16096600	1.48435657
C	2.24066999	1.17158266	-0.05504099
C	0.79608959	1.18225032	-0.55661307
H	1.42750835	0.05679901	3.15187148
H	-0.52770527	0.89159883	1.89178348
H	-0.54566255	-0.87114359	1.90317868
H	0.45154068	-0.92808304	-0.36659421
H	1.87521093	2.11350141	1.85953939
H	3.30126186	1.09654555	1.82669251
H	2.75182151	0.27996081	-0.44016442
H	0.30634397	2.11216120	-0.24913770
H	1.92345313	-0.95301501	1.80892829
N	0.67541617	1.13938763	-2.05708216
H	0.92394459	2.03998590	-2.46894591
H	1.33180526	0.45909880	-2.44633179
Pt	-1.22461106	0.61845590	-2.62159822
O	-3.13085691	0.12699152	-3.33772858
O	-1.00592079	1.20873088	-4.54530686
C	-3.23478925	0.41092939	-4.54804262
C	-2.04643851	1.04548674	-5.32472385
O	-4.32182948	0.19737743	-5.21587632
O	-2.15192086	1.31967535	-6.48381399
N	-1.37602137	0.04878797	-0.61276010
H	-1.83598724	-0.85483760	-0.50567578
H	-1.95440139	0.72321080	-0.10868444
H	2.77748773	2.04260896	-0.44139750
H	-5.00573411	-0.19933355	-4.64768433

30
Oxal_H3

C	0.00000000	0.00000000	0.00000000
C	0.00000000	0.00000000	1.52915818
C	1.44559067	0.00000000	2.06008286
C	2.26695817	1.16060575	1.48187228
C	2.24073478	1.17049510	-0.05765334
C	0.79521317	1.18161595	-0.55679661
H	1.42851649	0.05741482	3.15025983
H	-0.52725774	0.89171777	1.89203468
H	-0.54487320	-0.87140137	1.90368169
H	0.45051770	-0.92826223	-0.36726300
H	1.87669666	2.11353066	1.85691394
H	3.30201250	1.09580072	1.82312016
H	2.75105126	0.27849806	-0.44284725
H	0.30648658	2.11271875	-0.25165722
H	1.92361641	-0.95337530	1.80789431
N	0.67358739	1.13305138	-2.05624706
H	0.92016367	2.03074586	-2.47727697
H	1.32599666	0.44827080	-2.44531647
Pt	-1.21666663	0.62809137	-2.62922332
O	-3.07917352	0.21423623	-3.51570205
O	-0.87837687	1.25945779	-4.51277221
C	-3.17254380	0.56089549	-4.91434250
C	-1.82880015	1.17216390	-5.41314669
O	-4.17411870	0.36454635	-5.49412973
O	-1.76475143	1.51017433	-6.55793222
N	-1.37933515	0.04783207	-0.61191940
H	-1.83174103	-0.85762580	-0.49046483
H	-1.95222992	0.72343358	-0.10302820
H	2.77708896	2.04131933	-0.44482409
H	-3.91197158	-0.16494742	-3.19038896

```
30
Oxal_H4
 C                  0.00000000    0.00000000    0.00000000
 C                  0.00000000    0.00000000    1.52797901
 C                  1.44862247    0.00000000    2.05312266
 C                  2.27357885    1.15461792    1.46727436
 C                  2.24652090    1.16228234   -0.07347049
 C                  0.79465850    1.18290341   -0.55684969
 H                  1.43549591    0.06348542    3.14297905
 H                 -0.52638163    0.89195244    1.89118655
 H                 -0.54319244   -0.87141223    1.90442406
 H                  0.45573234   -0.92619865   -0.36667967
 H                  1.89046310    2.11120822    1.83978729
 H                  3.30969277    1.08490293    1.80457877
 H                  2.74828016    0.26589216   -0.45907413
 H                  0.31648937    2.11888080   -0.25275033
 H                  1.92264540   -0.95639957    1.80487967
 N                  0.66763745    1.12498806   -2.04831663
 H                  0.90709494    1.99146310   -2.57857773
 H                  1.24763778    0.37540231   -2.43523378
 Pt                -1.23115240    0.77205322   -2.59530624
 N                 -1.37708065    0.04540762   -0.62025359
 H                 -1.81071116   -0.87581000   -0.55948350
 H                 -1.97272644    0.67424285   -0.07805850
 H                  2.78421898    2.02953643   -0.46481539
 O                 -1.20363818    1.51058155   -4.43334298
 O                 -1.78190757    2.84254219   -6.72143524
 C                 -0.34813760    2.42148098   -4.82125444
 C                 -0.70686637    2.98355658   -6.21533023
 O                  0.61793231    2.80889994   -4.18482013
 O                  0.33375006    3.64067345   -6.73069568
 H                  0.06297279    3.98829821   -7.59534458
```

```
30
Oxal_H5
 C                  0.00000000    0.00000000    0.00000000
 C                  0.00000000    0.00000000    1.52804277
 C                  1.44880863    0.00000000    2.05277143
 C                  2.27335148    1.15492340    1.46715731
 C                  2.24615812    1.16290791   -0.07388961
 C                  0.79416589    1.18313702   -0.55650167
 H                  1.43564983    0.06362539    3.14256591
 H                 -0.52656983    0.89171870    1.89148621
 H                 -0.54287553   -0.87167727    1.90415524
 H                  0.45528654   -0.92634151   -0.36677188
 H                  1.89045926    2.11145140    1.83996794
 H                  3.30967347    1.08519144    1.80368164
 H                  2.74815357    0.26673940   -0.45962016
 H                  0.31533915    2.11900662   -0.25325341
 H                  1.92293967   -0.95635070    1.80476318
 N                  0.66740171    1.12484969   -2.04988295
 H                  0.91521936    1.98957034   -2.57224992
 H                  1.24796426    0.37477485   -2.43539917
 Pt                -1.23078800    0.76409420   -2.59524802
 N                 -1.37737580    0.04595636   -0.61999561
 H                 -1.81222408   -0.87477380   -0.55730120
 H                 -1.97250847    0.67666676   -0.07907753
 H                  2.78381744    2.03067103   -0.46437185
 O                 -1.20316278    1.48862813   -4.44291461
 O                 -1.60410664    2.57327781   -6.92320446
 C                 -0.35713566    2.37713356   -4.86015912
 C                 -0.66319703    2.92506322   -6.28285787
 O                  0.62475238    2.78583771   -4.24115553
 O                  0.24378757    3.82036544   -6.67589224
 H                  0.90055004    3.93031512   -5.96889675
```

25
CarboPt neutral

Pt	0.00000000	0.00000000	0.00000000
N	0.00000000	0.00000000	2.10725111
N	2.04107912	0.00000000	-0.52733892
H	2.55401864	0.84623684	-0.29309329
H	1.96742460	-0.05782213	-1.54760531
H	2.57639763	-0.80163713	-0.20291090
H	-1.00693704	-0.04152312	2.29190046
H	0.37022211	0.83915752	2.54634775
H	0.43471299	-0.81024841	2.54192269
O	-0.14537461	-0.07572770	-1.99449268
C	-1.27969579	0.14572744	-2.65453687
O	-1.35269958	-0.09594742	-3.83859374
C	-2.88713761	0.13865719	-0.58127200
O	-1.96657739	-0.08508030	0.35457133
O	-4.05169155	-0.10719835	-0.36137492
C	-2.43823384	0.81557690	-1.88681592
C	-2.12285555	2.35735525	-1.71222436
C	-3.59586498	1.21396340	-2.83906127
C	-3.00756561	2.64380316	-2.95192290
H	-1.07037850	2.64314327	-1.75401586
H	-2.55591639	2.74397817	-0.78723145
H	-3.65553378	0.63131316	-3.75573870
H	-4.54565524	1.18156876	-2.30778857
H	-2.41237647	2.77140002	-3.85740224
H	-3.70723846	3.47741712	-2.86751838

```
26
Carb_H1
 Pt                  0.00000000    0.00000000    0.00000000
 N                   0.00000000    0.00000000    2.11146452
 N                   2.03857766    0.00000000   -0.32598446
 H                   2.51907954    0.85187332   -0.03965874
 H                   2.10557436   -0.06878219   -1.34716304
 H                   2.53676010   -0.79575815    0.07068586
 H                  -0.96964988   -0.05008680    2.42597228
 H                   0.39937037    0.84278440    2.52276875
 H                   0.48025167   -0.80063738    2.52078323
 O                  -0.00436220   -0.06770992   -1.99803706
 C                  -1.03924485    0.18796841   -2.78510160
 O                  -0.98903186    0.01517813   -3.97300143
 C                  -2.77017282    0.16731516   -0.89989522
 O                  -2.05495486   -0.09770741    0.09946878
 O                  -4.04770799   -0.11165749   -0.82650984
 C                  -2.30762056    0.83530587   -2.14416124
 C                  -2.03865310    2.39653445   -1.94493850
 C                  -3.36888906    1.21212150   -3.21527231
 C                  -2.77151701    2.64074656   -3.28698400
 H                  -0.99036190    2.68144782   -1.85946983
 H                  -2.58814615    2.79029792   -1.08770507
 H                  -3.32385955    0.61029020   -4.11910402
 H                  -4.37894967    1.20246393   -2.80917525
 H                  -2.07497289    2.74948050   -4.11727589
 H                  -3.47849603    3.46877615   -3.29998355
 H                  -4.24873075   -0.52641968    0.02943370
```

```
26
Carb_H2
 Pt                 0.00000000    0.00000000    0.00000000
 N                  0.00000000    0.00000000    2.10564233
 N                  2.03589778    0.00000000   -0.34719256
 H                  2.51527711    0.85724424   -0.07525112
 H                  2.10128133   -0.08437893   -1.36679667
 H                  2.53842501   -0.78791495    0.05962465
 H                 -0.97363054   -0.08299952    2.40368772
 H                  0.36690771    0.85461984    2.52257858
 H                  0.49976847   -0.78605798    2.51959024
 O                 -0.03990105   -0.08281748   -2.00357735
 C                 -1.10464908    0.10740615   -2.76036175
 O                 -1.10840271   -0.12091726   -3.94084620
 C                 -2.78963723    0.08824029   -0.82926634
 O                 -2.04207529   -0.11534203    0.15297091
 O                 -4.03206675   -0.29042442   -0.66480357
 C                 -2.35850828    0.76544113   -2.09013605
 C                 -2.07916450    2.32202331   -1.91729827
 C                 -3.43396543    1.13116755   -3.15387686
 C                 -2.81353914    2.54880117   -3.26174013
 H                 -1.03025206    2.60507907   -1.84155444
 H                 -2.62422432    2.73509721   -1.06634353
 H                 -3.42828637    0.50809311   -4.04462377
 H                 -4.45022714    1.19215652   -2.74723413
 H                 -2.12173470    2.61595834   -4.10008964
 H                 -3.50732859    3.38671749   -3.29866216
 H                 -4.55382593   -0.10779076   -1.46150422
```

```
42
Carbo_N3
 Pt                 0.00000000    0.00000000    0.00000000
 N                  0.00000000    0.00000000    2.10869069
 N                  2.07770887    0.00000000   -0.25952121
 H                  2.67602704    0.27976647    0.51455820
 H                  2.24906105    0.63974958   -1.03731188
 H                  2.36718921   -0.92639571   -0.57981542
 H                 -0.72755222   -0.64734281    2.42572049
 H                 -0.22383812    0.92608605    2.47241395
 H                  0.87368442   -0.29139014    2.54241064
 O                  0.03984350    0.17780130   -2.01117377
 C                 -0.00252810   -0.76118911   -2.96835428
 O                  0.25542271   -0.46632408   -4.10611654
 C                  0.09237971   -2.78485935   -1.36870338
 O                 -0.50493609   -3.22524337   -0.40692741
 O                  1.44471257   -2.89870011   -1.45285799
 C                 -0.51013825   -2.17587071   -2.60332322
 C                 -2.07296368   -2.23438905   -2.70448155
 C                 -0.44330372   -3.14287629   -3.84164355
 C                 -1.93864247   -2.85032478   -4.12061134
 H                 -2.60028353   -1.28398104   -2.61953507
 H                 -2.47772291   -2.93691882   -1.97519125
 H                  0.27705452   -2.84515010   -4.59969390
 H                 -0.26338231   -4.17678737   -3.54164132
 H                 -2.06357438   -2.10850510   -4.90845480
 H                 -2.57268070   -3.70966836   -4.33498401
 H                 -1.24702379    1.81802524   -2.00607202
 N                 -2.15895844    1.95373090   -1.57729598
 C                 -3.17453898    2.81160963   -1.96274425
 H                 -3.01343782    3.57735880   -2.70594520
 N                 -4.29629179    2.57908106   -1.33789041
 C                 -4.02746011    1.51360971   -0.51363070
 C                 -4.90853841    0.77355865    0.35108725
 O                 -6.06297790    0.91053343    0.64287916
 N                 -4.17759414   -0.37464621    0.90154620
 H                 -4.77599660   -0.99787635    1.43130364
 C                 -2.87524881   -0.68604482    0.74345910
 N                 -2.35398532   -1.78222442    1.38675599
 H                 -3.02780060   -2.36985814    1.85998613
 H                 -1.69465647   -2.32502273    0.82043377
 N                 -2.06820055    0.08803328    0.01648863
 C                 -2.70549480    1.11839894   -0.65342138
 H                  1.72391159   -3.49043843   -0.73582807
```

42
Carbo_NH2-1

Pt	0.00000000	0.00000000	0.00000000
N	0.00000000	0.00000000	2.09915515
N	2.07051118	0.00000000	-0.20127795
H	2.45091540	0.93615668	-0.33058328
H	2.19348582	-0.53150799	-1.08770278
H	2.60337573	-0.45762214	0.53470463
H	0.30410091	0.88863985	2.49476098
H	0.58010032	-0.73317711	2.50427156
H	-0.97012794	-0.17310505	2.40547805
O	-0.24364731	0.03110627	-2.01290235
C	0.38005397	-0.80694018	-2.80396403
O	1.48798207	-1.28228924	-2.59002366
C	-1.74910565	-1.77224011	-3.69946375
O	-2.26660299	-2.47562929	-4.70464601
O	-2.33998639	-1.65887071	-2.63499502
C	-0.42225480	-1.13285389	-4.06679727
C	-0.55836397	0.13368403	-5.01024904
C	0.44401508	-1.79152369	-5.18349808
C	0.63440328	-0.40048173	-5.84117807
H	-0.46605568	1.09903118	-4.51417654
H	-1.49632260	0.10247339	-5.56575907
H	1.33225749	-2.30339944	-4.81992119
H	-0.14769038	-2.46458768	-5.80016222
H	1.57790778	0.06598362	-5.55360717
H	0.53373265	-0.34839342	-6.92439247
H	-3.64923145	-1.12051130	4.65714890
N	-3.84139201	-1.84787991	3.98469504
C	-4.53797819	-3.02152515	4.20605353
H	-4.90443658	-3.28660385	5.18619669
N	-4.68522241	-3.73197424	3.12016892
C	-4.07195547	-3.00034336	2.13446576
C	-3.94017287	-3.28525385	0.72347684
O	-4.30035893	-4.21984796	0.05922298
N	-3.24682302	-2.17892796	0.07913307
H	-3.12383303	-2.27533329	-0.92927936
C	-2.77434984	-1.08511229	0.70536535
N	-2.10549649	-0.10498316	-0.11626087
H	-2.22416056	-0.31404082	-1.12003281
N	-2.86000624	-0.84151061	1.98195982
C	-3.54109376	-1.82301863	2.65133175
H	-2.49743821	0.81565631	0.08161453
H	-3.12585903	-2.82770356	-4.42221590

42
Carbo_NH2-2

Pt	0.00000000	0.00000000	0.00000000
N	0.00000000	0.00000000	2.07581735
N	2.09992268	0.00000000	-0.21214778
H	2.55363909	0.79960843	0.22922513
H	2.28644523	0.07417482	-1.21383466
H	2.56459409	-0.84301972	0.12305735
H	0.72286540	0.59065759	2.48413578
H	0.10827906	-0.93385679	2.46987499
H	-0.92922894	0.38367802	2.36979305
O	0.01020957	0.12928197	-2.06700824
C	-0.71333962	-0.53217528	-2.87080586
O	-1.06318762	-1.77586029	-2.60061216
C	-2.63241996	0.82180397	-3.56755310
O	-3.25888090	1.38069153	-4.43217318
O	-2.87596025	0.74942885	-2.30901071
C	-1.28384186	0.07735264	-4.06969233
C	-0.32643541	0.99726429	-4.89508006
C	-1.44476641	-0.82471648	-5.32950666
C	-0.22951915	-0.11039079	-5.97685561
H	0.59229902	1.31654210	-4.40254470
H	-0.87873021	1.86958220	-5.24112370
H	-1.38335640	-1.90176002	-5.17633900
H	-2.38242439	-0.57874208	-5.82574660
H	0.69003570	-0.69503267	-5.89596337
H	-0.34902687	0.21111140	-7.01082442
H	-2.94595101	1.91858366	4.75026820
N	-3.29496144	2.48951604	3.99548339
C	-4.03917667	3.64934796	4.11151002
H	-4.26638694	4.08246842	5.07385398
N	-4.41134404	4.12599514	2.95428230
C	-3.90558133	3.24720911	2.03019525
C	-4.02521724	3.26269332	0.58654351
O	-4.56361911	4.03887378	-0.15177355
N	-3.35461744	2.08829253	0.04051234
H	-3.43046023	1.94054716	-0.97960953
C	-2.69672136	1.17055204	0.76333944
N	-2.09015819	0.08136376	0.01789004
H	-2.46504021	-0.79324463	0.38491500
N	-2.56265377	1.16795038	2.06474428
C	-3.20819759	2.22142837	2.65671654
H	-2.38532827	0.18932755	-1.02583426
H	-0.67764649	-2.05796697	-1.75516247

42
Carbo_N7-1

Pt	0.00000000	0.00000000	0.00000000
N	0.00000000	0.00000000	2.08288151
N	2.07949245	0.00000000	-0.00946377
H	2.48233497	0.86162656	0.35425257
H	2.32460917	-0.07427916	-1.02585640
H	2.50069470	-0.78451193	0.48384082
H	0.88369067	0.30010457	2.48872806
H	-0.19855215	-0.92917520	2.45065658
H	-0.73987760	0.64875963	2.42058498
O	-0.11455908	-0.05323220	-2.03926903
C	0.83647924	-0.19843641	-2.91328138
O	2.04287051	-0.19899780	-2.68368514
C	-0.56060856	-1.62539416	-4.37223375
O	-1.69045672	-1.71808836	-3.94333984
O	0.08212697	-2.66227044	-4.93251458
C	0.28724611	-0.36719537	-4.34388447
C	-0.42794516	0.93639027	-4.84275607
C	1.36241640	-0.16352673	-5.44524224
C	0.86139249	1.29434356	-5.62818718
H	-0.76883933	1.62282851	-4.06846095
H	-1.26979485	0.69636763	-5.49412410
H	2.39120165	-0.30883651	-5.12323346
H	1.16364259	-0.78872160	-6.31535653
H	1.48373642	2.01290244	-5.09220539
H	0.72687325	1.64333735	-6.65168139
H	-4.68938702	-0.58738183	-1.84382447
N	-4.01997357	-0.29498085	-1.14562123
C	-2.67939226	-0.50402438	-1.20049667
H	-2.19176058	-0.98510998	-2.03654234
N	-2.07489247	0.01895269	-0.14540032
C	-3.08328799	0.60189257	0.63161253
C	-3.07555773	1.32846226	1.86086442
O	-2.14447518	1.60392280	2.61644115
N	-4.37487419	1.75603568	2.20589617
H	-4.41211862	2.26824672	3.07919286
C	-5.52612383	1.50865729	1.49316942
N	-6.68812455	1.97526207	1.99047386
H	-6.73389036	2.59989589	2.77728889
H	-7.51831601	1.83669385	1.43679936
N	-5.52502912	0.82442832	0.36882080
C	-4.30776965	0.41017346	-0.00558259
H	-0.52106639	-3.42180491	-4.91705741

42
Carbo_N7-2

Pt	0.00000000	0.00000000	0.00000000
N	0.00000000	0.00000000	2.08161398
N	2.08077880	0.00000000	-0.02809707
H	2.48132491	0.90322988	0.21899127
H	2.31877539	-0.20480643	-1.02537641
H	2.51117024	-0.71211999	0.55819071
H	0.89095413	0.27283449	2.49086614
H	-0.23139978	-0.92072814	2.45147115
H	-0.71957663	0.67568213	2.41051523
O	-0.12091587	-0.02632470	-2.04134791
C	0.79226163	-0.35896719	-2.90151289
O	1.99219226	-0.51055011	-2.67925128
C	-0.60114956	-1.90024102	-4.17897357
O	-1.75483919	-1.94413074	-3.83180816
O	0.07030980	-3.03705582	-4.44136842
C	0.19883433	-0.60530930	-4.30138010
C	-0.57194335	0.62382173	-4.87348158
C	1.23553061	-0.46629145	-5.45639102
C	0.66582448	0.94860147	-5.75130647
H	-0.89031861	1.36771320	-4.14504743
H	-1.43873876	0.30610862	-5.45426531
H	2.28176723	-0.53555268	-5.16111433
H	1.03662741	-1.16336895	-6.27428650
H	1.28674527	1.73547807	-5.32032374
H	0.47497667	1.18695959	-6.79698027
H	-4.70847507	-0.69813191	-1.75277523
N	-4.02997184	-0.36653447	-1.08100272
C	-2.69035614	-0.57804386	-1.14405563
H	-2.22025077	-1.10706674	-1.96020484
N	-2.07177128	-0.00346817	-0.12460450
C	-3.06922744	0.61532676	0.63742414
C	-3.04263800	1.38988796	1.83625687
O	-2.09953130	1.68659515	2.56871546
N	-4.33561554	1.83724206	2.17899262
H	-4.36123028	2.38448058	3.03122612
C	-5.49701499	1.56107627	1.49285452
N	-6.65087217	2.05367007	1.98336746
H	-6.68550104	2.71039160	2.74417082
H	-7.48951434	1.88960597	1.44971720
N	-5.51314605	0.82617771	0.40084734
C	-4.30216855	0.39353620	0.02755280
H	0.97894813	-2.84168262	-4.70648154

42
Carbo_O-1

Pt	0.00000000	0.00000000	0.00000000
N	0.00000000	0.00000000	2.08313585
N	2.05657830	0.00000000	-0.17659531
H	2.52714558	-0.65179340	0.44751948
H	2.46221837	0.92375585	-0.03565165
H	2.23184782	-0.29182938	-1.16276243
H	0.40114842	0.83364406	2.50994639
H	0.43707956	-0.81605631	2.50849202
H	-0.99706061	-0.02466771	2.31879840
O	-0.29421644	0.01650539	-2.03782488
C	0.59030328	-0.26983939	-2.96277914
O	1.75670912	-0.58117377	-2.76468269
C	-0.67892902	1.13192250	-4.55431428
O	0.19679772	2.12727324	-4.73459260
O	-1.87794657	1.32077965	-4.53671180
C	0.00924467	-0.20207950	-4.38244107
C	1.02786828	-0.61927098	-5.48561015
C	-0.83094707	-1.47790828	-4.72266288
C	0.39021117	-2.03356811	-5.50181394
H	2.07450006	-0.53944317	-5.20152613
H	0.85833446	-0.06919880	-6.41228711
H	-1.20481674	-2.05834073	-3.87845704
H	-1.66929997	-1.22682516	-5.37322600
H	0.96688567	-2.74730038	-4.91257159
H	0.18390960	-2.46852935	-6.47899628
H	-7.46322686	-0.89169863	0.12359404
N	-6.50026931	-0.75350650	0.39360993
C	-5.97396626	-0.76412642	1.67846500
H	-6.60082986	-0.93339213	2.54099753
N	-4.68879065	-0.55380944	1.70706929
C	-4.34291172	-0.39377729	0.37858349
C	-3.10679055	-0.15621779	-0.23717658
O	-2.01592929	-0.02227586	0.40695173
N	-3.15904004	-0.06483583	-1.61156300
H	-2.26483385	0.07572042	-2.08839312
C	-4.33137811	-0.18516765	-2.34836340
N	-4.22256185	-0.08527530	-3.68406557
H	-0.30356244	2.95121486	-4.84653952
H	-5.09324449	-0.09020793	-4.19199686
N	-5.50505975	-0.41645896	-1.79094051
C	-5.46165126	-0.51577291	-0.45850055
H	-3.41197119	0.36004649	-4.10946603

42
Carbo_O-2

Pt	0.00000000	0.00000000	0.00000000
N	0.00000000	0.00000000	2.08979967
N	2.05322618	0.00000000	-0.25860877
H	2.49937141	-0.84669637	0.08978028
H	2.52282910	0.80191421	0.15705757
H	2.18106092	0.04023956	-1.29220716
H	0.85605901	0.30368482	2.54835543
H	-0.22038554	-0.93254230	2.43855271
H	-0.76166205	0.62696832	2.39873524
O	-0.40026073	0.06296796	-1.99491589
C	0.40511485	0.09716006	-3.00651185
O	1.63288188	0.10640449	-2.97013260
C	-1.43745310	1.16989520	-4.27589673
O	-1.05725298	2.40816740	-4.63282800
O	-2.57974372	0.98638068	-3.91070107
C	-0.37169720	0.09398686	-4.34302555
C	0.55352497	0.05153980	-5.59913699
C	-0.86945531	-1.34635402	-4.69656415
C	0.32512864	-1.48276952	-5.67634741
H	1.57585918	0.39141725	-5.43835167
H	0.11435815	0.57440100	-6.45248790
H	-0.93743182	-2.04905582	-3.86705569
H	-1.83652804	-1.30680256	-5.19878511
H	1.15790714	-2.03671409	-5.24262362
H	0.10327804	-1.89181609	-6.66113774
H	-4.24331596	4.59984797	2.20219324
N	-3.74131174	3.74084848	2.02794236
C	-2.94426787	3.04698285	2.92028599
H	-2.79290343	3.39486736	3.93086821
N	-2.42064786	1.96730870	2.40274948
C	-2.90079281	1.94438032	1.10464056
C	-2.69474932	1.03094221	0.06748334
O	-2.05985937	-0.07470238	0.13339147
N	-3.28613521	1.39369462	-1.12162042
H	-3.07199175	0.80980208	-1.93259780
C	-4.02898887	2.54631976	-1.30311301
N	-4.49371675	2.77293592	-2.54060048
H	-4.07641819	2.28500023	-3.32716396
H	-4.96349583	3.65051781	-2.69710569
N	-4.28900219	3.39019562	-0.31304832
C	-3.71408657	3.05599749	0.84239698
H	-0.14095535	2.40937872	-4.94225466

```
46
Oxal_N3
 H                  0.00000000    0.00000000    0.00000000
 N                  0.00000000    0.00000000    1.01319515
 C                  1.09279529    0.00000000    1.86606850
 H                  2.09391159   -0.16638024    1.49910467
 N                  0.76132824    0.21775743    3.10803719
 C                 -0.60276461    0.38881782    3.08678240
 C                 -1.50534207    0.73644186    4.15354760
 O                 -1.34291570    0.89666081    5.33084105
 N                 -2.84293773    0.95719279    3.59325870
 H                 -3.49874894    1.31329404    4.27883455
 C                 -3.24700685    0.78470027    2.31772659
 N                 -4.55616713    0.99705600    1.97499068
 H                 -5.13194785    1.43439730    2.68201223
 H                 -4.66063445    1.42682111    1.05421149
 N                 -2.39789241    0.35745862    1.38219651
 C                 -1.08454935    0.25546819    1.79392962
 O                 -1.64213999    0.93458792   -1.33940009
 O                 -3.00130459    4.24037332   -1.33324027
 C                 -1.74818006    2.21837168   -1.50533354
 C                 -3.06670776    2.95130901   -1.07568417
 O                 -0.88424302    2.92627941   -1.98518155
 O                 -4.03341329    2.42521372   -0.56841506
 H                 -2.11891052    4.39331503   -1.73486082
 C                 -5.17224225   -2.28243441   -0.86757221
 C                 -5.87512103   -3.60158432   -0.54214228
 C                 -6.69535406   -4.08511256   -1.75144701
 C                 -5.83499956   -4.18851558   -3.01820640
 C                 -5.11257351   -2.86529491   -3.32722658
 C                 -4.29559459   -2.40820320   -2.11715426
 H                 -7.14364463   -5.05355607   -1.51998252
 H                 -5.12272557   -4.35698653   -0.28093635
 H                 -6.51994852   -3.47500584    0.33238675
 H                 -5.92049497   -1.50259496   -1.04605635
 H                 -5.09351756   -4.98651853   -2.89686603
 H                 -6.45435705   -4.47046234   -3.87218427
 H                 -5.84967780   -2.09171963   -3.57859649
 H                 -3.50108343   -3.13413994   -1.91447250
 H                 -7.52694240   -3.39259401   -1.92537261
 N                 -3.59875563   -1.09078252   -2.31729518
 H                 -2.79978539   -1.19452766   -2.94289764
 H                 -4.23003572   -0.42601004   -2.76808642
 Pt                -2.99432785   -0.32938477   -0.47633182
 N                 -4.31026579   -1.76483088    0.25438593
 H                 -4.89194194   -1.36494406    0.99236786
 H                 -3.78844747   -2.53542833    0.67434494
 H                 -4.45845019   -2.97946461   -4.19639068
```

```
46
Oxal_O
 H                 0.00000000    0.00000000    0.00000000
 N                 0.00000000    0.00000000    1.00946800
 C                 1.10100668    0.00000000    1.85458836
 H                 2.10807423   -0.00836850    1.46560685
 N                 0.77801204    0.01019425    3.11610974
 C                -0.60364602    0.01502732    3.11379199
 C                -1.54424775    0.02008890    4.15604754
 O                -1.25767062    0.04436993    5.39992127
 N                -2.85097312   -0.00261867    3.72624265
 H                -3.56515891   -0.05990101    4.46110034
 C                -3.24742168    0.04450392    2.40332105
 N                -4.57798866    0.07006222    2.18997817
 H                -5.19594631    0.37734642    2.93445141
 H                -4.87555920    0.19720949    1.23570434
 N                -2.38909696    0.04166984    1.40268540
 C                -1.11047308    0.01092950    1.80173969
 O                -4.20378609    0.18925481    6.10009602
 O                -4.90903228    2.04245483    8.15797078
 C                -5.03808315    1.16556186    5.86797635
 C                -5.29795467    2.17580691    7.01859957
 O                -5.63906377    1.29033606    4.82119668
 O                -6.01787777    3.20423043    6.59745887
 H                -6.17039172    3.79589267    7.35180655
 C                -0.89083325    0.14567137    9.58620084
 C                 0.23018413   -0.28410815   10.53299627
 C                -0.12207199    0.10033838   11.98150846
 C                -1.48504562   -0.46369405   12.40730912
 C                -2.60438357   -0.05566372   11.43312744
 C                -2.23649674   -0.45776683   10.00380634
 H                 0.66100038   -0.25981195   12.65215458
 H                 0.36953918   -1.37051402   10.46170897
 H                 1.17326614    0.18097502   10.23162982
 H                -0.98021602    1.23661312    9.59136690
 H                -1.43081723   -1.55734026   12.45889653
 H                -1.73644843   -0.11970439   13.41291086
 H                -2.75707916    1.02991146   11.47380087
 H                -2.15345575   -1.54889063    9.94380121
 H                -0.13036676    1.19255634   12.07313477
 N                -3.26598058   -0.06948518    8.98113342
 H                -4.04409295   -0.72821337    8.99392752
 H                -3.68541399    0.85071358    9.15007789
 Pt               -2.41524993    0.00682249    7.11102805
 N                -0.65626368   -0.23114948    8.14874809
 H                 0.07673855    0.33994699    7.72606707
 H                -0.33865405   -1.19983310    8.07953434
 H                -3.55099615   -0.52284551   11.71946219
```

```
46
Oxal_NH2
 H                  0.00000000    0.00000000    0.00000000
 N                  0.00000000    0.00000000    1.00992652
 C                  1.09372542    0.00000000    1.85108310
 H                  2.10338080    0.02084091    1.46988914
 N                  0.75975692   -0.02813851    3.11571899
 C                 -0.61156125   -0.05531301    3.11294946
 C                 -1.53532684   -0.11853253    4.21872483
 O                 -1.37184269   -0.14636853    5.41153384
 N                 -2.89670557   -0.13512228    3.69413914
 H                 -3.59455749   -0.30952394    4.40770662
 C                 -3.24161062   -0.10983682    2.37100858
 N                 -4.64679116   -0.07350871    2.07727893
 H                 -4.83080567   -0.36414280    1.08262967
 H                 -5.16902015   -0.72029273    2.66931033
 N                 -2.40355325   -0.04676975    1.39416323
 C                 -1.10550499   -0.03707423    1.80943429
 O                 -6.76855818    1.42275878    0.51301629
 O                 -8.12530293    1.69922500   -1.73096471
 C                 -6.61579890    0.45403705   -0.33755992
 C                 -7.65435080    0.46431579   -1.48442186
 O                 -5.78624025   -0.44081771   -0.30499128
 O                 -7.97112422   -0.52778331   -2.06963940
 H                 -8.75042927    1.61987006   -2.46943704
 C                 -4.75479592    4.12781747    3.77525162
 C                 -4.38671003    4.78835598    5.10496285
 C                 -4.63658654    6.30554372    5.03611691
 C                 -6.07683940    6.62658336    4.61426024
 C                 -6.44979471    5.94048113    3.28821720
 C                 -6.20226315    4.43305495    3.37840839
 H                 -4.42008863    6.75101786    6.00923590
 H                 -4.99504220    4.35064410    5.90714395
 H                 -3.34024299    4.58245774    5.34771011
 H                 -4.09076717    4.49472596    2.98556841
 H                 -6.77201950    6.30362590    5.39769695
 H                 -6.20790561    7.70578475    4.51172915
 H                 -5.84391030    6.35694452    2.47319805
 H                 -6.86952917    3.99674694    4.12966538
 H                 -3.93398112    6.75659307    4.32607137
 N                 -6.48838915    3.69545593    2.10261050
 H                 -7.49104671    3.58665262    1.94704125
 H                 -6.13407068    4.21679825    1.29855728
 Pt                -5.58314641    1.82618989    2.11836401
 N                 -4.58302779    2.62846840    3.78248282
 H                 -3.59068242    2.39377135    3.81265931
 H                 -4.98315902    2.25586354    4.64525310
 H                 -7.49747685    6.13056695    3.03842707
```

```
46
Oxal_N7-1
 H                  0.00000000    0.00000000    0.00000000
 N                  0.00000000    0.00000000    1.01069142
 C                  1.09953478    0.00000000    1.80838364
 H                  2.11353590    0.03781439    1.44421698
 N                  0.75701891    0.03200892    3.08507969
 C                 -0.63748469    0.06797559    3.11648150
 C                 -1.58118750    0.17991180    4.18530024
 O                 -1.40618218    0.23420068    5.39850480
 N                 -2.90088859    0.23041323    3.67959066
 C                 -3.26534598    0.18966199    2.35226404
 N                 -4.57956500    0.22777395    2.05834193
 H                 -5.28833340    0.41313603    2.74728177
 H                 -4.83593216    0.25677281    1.08436645
 N                 -2.38320467    0.10012069    1.37876982
 C                 -1.11615202    0.05169387    1.80882961
 O                  3.28011222    1.04256620    3.10318252
 O                  4.40800863    2.03133170    0.83841962
 C                  4.27983944    1.83053186    3.25700653
 C                  4.85209623    2.34595615    1.90460827
 O                  4.80872504    2.20160290    4.30554508
 O                  5.88430250    3.17023689    2.08224133
 H                  6.02877723    3.24783647    3.04202835
 H                 -3.60754484    0.30261624    4.40181938
 C                  1.90121741   -0.75782424    7.39413006
 C                  1.04645135   -0.81036704    8.66113377
 C                  1.94758564   -0.82935992    9.90904338
 C                  2.93753075    0.34452223    9.92046797
 C                  3.77297376    0.40353216    8.62916122
 C                  2.85214887    0.44149375    7.40866584
 H                  1.32535472   -0.80535120   10.80652911
 H                  0.38906994    0.06723306    8.68773824
 H                  0.40038225   -1.69296491    8.64189473
 H                  2.51138941   -1.66684585    7.33334239
 H                  2.38920672    1.28636464   10.03816459
 H                  3.60414438    0.26567602   10.78212769
 H                  4.42325347   -0.47876183    8.56724936
 H                  2.25927585    1.36143054    7.42593611
 H                  2.50047863   -1.77558890    9.94119727
 N                  3.56764417    0.44174523    6.09656717
 H                  4.07330408    1.31332845    5.88481147
 H                  4.26814695   -0.30078683    6.07409068
 Pt                 2.17531937    0.18377324    4.58843688
 N                  1.09824427   -0.71437593    6.12344965
 H                  0.82654000   -1.66184196    5.86624312
 H                  0.21042873   -0.20000863    6.21758060
 H                  4.42448941    1.28175203    8.631430864
```

Oxal_N7-2
46

H	0.00000000	0.00000000	0.00000000
N	0.00000000	0.00000000	1.01045960
C	1.10085498	0.00000000	1.80703216
H	2.11445918	-0.03232855	1.43603282
N	0.75944094	-0.02209998	3.08506609
C	-0.63657175	-0.04324185	3.11648767
C	-1.58658055	-0.10402613	4.18318146
O	-1.42128045	-0.11582152	5.40022622
N	-2.90522991	-0.15033574	3.67692526
C	-3.26759018	-0.13386198	2.34910160
N	-4.58278876	-0.15930492	2.05451060
H	-5.29177074	-0.34001733	2.74454751
H	-4.83705186	-0.20979349	1.08088100
N	-2.38292585	-0.07469726	1.37642301
C	-1.11555454	-0.03581093	1.80828438
Pt	2.19296656	-0.14563942	4.58578293
O	3.34914361	-0.90499439	3.08105124
O	4.43913982	-0.68838171	0.60380880
C	4.63144780	-0.73377334	3.01490268
C	5.11982119	-0.94814776	1.56395261
O	5.40160049	-0.39749405	3.89862996
O	6.37133677	-1.40152143	1.51828715
H	6.62379824	-1.47966446	0.58458357
H	-3.61357979	-0.18298267	4.40033213
C	1.79131760	0.44423665	7.44602661
C	1.32568949	1.35568194	8.58254977
C	2.10711623	1.04420951	9.87153663
C	3.62518139	1.12080166	9.65373144
C	4.08397080	0.22018624	8.49344382
C	3.30255800	0.55441694	7.22192776
H	1.80397539	1.73952569	10.65766660
H	1.49004790	2.40282271	8.29602601
H	0.25111829	1.23203636	8.74392524
H	1.55287270	-0.59592903	7.69402969
H	3.91423126	2.15701673	9.44254986
H	4.15127271	0.83415957	10.56709758
H	3.91585372	-0.83284190	8.75442367
H	3.53577961	1.57833440	6.90995360
H	1.83677642	0.04182818	10.22371506
N	3.63804598	-0.31598815	6.05473239
H	4.53945586	-0.10382124	5.60172335
H	3.69553214	-1.29185268	6.34928544
N	1.11347323	0.71515594	6.13739626
H	0.13990375	0.37051571	6.11537363
H	1.06911383	1.72286169	5.98184256
H	5.15617037	0.33794264	8.31386500

46
Oxal_N7-3

H	0.00000000	0.00000000	0.00000000
N	0.00000000	0.00000000	1.01026372
C	1.09709221	0.00000000	1.81388080
H	2.11334112	0.03898554	1.45834909
N	0.74976949	0.02019499	3.08766645
C	-0.64439341	0.04585072	3.11421305
C	-1.59253711	0.12956077	4.18266344
O	-1.42216022	0.15955571	5.39629314
N	-2.91137107	0.17831888	3.67208757
C	-3.27096785	0.15219287	2.34337752
N	-4.58477344	0.18404788	2.04582390
H	-5.29617150	0.35948802	2.73468539
H	-4.83841639	0.22437853	1.07160482
N	-2.38534341	0.08085557	1.37127630
C	-1.11909570	0.03794044	1.80545813
O	3.24769397	1.13033264	3.16195823
O	4.24951380	2.16429057	1.00970510
C	4.19616433	1.97603768	3.42067702
C	4.82616175	2.60314927	2.14989192
O	4.62963903	2.31006436	4.50948786
O	5.72638164	3.38776174	2.19295988
H	-3.62129930	0.23106941	4.39280765
H	4.71567761	2.60779230	0.28330612
C	2.80364904	0.31485374	7.43836980
C	3.72105618	0.24748296	8.66039662
C	2.88442186	0.09897722	9.94343869
C	1.93241190	-1.10383494	9.87060183
C	1.03459116	-1.05233307	8.62117711
C	1.89081469	-0.91109068	7.36204156
H	3.55052908	-0.00065150	10.80340135
H	4.39974953	-0.60941489	8.55868577
H	4.34398146	1.14481750	8.70721552
H	2.18193586	1.21390351	7.49784829
H	2.51533369	-2.03239611	9.85839849
H	1.30734114	-1.14395246	10.76561423
H	0.35023366	-0.19773920	8.68796684
H	2.52871347	-1.79685707	7.25818608
H	2.30584054	1.01599641	10.10451876
N	1.09146288	-0.82761832	6.09166727
H	0.83576300	-1.76725173	5.79327985
H	0.19797628	-0.32910729	6.20745545
Pt	2.15666917	0.16569871	4.60086894
N	3.52335225	0.40145421	6.13358402
H	3.98891679	1.30513469	5.95278977
H	4.25476542	-0.30889859	6.08217480
H	0.41625719	-1.95263673	8.55670071

46
Oxal_N7-4

H	0.00000000	0.00000000	0.00000000
N	0.00000000	0.00000000	1.01078862
C	1.09524595	0.00000000	1.81611985
H	2.10880175	-0.02664621	1.45589504
N	0.75158759	-0.01070889	3.09106335
C	-0.64370543	-0.01517761	3.11620024
C	-1.59694137	-0.02428710	4.18329402
O	-1.42818072	0.01393264	5.39805794
N	-2.91415390	-0.07242775	3.67506410
C	-3.27295408	-0.08067360	2.34528432
N	-4.58437914	-0.11071086	2.04657339
H	-5.30427797	-0.21592046	2.74084465
H	-4.84095004	-0.15250991	1.07310657
N	-2.38422446	-0.04657285	1.37293105
C	-1.11900599	-0.01801872	1.80674882
O	3.28157967	-1.18023313	3.22865743
O	4.25270314	-2.62022266	1.30215202
C	4.59545996	-1.20426843	3.25367866
C	5.18053450	-1.95697136	2.01935232
O	5.32830282	-0.71786758	4.08966542
O	6.33782912	-1.92733434	1.74326134
H	-3.62539358	-0.07847272	4.39667233
H	3.40488309	-2.50339973	1.75845456
C	1.75125434	0.77218732	7.38933289
C	1.33192560	1.83267783	8.40802454
C	2.06916184	1.61125952	9.74127965
C	3.59205938	1.55758119	9.55210436
C	4.00384419	0.50475350	8.50789179
C	3.26818695	0.75213253	7.19013647
H	1.80423145	2.40857536	10.43933757
H	1.57484141	2.82829851	8.01387132
H	0.24890921	1.80104852	8.55695237
H	1.43445840	-0.21565476	7.74159280
H	3.95853653	2.54148493	9.23686376
H	4.08146246	1.33689017	10.50328972
H	3.75631735	-0.49890171	8.87751363
H	3.58004567	1.71651821	6.77457776
H	1.72186983	0.67525070	10.19408780
N	3.55722023	-0.26247927	6.13173725
H	4.47951302	-0.16268145	5.68224542
H	3.53795669	-1.20166075	6.53188942
Pt	2.16154729	-0.13697533	4.61045125
N	1.11551341	0.94398438	6.04151816
H	0.12954619	0.63661851	6.03850227
H	1.12391823	1.93184911	5.78558512
H	5.08430536	0.52736786	8.34184155

46
Oxal_N7-5

H	0.00000000	0.00000000	0.00000000
N	0.00000000	0.00000000	1.01056211
C	1.09986319	0.00000000	1.80879440
H	2.10772325	0.03068907	1.42351748
N	0.75741433	0.02549332	3.08580497
C	-0.63909533	0.05942359	3.11524786
C	-1.58745660	0.16833868	4.18226735
O	-1.42012283	0.21996091	5.39583803
N	-2.90620219	0.21895091	3.67127087
H	-3.61432576	0.29045517	4.39212601
C	-3.26743734	0.18069705	2.34365758
N	-4.58077689	0.21839275	2.04598442
H	-5.29250292	0.39472542	2.73417877
H	-4.83513314	0.24687283	1.07153631
N	-2.38226626	0.09455739	1.37268149
C	-1.11648940	0.04689324	1.80707872
O	3.31601321	1.18303196	3.23946018
O	5.55873957	-0.10682327	4.56537909
C	4.28548111	0.63490176	2.58533972
C	5.49371950	0.01671610	3.36559607
O	4.36166067	0.58012901	1.36414310
O	6.45441582	-0.37821183	2.54795027
H	6.14038090	-0.17984754	1.64261694
C	1.91948899	-0.97332320	7.30699747
C	1.12655891	-1.30949243	8.57063649
C	2.08075021	-1.46835645	9.76820359
C	2.97544691	-0.23442354	9.95475726
C	3.74546927	0.11503850	8.66905318
C	2.77344891	0.27942219	7.49929567
H	1.49876205	-1.65203295	10.67417866
H	0.40757828	-0.50539747	8.77031986
H	0.54801201	-2.22553103	8.41824738
H	2.58867887	-1.80599833	7.06348839
H	2.36078542	0.62301483	10.25293050
H	3.68427270	-0.40397474	10.76830754
H	4.46177624	-0.68165403	8.43374717
H	2.10403139	1.12411649	7.69644980
H	2.70645543	-2.35557775	9.61640164
N	3.43641223	0.57552076	6.19154440
H	3.74453912	1.54673705	6.15458664
H	4.28501899	0.02600561	6.01291163
Pt	2.13101470	0.22929372	4.62891511
N	1.06167353	-0.76946449	6.09024869
H	0.75183833	-1.67587344	5.74328315
H	0.19471789	-0.24717941	6.27412465
H	4.32382094	1.03330849	8.80536045

46
Oxal_N7-6

H	0.00000000	0.00000000	0.00000000
N	0.00000000	0.00000000	1.01066480
C	1.09621653	0.00000000	1.81585393
H	2.11020099	0.02235659	1.45401606
N	0.74959764	0.01906405	3.08956248
C	-0.64385519	0.03553119	3.11464415
C	-1.58993052	0.07559330	4.18770907
O	-1.41117130	0.05812269	5.40033442
N	-2.90894385	0.13104079	3.68209352
H	-3.61877122	0.15970019	4.40455339
C	-3.27068932	0.12628174	2.35274737
N	-4.58334038	0.16376379	2.05791907
H	-5.29675567	0.30934290	2.75175260
H	-4.84074546	0.20906691	1.08478812
N	-2.38640798	0.07019933	1.37692376
C	-1.11973709	0.03209061	1.80682996
O	3.17934764	1.37447699	3.27327822
O	3.69495977	3.03998430	5.71739333
C	3.67747994	2.51786655	3.32680562
C	3.93891620	3.47148451	4.57955447
O	4.07549313	3.07992886	2.23403489
O	4.38615860	4.55091815	4.17198322
H	4.39669026	3.97260159	2.59702525
C	1.90355725	-1.13069968	7.26469810
C	1.03992054	-1.49162452	8.47269669
C	1.91870617	-1.58391719	9.73421390
C	2.73924504	-0.30490560	9.95846104
C	3.57860694	0.06613618	8.72279696
C	2.67989082	0.16540853	7.48974438
H	1.28590381	-1.78264022	10.60217813
H	0.27120024	-0.72135250	8.60919330
H	0.51947465	-2.43838467	8.29873598
H	2.62659559	-1.93332507	7.07940741
H	2.06599320	0.52603693	10.19837909
H	3.39665106	-0.42852752	10.82197943
H	4.34733954	-0.69921414	8.55277011
H	1.96745793	0.98550269	7.62784596
H	2.59463081	-2.44216514	9.64092466
N	3.40669066	0.47635966	6.22456730
H	3.66445917	1.49777793	6.15839812
H	4.25016576	-0.09109971	6.14179502
Pt	2.12235154	0.21019372	4.64028098
N	1.12155938	-0.97950170	5.98539967
H	0.93140871	-1.90035101	5.59259623
H	0.19862973	-0.54058946	6.12881490
H	4.09747563	1.01541351	8.87774242

Table S2: Experimental spectrum of the [OxaliPt + H]$^+$ ion and computed vibrational modes for the **Oxal_H1** structure.

Wavenumber (cm^{-1})		Vibrational mode[b]
IRMPD	Calculated[a]	
Fingerprint region (FEL)		
1003	988 (41)	ν C-N DACH
1063	1045 (22)	NH_2 twisting
1150	1153 (96)	NH_2 and CH_2 wagging
1248	1217 (153)	δ C-OH
	1254 (82)	δ C-H DACH
	1257 (354)	ν C-O···Pt
1444	1449 (251)	ν C$^{\cdots}$ OH
1669	1662 (279)	ν C=O(OH)
1759	1765 (781)	ν C=O(OPt)
X-H stretch region (OPO)		
~ 3285	3288 (31)	ν NH_2 sym
	3294 (26)	ν NH_2 sym
~ 3340	3347 (45)	ν NH_2 asym
	3354 (41)	ν NH_2 asym
	3371 (216)	ν OH

[(a)] Calculated vibrational modes at the B3LYP/6-311G** level of theory. The computed intensities (km mol^{-1}) are given in parenthesis. In the fingerprint region, bands with intensity lower than 20 km mol^{-1} are not included.

Table S3: Experimental spectrum of the [CarboPt + H]$^+$ ion and computed vibrational modes for the **Carbo_H1** structure.

Wavenumber (cm^{-1})		Vibrational mode[b]
IRMPD	Calculated[a]	
Fingerprint region (FEL)		
–	1094	ν C-C cyclobutane ring
1180-1255	1176 (183)	δ C-OH + δ C-H
	1185 (95)	δ C-H
	1203 (113)	δ C-OH + δ C-H
	1225 (23)	δ C-H
1305	1312 (144)	NH_3 umbrella
	1322 (74)	NH_3 umbrella
1390-1460	1416 (174)	ν C$^{\cdots}$ OH
1560-1630	1563 (628)	ν C=O(OH)
	1606 (23)	NH_2 scissoring
	1622 (47)	NH_2 scissoring
	1634 (57)	δ NH
1745	1752 (384)	ν C=O(OPt)
X-H stretch region (OPO)		
3300	3292 (22)	ν NH_3 sym
3350	3350 (66)	ν NH + ν NH_2 asym of NH_3
3380-3390	3374 (46)	ν NH + ν NH_2 asym of NH_3
	3384 (37)	ν NH_2 asym of NH_3
	3389 (65)	ν NH_2 asym of NH_3
3545	3562 (154)	ν OH

[(a)] Calculated vibrational modes at the B3LYP/6-311G** level of theory. The computed intensities (km mol^{-1}) are given in parenthesis. In the fingerprint region, bands with intensity lower than 20 km mol^{-1} are not included.

Table S4: Experimental spectrum of the [CarboPt + H + G]$^+$ complex and computed vibrational modes for the global minimum **Carbo_N7-1**.

Wavenumber (cm^{-1})		Vibrational mode[b]
IRMPD	Calculated[a]	
Fingerprint region (FEL)		
1130	1121 (49)	δ C8-H + δ N9-H
	1130 (169)	CH_2 rocking
1185	1158 (34)	δ C8-H + δ N9-H
	1165 (136)	δ O-H
1285-1355 (1320)	1295(431)	ν C⋯O-Pt
	1314 (35)	ν C5N9
	1328 (81)	δ N1-H
	1334 (81)	ν C⋯O-H
	1341 (115)	NH_3 umbrella
	1353 (143)	NH_3 umbrella
1565-1750 (1595+1635+ 1700+1740)	1585 (126)	NH_2 scissoring of NH_3
	1595 (489)	ν N3C4
	1636 (1145)	ν C2N2
	1646 (88)	ν C=O(OPt)
	1662 (126)	δ N-H of NH_3, H bonded to C=O of G
	1699 (465)	ν C=O (of G)
	1733 (393)	ν C=O(OH)
X-H stretch region (OPO)		
~3150 (broad)	3089 (303)	ν C8-H
~3345	3332 (43)	ν NH_2 sym of NH_3
	3334 (37)	ν NH_2 sym of NH_3
~3390	3393 (21)	ν NH_2 asym of NH_3
	3398 (37)	ν NH_2 asym of NH_3
~3425	3423 (63)	ν N1H
~3445	3452 (229)	ν NH_2 sym of G
~3480	3473 (158)	ν N9H
3550+3575	3570 (80)	ν NH_2 asym of G
	3584 (87)	ν OH

[(a)] Calculated vibrational modes at the B3LYP/6-311G** level of theory. The computed intensities (km mol^{-1}) are given in parenthesis. In the fingerprint region, bands with intensity lower than 30 km mol^{-1} are not included.

Table S5: Experimental spectrum of the [OxaliPt + H + G]$^+$ complex and computed vibrational modes for the global minimum **Oxal_N7-2**.

Wavenumber (cm^{-1})		Vibrational mode[b]
IRMPD	Calculated[a]	
Fingerprint region (FEL)		
1125-1210 (1160)	1115 (93)	δ C8-H + δ N9-H
	1133 (35)	δ N-H (DACH)
	1154 (401)	δ O-H
	1156 (176)	δ C8-H + δ N9-H
	1169 (125)	NH_2 (DACH) wagging + twisting + δ CH (DACH)
1250-1340 (1295)	1242 (100)	δ N-H (DACH)
	1273(71)	δ C8-H
	1282 (175)	ν C⁼⁼ O-Pt
	1285 (79)	δ CH_2 DACH
	1315 (73)	ν C5N7
	1329 (34)	δ N1-H
1410	1396 (30)	δ N9-H
1585	1595 (533)	ν N3C4
1625	1623 (38)	NH_2 scissoring of DACH (H bonded NH_2 to C=O of oxalate)
	1629 (371)	NH_2 scissoring of DACH (H bonded NH_2 to C=O of G)
	1637 (681)	ν C2N2
1680	1693 (360)	ν C=O(O-Pt)
	1705 (566)	ν C=O (of G)
1755 (shoulder)	1762 (318)	ν C=O(OH)
1800	–	
X-H stretch region (OPO)		
~2960 (broad)	2942 (25)	ν CH DACH
	2950 (26)	ν CH DACH
	2952 (27)	ν CH DACH
3110 (broad)	3101 (421)	ν NH of DACH (H bonded to C=O of G)
	3107 (345)	ν C8H (interacting with C=O(OH)
3335	3321 (29)	ν NH of NH_2 (DACH)
3335	3322 (31)	ν NH of NH_2 (DACH)
3395	–	
3418	3425 (54)	ν N1H
3445	3451 (228)	ν NH_2 sym of G
3475	3473 (177)	ν N9H
3530+3555	3568 (77)	ν NH_2 asym of G
	3580 (108)	ν OH

Calculated vibrational modes at the B3LYP/6-311G** level of theory. The computed intensities ($km.mol^{-1}$) are given in parenthesis. In the fingerprint region, bands with intensity lower than 30 km mol^{-1} are not included.

Table S6: Experimental spectrum of the [OxaliPt + H + G]$^+$ complex and computed vibrational modes for the local minimum **Oxal_N7-1**.

Wavenumber (cm^{-1})		Vibrational mode[b]
IRMPD	Calculated[a]	
Fingerprint region (FEL)		
1125-1210 (1160)	1112 (93)	δ C8-H + δ N9-H
	1128 (38)	δ N-H (DACH) twinsting ?
	1157 (40)	δ C8-H + δ N9-H
	1158 (95)	NH_2 (DACH) wagging + twisting + δ CH (DACH)
	1164 (60)	ν C⁼⁼⁼O-H
	1191 (42)	NH_2 (DACH) wagging + twisting + δ CH (DACH)
1250-1340 (1295)	1240 (54)	NH_2 (DACH) wagging (NH_2 H bonded to C=O of G)
	1276 (30)	δ C8-H
	1283 (38)	δ CH DACH
	1302 (167)	δ CH DACH
	1316 (53)	ν C1N9
	1329 (34)	δ N1-H
1410	1385 (75)	δ O-H
1585	1595 (612)	ν N3C4
1625	1613 (203)	NH_2 scissoring of DACH (H bonded NH_2 to C=O of G)
	1620 (59)	NH_2 scissoring of DACH (H bonded NH_2 to C=O of oxalate)
	1638 (834)	ν C2N2
1680	1665 (336)	ν C=O(OPt)
	1713 (517)	ν C=O (of G)
1755 (shoulder)	–	
1800	1816 (264)	ν C=O(OH)
X-H stretch region (OPO)		
~2960 (broad)	2943 (23)	ν CH DACH
	2951 (23)	ν CH DACH
	2954 (26)	ν CH DACH
3110 (broad)	3132 (52)	ν C8H
	3168 (363)	ν NH of DACH (H bonded to C=O of G)
	3182 (345)	ν NH of DACH (H bonded to C=O of oxalate)
3335	3322 (31)	ν NH of NH_2 (DACH)
	3349 (31)	ν NH of NH_2 (DACH)
3395	–	
3418	3425 (54)	ν N1H
3445	3451 (230)	ν NH_2 sym of G
3475	3470 (186)	ν N9H
3530+3555	3510 (113)	ν OH
	3569 (79)	ν NH_2 asym of G

[(a)] Calculated vibrational modes at the B3LYP/6-311G** level of theory. The computed intensities (km mol^{-1}) are given in parenthesis. In the fingerprint region, bands with intensity lower than 30 km mol^{-1} are not included.

Complete citation for the Gaussian code of programs

Gaussian 16. Revision C.01.
Frisch, M. J., Trucks, G. W., Schlegel, H. B., Scuseria, G. E., Robb, M. A., Cheeseman, J. R., Scalmani, G., Barone, V., Petersson, G. A., Nakatsuji, H., Li, X., Caricato, M., Marenich, A. V., Bloino, J., Janesko, B. G., Gomperts, R., Mennucci, B., Hratchian, H. P., Ortiz, J. V., Izmaylov, A. F., Sonnenberg, J. L., Williams, Ding, F., Lipparini, F., Egidi, F., Goings, J., Peng, B., Petrone, A., Henderson, T., Ranasinghe, D., Zakrzewski, V. G., Gao, J., Rega, N., Zheng, G., Liang, W., Hada, M., Ehara, M., Toyota, K., Fukuda, R., Hasegawa, J., Ishida, M., Nakajima, T., Honda, Y., Kitao, O., Nakai, H., Vreven, T., Throssell, K., Montgomery Jr., J. A., Peralta, J. E., Ogliaro, F., Bearpark, M. J., Heyd, J. J., Brothers, E. N., Kudin, K. N., Staroverov, V. N., Keith, T. A., Kobayashi, R., Normand, J., Raghavachari, K., Rendell, A. P., Burant, J. C., Iyengar, S. S., Tomasi, J., Cossi, M., Millam, J. M., Klene, M., Adamo, C., Cammi, R., Ochterski, J. W., Martin, R. L., Morokuma, K., Farkas, O., Foresman, J. B. and Fox, D. J.. Wallingford CT.